Force Modification Factors for the Seismic Design of Bridges

Tianyou Xie

A Thesis in

The Department of

Building, Civil and Environmental Engineering

Presented in Partial Fulfillment of the Requirements

for the Degree of Master of Applied Science (Civil Engineering) at

Concordia University

Montreal, Quebec, Canada

August 2017

CONCORDIA UNIVERSITY

School of Graduate Studies

This is to certify that the thesis prepared

By: Tianyou Xie

Entitled: Force Modification Factors for the Seismic Design of Bridges

and submitted in partial fulfillment of the requirements for the degree of

Master of Applied Science (Civil Engineering)

complies with the regulations of the University and meets the accepted standards with respect to originality and quality.

Signed by the final examining committee:

Dr. A. M. Hanna Chair

Dr. A. Bagchi Examiner

Dr. Y. Zeng Examiner

Dr. L. Lin Supervisor

Approved by _____

Chair of Department or Graduate Program Director

August 2017 _____

Dean of Faculty

Abstract

Force Modification Factors for the Seismic Design of Bridges

Tianyou Xie

The current seismic design of bridges is based on a well-known principle, i.e., capacity design, in which the superstructure should remain elastic during earthquake events while the nonlinear deformation (i.e., plastic hinges) should occur in the substructure and should be ductile in term of flexure. Given this, the Canadian Highway Bridge Design Code (CHBDC) allows reducing the demands for the design of substructure elements (mainly columns) by a response modification factor R. Since the R-factor will affect the design forces significantly, the objective of the study is to determine its value from detailed finite element analyses, and evaluate its dependency on the ductility and bridge dominant period. For the purpose of the study, eight existing typical highway bridges in Montreal are examined including slab type bridges, slab-girder type bridges, and box-girder bridges. The substructure of the bridges consists of multiple columns from two to four. Nonlinear time-history analyses are conducted on each bridge model using IDARC. Thirty simulated accelerograms are used as input for the seismic excitations, and they are scaled to three intensity levels based on the first mode period of the bridge, namely, $1.0Sa(T_1)$, $2.0Sa(T_1)$, and $3.0Sa(T_1)$. It is found in the study that the configuration of the substructure affects the R-factor, such as, number of columns in the bent, using of crush struts, type of the bearings, etc. In addition, neither the equal displacement rule nor equal energy rule is observed in this study.

Acknowledgments

I wish to express my sincere gratitude to my supervisor Dr. Lan Lin for her continuous guidance and support during my study. She is the most patient advisor and one of the most diligent people I have ever met. The joy and enthusiasm she has for the research work is motivational and contagious for me.

Thanks are also due to professors for sharing their knowledge by offering courses that helped me in my graduate study at Concordia University.

I am grateful to the love and encouragement that my family has given to me. Their continuous encouragement helps me a lot whenever I have difficult times.

In regards to all my friends and staffs at Concordia University who made my journey to higher education successful.

Table of Contents

List of Tables

List of Figures

Chapter 1

Introduction

1.1 Motivation

Studies on damage to bridges during earthquakes could be dated back to the early beginning of the 19th century. For example, Hobbs (1908) examined failure modes of railways bridges based on the data from the most powerful earthquakes recorded up to 1907 including the M_w 7.3 Charleston (US) earthquake of 1886, the Japanese earthquakes of 1891 (M_w = 8.0) and 1894 (M_w = 6.6), the M_w 8.0 Indian earthquake of 1897, the M_w 7.8 California earthquake of 1906, and the M_w 6.5 Kingston (Jamaica) earthquake of 1907. The severe damage to almost all types of structures, such as buildings, bridges, pipelines, dams, transmission lines, etc. from the 1971 M_w 6.8 San Fernando Earthquake, California was the most important lesson for the earthquake engineering community around the world that seismic loads should be considered in the structure design. The collapse of eighteen spans 630 m long the Hanshin Expressway Bridge in Fukae from the 1995 M_w 6.9 Kobe earthquake brought an attention to the Japanese code authorities and bridge design engineers to update their seismic design codes. Furthermore, Wilson(2003) stated that "the 1995 Kobe earthquake provided the world's first experience with earthquake damage to new long-span bridges designed to 1990s seismic standards". Mitchell et al. (2010) conducted a field visit on the damage to bridges after the 2010 Chile earthquake. It was reported that failure of most of the bridges was due to loss of superstructure support. Mitchell et al. also highlighted that skew supports and multi-span simply supported bridges

were vulnerable to earthquakes.

Given the lessons learned from past earthquakes, comprehensive studies on the performance of bridges subjected to earthquake loads have been undertaken for years. Most of them are focussed on, (i) risk analysis to prepare an emergency response plan in case of earthquakes and take an action on the vulnerable bridges; (ii) retrofit techniques to strengthen the bridges that do not satisfy the seismic requirements in the modern design codes. In the meantime, the seismic provisions are also required to be revised or modified since our knowledge of seismology and seismic performance of structures have been improved significantly in the past decades.

The principle of the capacity design is well accepted for the seismic design of bridges in the design standards or codes in several countries, e.g., AASHTO bridge design specifications by American Association of State Highway and Transportation Officials (AASHTO 2012), Canadian Highway Bridge Design Code (CHBDC 2014), New Zealand Bridge Manual (NZ 2013), etc. According to 2014 CHBDC, the seismic design should fulfill the following requirements, (i) the superstructure should remain elastic, (ii) all inelastic deformations should occur in predetermined locations (i.e., plastic hinges) in the substructure, (iii) the inelastic behavior should be ductile for flexure. Furthermore, CHBDC specifies response modification factors (R-factor) to be used to reduce the forces (i.e., moment, shear, and axial force) for the design of bridge substructure elements. These factors depend on the type and the material of the column bents. For example, for wall-type piers, the R-factor defined is 2.0; for single column bents, the factor is 3.0; for multiple-column bents, the factor is 5.0. Since the seismic design forces are well related to the R-factor, it is wise to assess the value of R-factor from detailed finite element analysis on some existing bridges.

1.2 Objective and Scope of the Study

The main objective of this study is to evaluate the force reduction factor used for the design of bridge substructure elements. To achieve this, the following tasks are carried out:

- Select typical highway bridges in Quebec. The selection is based on the statistics data available in the literature.
- Develop bridge models for the linear and nonlinear time-history analyses.
- Select thirty time series as input for seismic excitations for the time-history analysis.
- Run time-history analysis for three excitation levels, namely, $1.0Sa(T_1)$, $2.0Sa(T_1)$ and $3.0Sa(T_1)$ in which T_1 represents the dominant period of a bridge model.
- Evaluate the R-factor for each bridge model based on the analysis results; then compare it with the value defined in CHBDC and AASHTO, and the recommendations made by other researchers.
- Investigate the relation between R-factor and the ductility.
- Investigate the relation between R-factor and the bridge period.

1.3 Outline of the Thesis

This thesis is organized in 7 Chapters. Chapter 2 presents a literature view of similar research work related to the topic of this study. A description of the eight bridges selected for the study is provided in Chapter 3 while the modeling techniques are explained in Chapter 4.

Chapter 5 provides detailed information on the selection of accelerograms for the time-history analysis. Chapter 6 discusses the analysis results. Finally, the conclusions from this study and recommendations for future work are presented in Chapter 7.

Chapter 2

Literature Review

2.1 Force Reduction Factor

Currently, two approaches are available for the seismic design of bridges, namely, force-based design and performance-based design. For the forced-based design, the demand for the elements to be designed should be larger than or equal to their capacity. With respect to the performance-based design, the elements designed should meet certain performance level during possible earthquake events. The concept of performance-based design was introduced in the beginning of the 20^{th} century. Due to the lack of quantitative data to define the performance levels, this design approach is not well adopted by practicing engineers. Accordingly, the force-based approach is commonly used in practice (Erdem 2010). It is also necessary to mention that the performance of structures designed according to the force-based approach has been validated by a full-scale test conducted by Zafar (2009).

With respect to the force-based design method, the elastic design force is allowed being reduced by a factor larger than 1.0 to take into account the nonlinearity of the structural elements during significant earthquake events. Generally speaking, two factors are considered in the development of the force reduction factor, and they are the ductility-related factor R_μ, and the overstrength-related factor Ω as illustrated in Fig. 2.1 (Uang et al. 2000). It can be seen in the figure that the factor R_μ is used to account for the seismic design force reduced from elastic to inelastic while Ω is used to take into account the reduction from the maximum

inelastic response to the response corresponding to the first significant yielding. More specifically, the factor R_μ and Ω can be determined using Eqs. 2.1 and 2.2, respectively (Uang et al. 2000). The force reduction factor R in Eq. 2.3 is the ratio of the elastic seismic design force to the force when the first yielding occurs.

$$R_\mu = \frac{Q_e}{Q_y} \tag{2.1}$$

$$\Omega = \frac{Q_y}{Q_s} \tag{2.2}$$

$$R = \frac{Q_e}{Q_s} \tag{2.3}$$

Where,

Q_e = Required elastic force level,

Q_s = Design seismic force level,

Q_y = Yielding force level based on the idealized response curve.

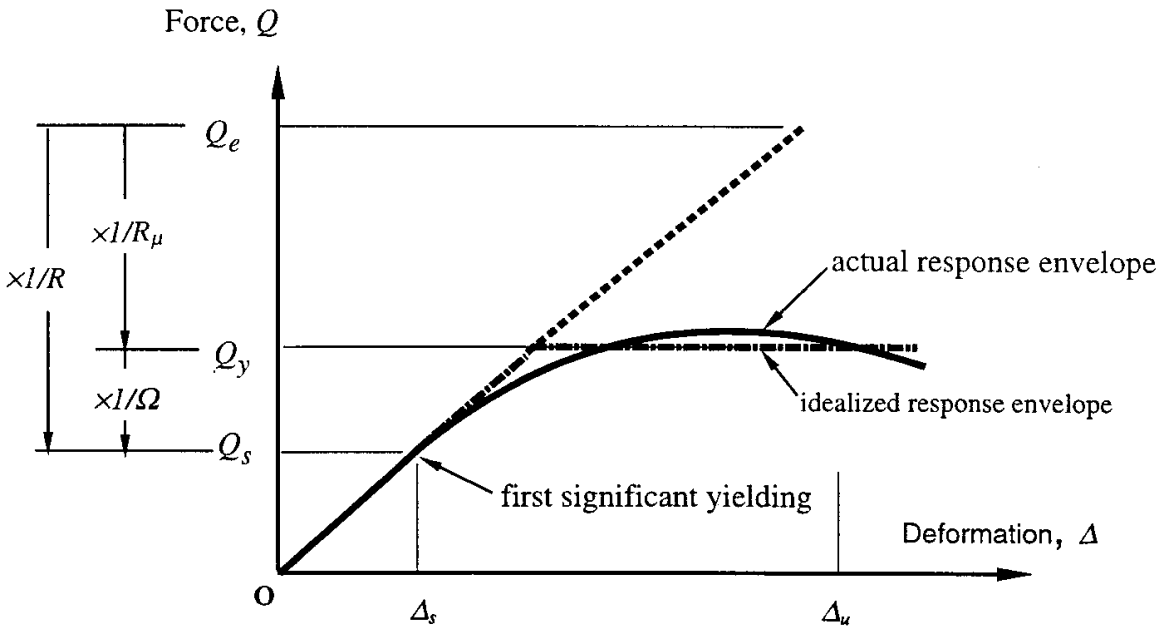

Figure 2.1 Concept of force reduction factor R (Uang et al. 2000).

It is necessary to mention that both the ductility-related factor and the overstrength-related factor are used to reduce the elastic seismic design force for buildings while there is only one factor, i.e., R-factor used in the seismic design of bridges. Tables 2.1 and 2.2 provide R-factors defined in CHBDC (2014) and AASHTO (2012), respectively. By comparing the R-factors given in CHBDC and AASHTO, it is noticed that CHBDC specifies R-factors only for the substructure elements while AASHTO specifies R-factors for not only the substructures but also the connections. Furthermore, CHBDC R-factors are the same as AASHTO factors for "Other bridge".

Table 2.1 Force reduction factor specified in CHBDC (2014).

Ductile substructure elements	**Response modification factor, R**
Wall-type piers in direction of larger dimension	2.0
Reinforced concrete pile bents	
Vertical piles only	3.0
With batter piles	2.0
Single columns	
Ductile reinforced concrete	3.0
Ductile steel	3.0
Steel or composite steel and concrete pile bents	
Vertical piles only	5.0
With batter piles	3.0
Multiple-column bents	
Ductile reinforced concrete	5.0
Ductile steel columns or frames	5.0
Braced frames	
Ductile steel braces	4.0
Nominally ductile steel braces	2.5

Table 2.2 Force reduction factor specified in AASHTO (2012).

Substructure	Operational Category		
	Critical	**Essential**	**Other**
Wall-type piers—larger dimension	1.5	1.5	2.0
Reinforced concrete pile bents			
Vertical piles only	1.5	2.0	3.0
With batter piles	1.5	1.5	2.0
Single columns	1.5	2.0	3.0
Steel or composite steel and concrete pile bents			
Vertical piles only	1.5	3.5	5.0
With batter piles	1.5	2.0	3.0
Multiple column bents	1.5	3.5	5.0
Connection	**All Operational Categories**		
Superstructure to abutment	0.8		
Expansion joints within a span of the superstructure	0.8		
Columns, Piers, or pile bents to cap beam or superstructure	1.0		
Columns or piers to foundations	1.0		

2.2 Review of Previous Studies

Investigation of the force reduction factor for the seismic design of structures starts with buildings. The two well-known rules for the earthquake engineering community, i.e., equal displacement rule and equal energy rule, proposed by Newmark and Hall in 1973 were based on the performance of buildings. According to the equal displacement rule, the force reduction factor (R) is almost equal to the ductility (μ), i.e., $R = \mu$. For the equal energy rule, the relationship between R and is expressed as $\mu = (R^2 + 1)/2$. These two relationships proposed by Newmark and Hall (1973) still serve as a basis for the seismic analysis of structures. Naumoski and Tso (1990) conducted a study to assess the seismic force reduction factors proposed in the seismic provisions of the 1990 National Building Code of Canada (NBCC). They reported that the code reduction factor led to very high ductility demand for

short-period buildings. Given this, two types of period-dependent force reduction factor were recommended by Naumoski and Tso (1990). More specifically, Type I factor is linearly increased with the period, and it is used for a building with a period shorter than to 0.5 s, while Type II factor is constant for a building with a period longer than 0.5 s. Mitchell et al. (2003) discussed in detail about the seismic force reduction factors for the proposed 2005 edition NBCC, in particular, the overstrength-related factor should be related to the size of members, material factor, strain hardening of the material, and additional resistance developed before a collapse mechanism forms. Kim (2005) performed a pushover analysis on 30 steel braced frames with different span lengths and storey numbers to evaluate the R-factor. It was found that R-factor increased with the span length and the storey height. Most of the values of R-factor from the study were smaller than those defined in IBC (2000), and it indicates that the building seismic resistance was overestimated. Furthermore, a comparison was made between the results from pushover analysis and incremental dynamic analysis. It was found out the values of the R-factor from the two methods were compatible. Kim (2005) also suggested that the number of stories, target ductility ratios should be taken into account in order to determine the R-factor. Kang and Choi (2011) proposed a simplified method to estimate R-factor for steel moment-resisting frame buildings that could be determined based on the period of the building and the displacement ductility. In addition, Kang and Choi (2011) also reported that the R-factor changed with the seismic intensity level.

Compared with buildings, research work on the investigation of the R-factor for bridges is very limited. Ahmad (1997) conducted a pushover analysis on circular reinforced concrete bridge columns to evaluate the R-factors, which can be determined using the displacement, longitudinal reinforcement ratio, and displacement ductility. It was found that the R-factor and the displacement ductility decreased with the increasing of the reinforcement

ratio. Ahmad also reported that the R-factor changed significantly with the dominant period of the structure. Borzi (2000) conducted a regression analysis on earthquake records to evaluate the modification factor for the demand by using the ratio of inelastic to elastic spectra acceleration. It should be noted that, the methodology of Brozi's study was completely different from all others since it was performed based on seismology not structural analysis. The earthquake records were grouped in terms of the magnitude, distance and soil condition. The results of the study showed that the characteristics of ground motions had very minor effect on R-factor. The study also concluded that R-factors proposed in the code were underestimated, and they were smaller compared to those from structural analysis. Watanabe (2002) used a single-degree-of-freedom system to evaluate the R-factor subjected to seventy ground motions. The hysteretic behavior was represented by an elastic-perfectly-plastic model. The R-factor was determined as a ratio of the maximum elastic restoring force to the inelastic force hysteresis model in the oscillator. The results showed that R-factor scattered significantly with the input ground motion. The study also found out that the equal displacement rule is more appropriate than the equal energy rule for determining of R-factor. Kappos (2013) developed an approach for determining R-factors for bridges. Seven bridges located in southern Europe were selected for the study and they were categorized into two groups: bridges with yielding piers and bridges without yielding piers. Pushover analyses were conducted on the bridge models for the longitudinal and transverse directions. The ductility-related factor and overstrength-related factor were calculated in terms of the ultimate strength, yield strength, design strength, yield displacement, and ultimate displacement of the bridge column. The computed factors were compared with those specified in the Eurocode 8 (2005), AASHTO (2010). It was concluded that the energy absorption capacity of the bridge column was underestimated for modern bridges.

2.3 Summary

The concept for determination of the R-factor is introduced in this chapter followed by a review of the previous studies on the investigation of the R-factor for bridges, which is very limited. There were two studies related to the current research topic proposed. One was focused on bridge columns; the other followed the approach for buildings. Given this, the objective of this study is to examine the reduction of bridge responses by detailed finite element analysis.

Chapter 3

Description of Bridges

3.1 Introduction

According to Tavares et al. (2012), there are 2672 multi-span bridges in Québec of which 57% are concrete bridges, 15% are steel bridges. Regarding the concrete bridges, 25% of them are multi-span simply supported slab-on-girder type bridges, 21% are multi-span continuous slab-on-girder type bridges, and 11% are multi-span continuous slab bridges. Tavares et al. (2012) also reported that most of the bridges in Québec have three spans. Given this, eight existing bridges used in the research conducted by Keivani (2003) were selected for this study. More specifically, these include two of each following types of bridges, rigid frame bridges (i.e., Bridge #1 and Bridge #5), slab-on-girder bridges (i.e., Bridge #2 and Bridge #8), slab bridges (i.e., Bridge #4 and Bridge #6), and box girder bridges (i.e., Bridge #3 and Bridge #7). Most of the selected bridges have three spans except Bridges #2, #4, and #5 in which Bridges #2 and #4 have 2 spans while Bridge #5 has 4 spans. It is necessary to mention that all these bridges are located in Ottawa. Given the similar practice in the design and construction between Ottawa and Montreal, it is assumed that these bridges are representative of typical highway bridges in Montreal, Québec this besides that the seismic hazard in the two cities is very close (CHBDC 2014). Generally speaking, these bridges can be considered as representatives of typical highway bridges in Canada given the uniform construction techniques. The characteristics of the selected bridges are summarized in Table 3.1. A brief

description of each bridge is given in the section below, and details can be found in Keivani (2003).

Table 3.1 Characteristics of the selected bridges.

Bridge No.	Year of design	Span	Skew	Structural system	Bridge type	Superstructure	Substructure	Foundation
1	1957	3	6	Continuous	Rigid frame	Concrete girder	4 columns bent	Strip footing
2	1957	2	------	Simply-supported	Slab-on-girder	Steel girder	3 columns bent	Pile footing
3	1965	3	22.81	Continuous	Box girder	Prestressed concrete box girder	3 columns bent	Pile footing
4	1965	2	24.78	Continuous	Slab	Prestressed slab	2 columns bent	Square footing
5	1968	4	------	Continuous	Rigid frame	Concrete girder	4 columns bent	Strip footing
6	1968	3	28.62	Continuous	Slab	Prestressed slab	3 columns bent	Caisson footing
7	1970	3	------	Continuous	Box girder	Steel box girder	2 columns bent	Pile footing
8	1973	3	30	Continuous	Slab-on-girder	Precast girder	3 columns bent	Strip footing

3.2 Description of Bridges

3.2.1 Bridge #1

Bridge #1 is a three-span rigid frame bridge (Fig. 3.1) built in 1957. The two end spans are 21.34 m each and the middle span is 27.43 m long, which gives the total bridge length of about 70 m. The overall deck width measured from edge to edge of the sidewalk is 13.67 m. The bridge has a skew of 6 degrees. The superstructure consists of a 20 cm thick slab supported by four 1.98 m deep T-beams. The substructure includes two abutments and two bents. Each bent has four square columns (762×762 mm), and the height of the columns is 3.4 m. Twelve No. 11 bars (The unit for the steel bars is imperial unit, hereafter. It is equivalent to a diameter of 35.7 mm in metric unit) are used for the longitudinal reinforcement that provides a reinforcement ratio of 2.1%. The transverse reinforcement is provided by three sets of No. 3

stirrups (diameter d_b = 11.3mm) at a spacing of 305 mm. The transverse reinforcement ratio is about 0.34%. The strip footing is used for both the abutments and the bents. Each has two layers; the bottom one is 0.76 m, and the top one is 3.05 m.

The compressive strength of the concrete for all the components, such as slab, columns, etc. is 22.8 MPa. Due to the lack of information on the reinforcing steel in the design drawings, the yield strength of the steel bars is assumed to be 275 MPa in accordance with the minimum material strengths required by CHBDC (2014).

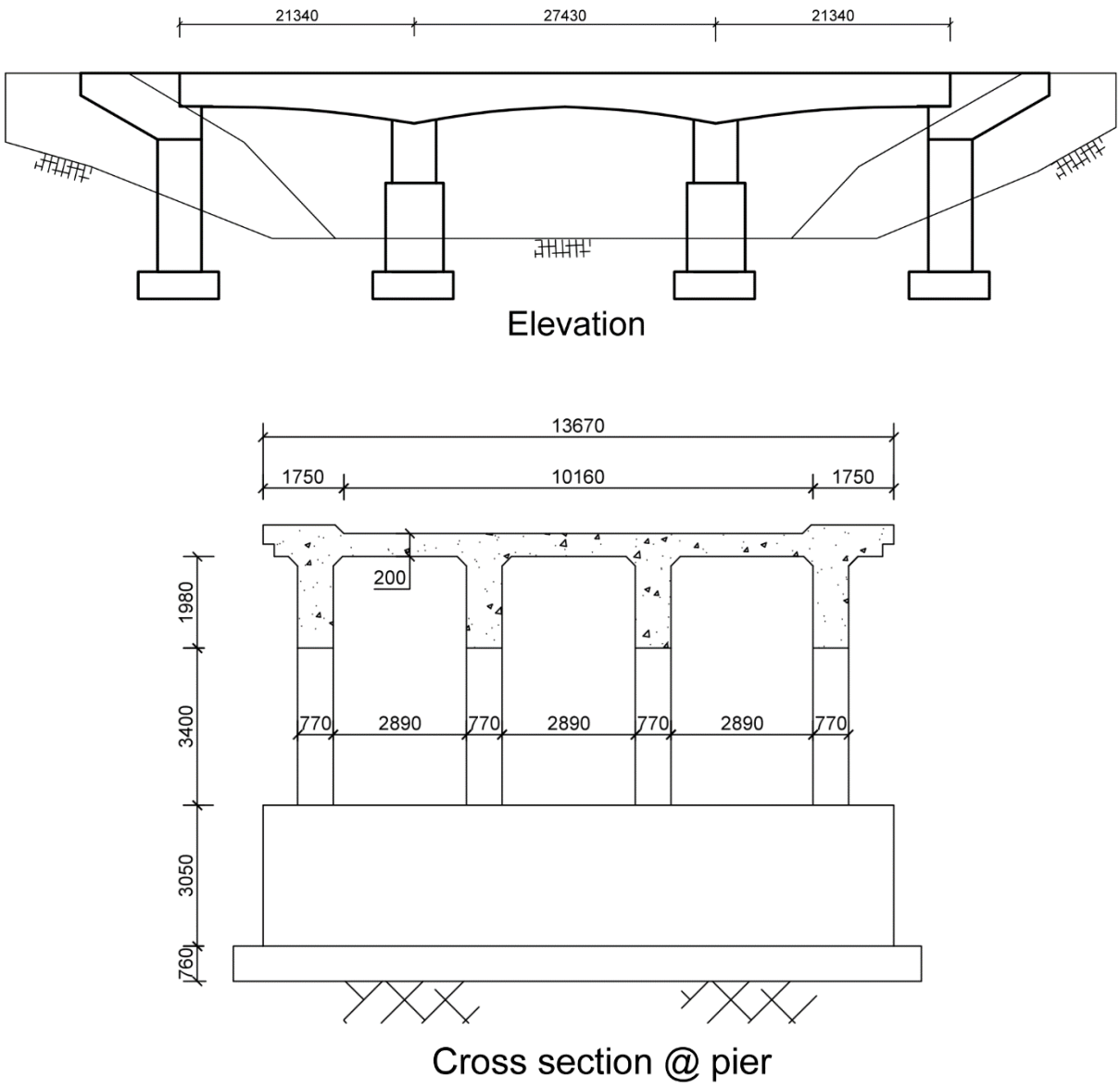

Figure 3.1 Geometric configuration of Bridge #1 adapted from Keivani (2003).

3.2.2 Bridge #2

Bridge #2 was also built in 1957 and has two equal spans (24.16 m each) without a skew angle. As shown in Fig. 3.2, the deck is provided by an 18 cm slab supported by six steel girders. The total deck width is 12.5 m.

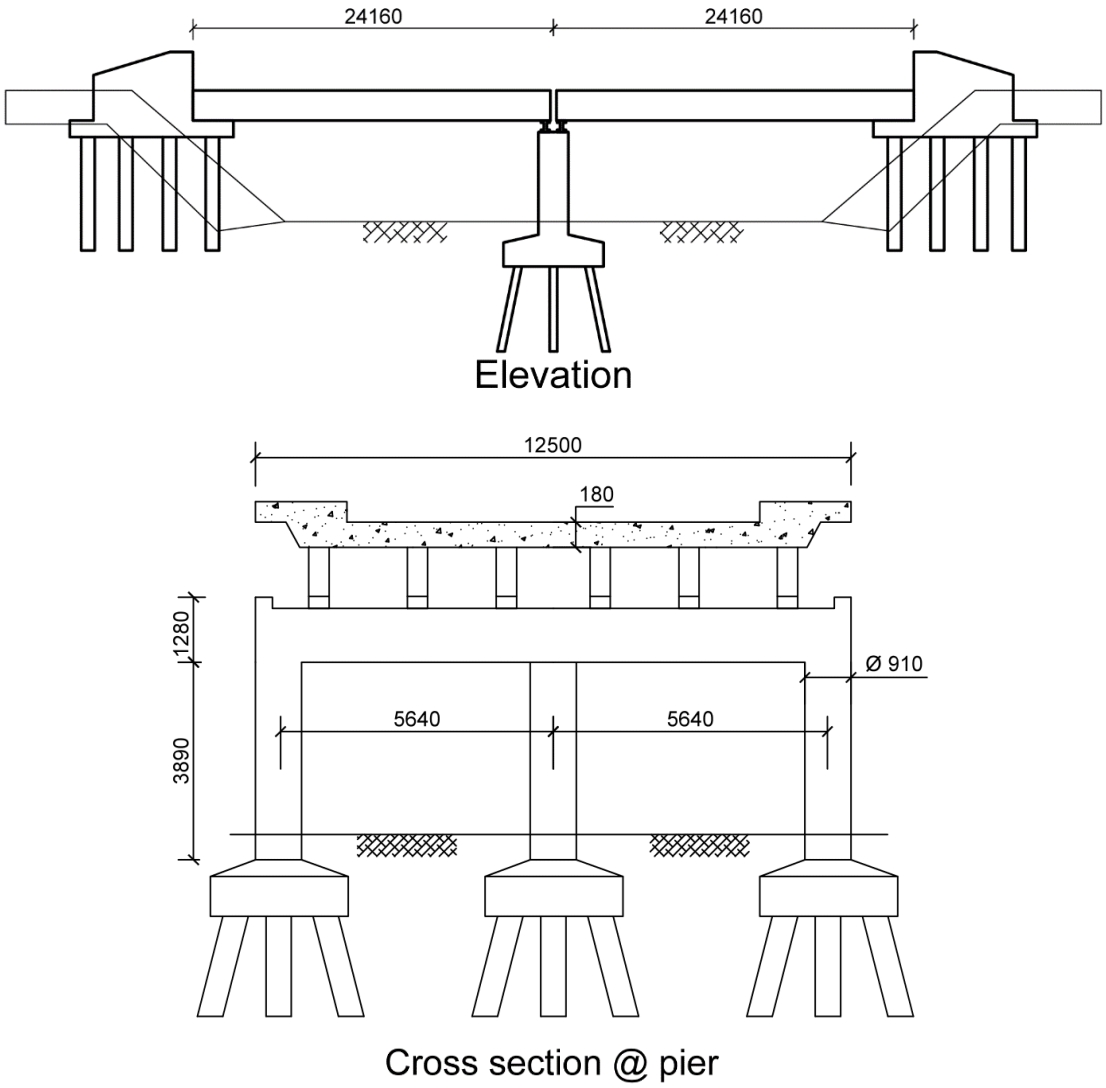

Figure 3.2 Geometric configuration of Bridge #2 adapted from Keivani (2003).

The bent consists of a cap beam and three columns. The cross-sectional dimension of the cap beam is 910 mm (depth) ×1280 mm (width). The diameter of the columns is 910 mm, and the height is 3.89 m. The center-to-center spacing of the columns is 5.64 m. The

longitudinal reinforcement of the column consists of twelve No. 11 bars providing a reinforcement ratio of 1.84%. A 12.7 mm spiral at a pitch of 51 mm is used for the transverse reinforcement, which results in a transverse reinforcement ratio of 0.83%. Piled foundation is used for abutments and the bent. Fixed bearings are used at the abutments while expansion bearings are used at the bent.

Based on the original construction drawings, it was found that the compressive strength of the concrete was 20.7 MPa, and the yield strength of the reinforcing steel is 375 MPa.

3.2.3 Bridge #3

Bridge #3 (Fig. 3.3) is a three-span continuous box girder bridge. The span on the west end is 19.41 m, on the east end is 16.44 m, and the middle span is 31.55 m. The total deck width is 20.34 m including a 2.55 m-wide sidewalk on each side. The bridge has a skew angle of 22.81 degrees. The superstructure consists of a three-cell box girder prestressed in the longitudinal direction only. The prestressing force is provided by 8 S-A-37 cables (i.e., 37Ø7mm wires) in each cell. The jacking force of each cable at the final stage is 1550 kN. Diaphragms are located at the abutments, bents, and the middle of each span to in order to provide the rigidity of the superstructure in the transverse direction. Each box girder is supported by a circular column with a diameter of 1.07 m. As illustrated in Fig. 3.3, the diameter of the column is reduced to 0.61 m over a height of 12.7 mm at the bottom. The column and the box girder is monolithically cast. Each column is reinforced with thirteen No. 11 longitudinal bars and a No. 5 spiral with a pitch of 64 mm. The longitudinal and transverse reinforcement ratios are 1.46% and 1.30%, respectively. Piled foundation is used for the bents.

The concrete compressive strength is 34.5 MPa, and the yield strength of the steel bars is 345 MPa. The bridge was designed according to 1961 AASHTO standard specifications.

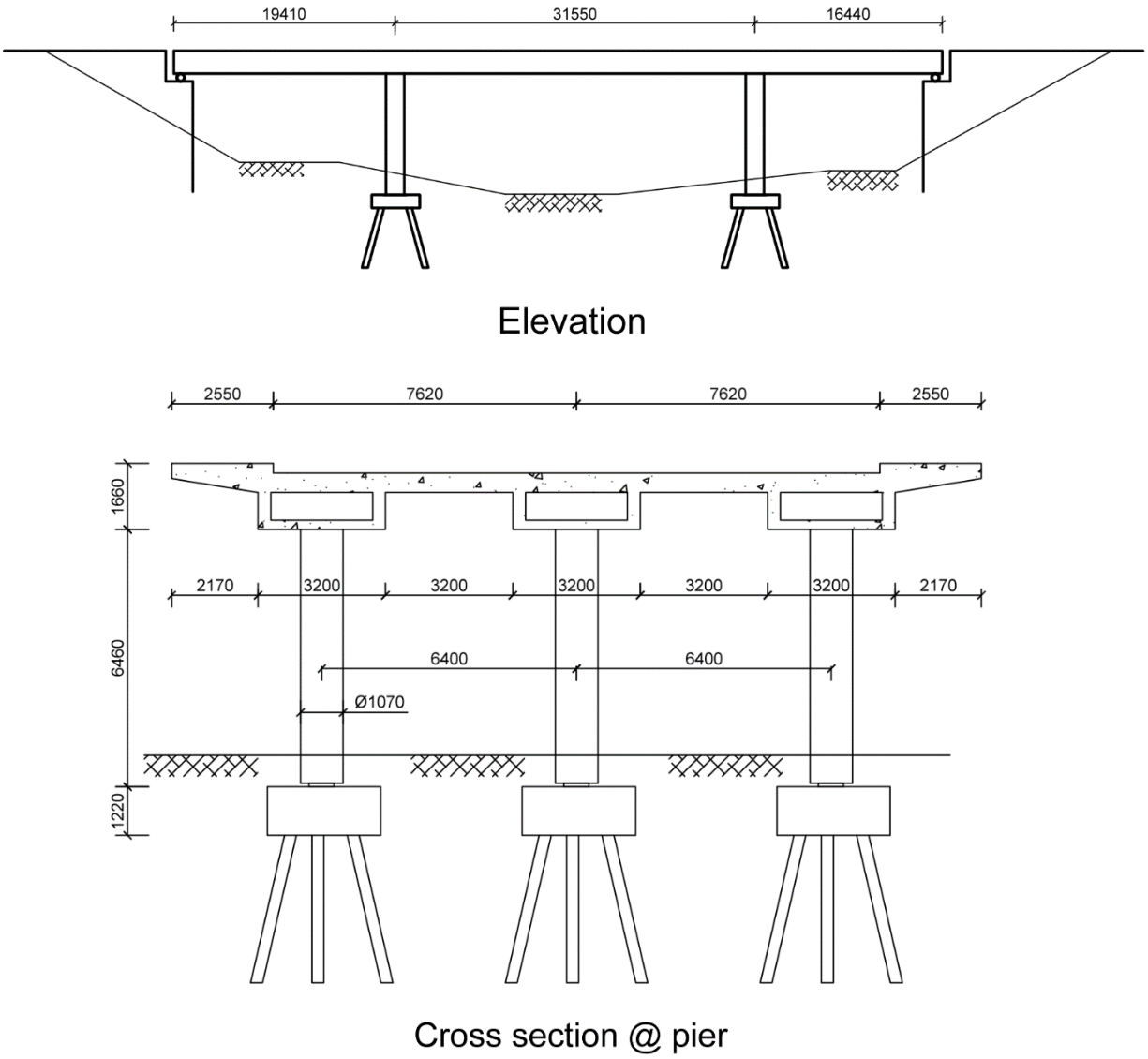

Figure 3.3 Geometric configuration of Bridge #3 adapted from Keivani (2003).

3.2.4 Bridge #4

Figure 3.4 presents a geometric configuration of Bridge #4. The bridge was built in 1965. It is a two equal span bridge, and each span is 19.34 m. The bridge has a skew angle of 24.78 degrees. The overall deck width is 15.80 m. The superstructure consists of a slab with a thickness of 84 cm in which prestressing was conducted in both longitudinal and transverse directions. The column bent consists of two circular columns (diameter = 0.76 m) with a center-to-center spacing of 8.23 m. The height of the columns is 4.95 m. The longitudinal

reinforcement in the columns is provided by twenty No. 11 bars. This gives a relatively high reinforcement ratio of about 4.4%. A spiral of No. 5 with a spacing of 64 mm is used as the transverse reinforcement. A mat foundation is considered for the abutments, and square footing for the bent. Expansion bearings are used at the abutments, and fixed bearings are used at the bent.

All the concrete members have a compressive strength of 34.5 MPa. The yield strength of the steel is assumed to 345 MPa.

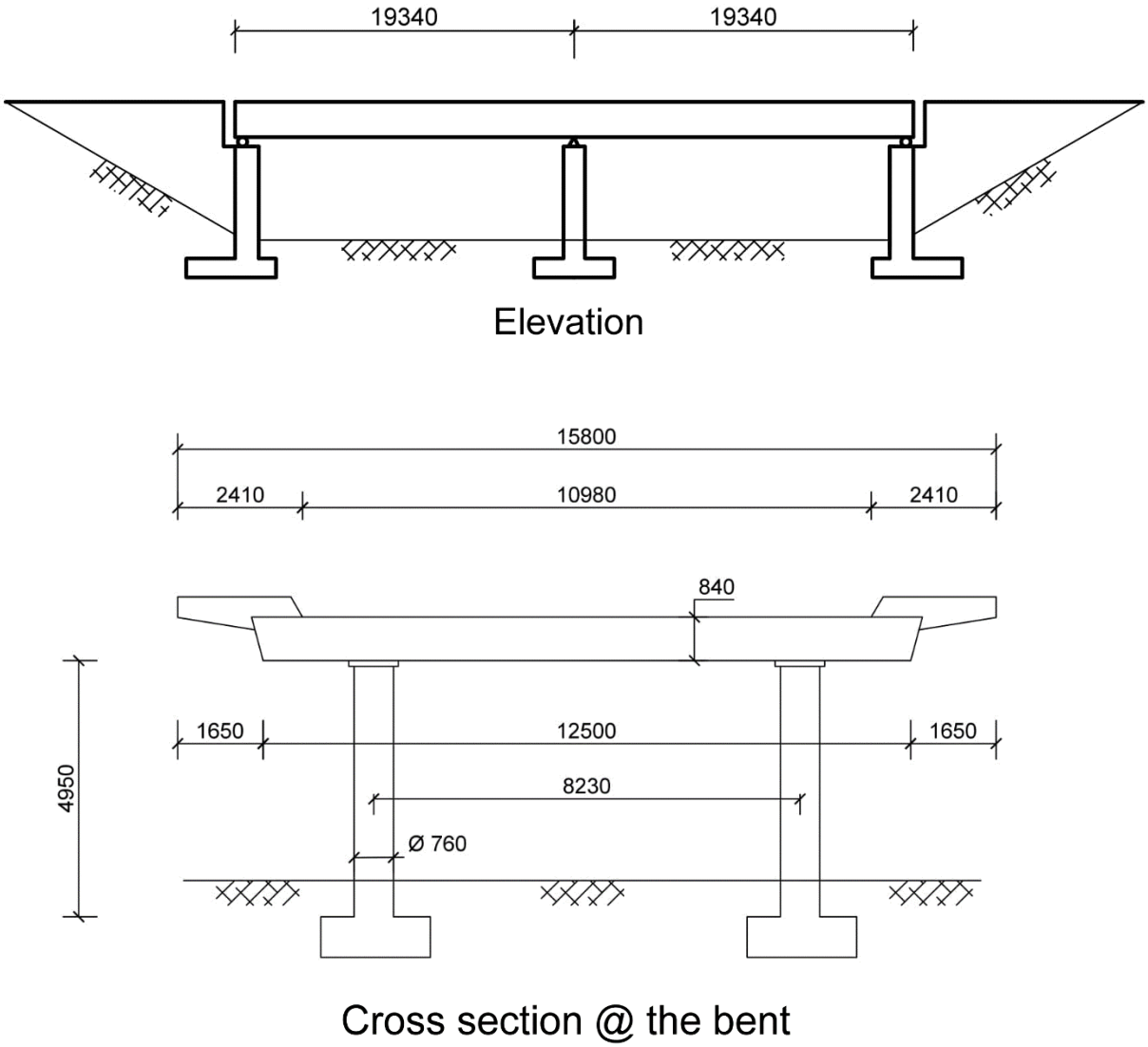

Figure 3.4 Geometric configuration of Bridge #4 adapted from Keivani (2003).

3.2.5 Bridge #5

From the structure point of view, Bridge #5 is very similar to Bridge #1 unless it has 4 spans while Bridge #1 has 3 spans. As shown in Fig. 3.5, its two end spans are 13.72 m, and the two middle spans are 18.90 m. The total length of the bridge is 64.24 m. It is a straight bridge without a skew angle.

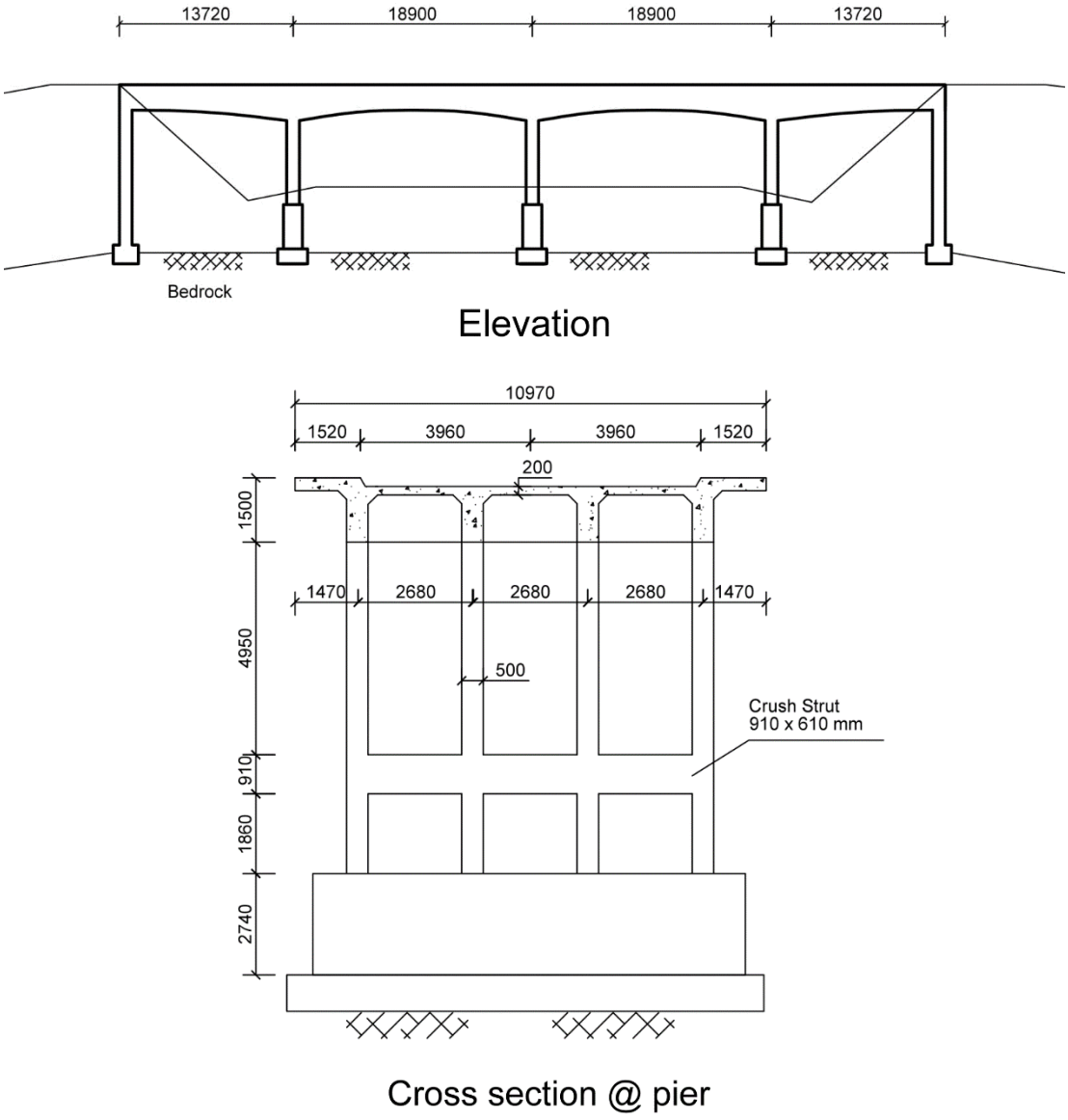

Figure 3.5 Geometric configuration of Bridge #5 adapted from Keivani (2003).

The depth of the beams is variable along the span length. More specifically, the beams'

depth is 0.69 m at the abutments, and at the middle of the 2nd and the 3rd spans while it is changed to 1.5 m at the bents following a parabolic function. There are four rectangular columns (610x500 mm) in each bent. Since the columns are relatively high, a crush strut is provided between the columns in order to provide rigidity of the columns in the transverse direction as illustrated in Fig. 3.5. Each column is reinforced with ten No. 11 bars. The transverse reinforcement is provided by No. 5 ties at a spacing of 305 mm. Shallow foundation is used for both the abutments and bents.

The compressive strength of the concrete is 27.6 MPa, and the yield strength of the steel bars was assumed to be 275 MPa due to the missing information in the construction drawings. This bridge was built in 1968. The design followed the Canadian Highway Bridge Design Code CSA-S-6 (1966).

3.2.6 Bridge #6

Bridge #6 was designed in 1968. It has three spans of 16.20 m, 23.28 m and 17.70 m as shown in Fig. 3.6. The total length of the bridge is 57.18 m. The overall deck width is 19.66 m. The bridge has a skew angle of 28.62 degrees. The superstructure consists of a 0.762 m prestressed slab with a slope of 5.4% in the transverse direction. Each bent has three circle columns with a diameter of 0.91 m. Like Bridge #5, a crush strut is provided between columns. The average height of columns is 8.84 m. The columns are reinforced longitudinally with twelve No. 11 bars with a reinforcement ratio of 1.84%. A spiral is used with No. 5 bar size with a pitch of 305 mm, and the transverse reinforcement ratio is 1.31%. Steel piles are used for the foundation at abutments while caisson foundation is used at the bents.

The compressive strength of all the concrete members including slab, cap beam, columns, etc. is 34.5 MPa. The reinforcing steel was assumed to have a yielding strength of

345 MPa.

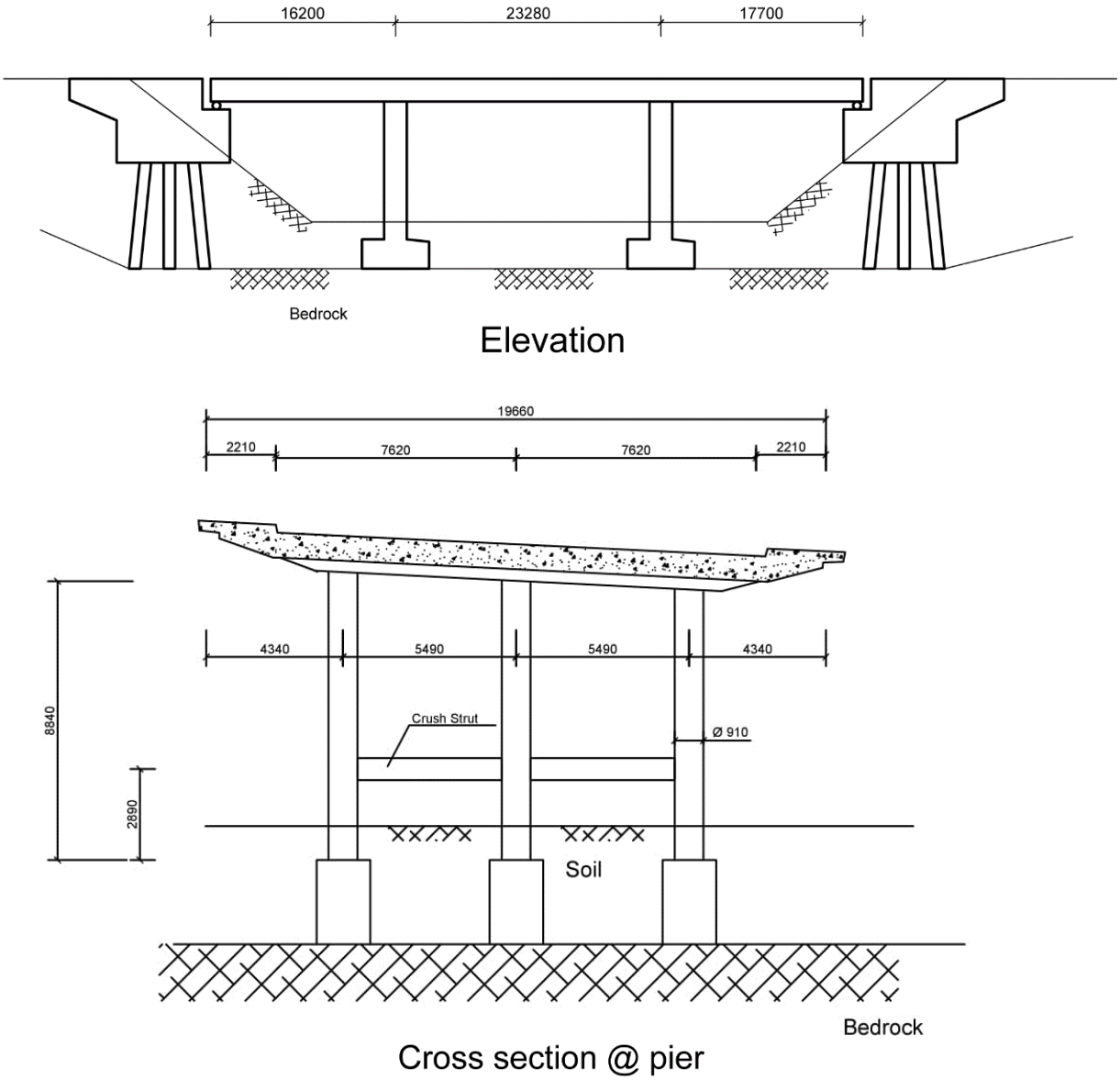

Figure 3.6 Geometric configuration of Bridge #6 adapted from Keivani (2003).

3.2.7 Bridge #7

Bridge #7 was constructed in 1970, and it is a steel bridge. The three spans of the bridge are 21.33 m, 38.10 m, and 21.33, respectively as shown in Fig. 3.7. The total length of the bridge is 80.76 m, the deck width is 13.12 m. This bridge was designed following the requirements in AASHO available at that time. It is a straight bridge. The superstructure

consists of an 18 cm concrete deck supported by three steel box girders. The substructure of the bents includes a cap beam and two columns. As shown in Fig. 3.7 the depth of the cap beam is 1.35 m right above the column, and it is reduced to 1.19 m at the mid-width. The cross section of the column on the top is 1.37 m x 0.97 m while on the bottom is 1.07 m x 0.64 m. The columns are reinforced with eighteen No. 11 bars over the entire height. The transverse reinforcement of the columns consists of stirrups of No. 3 at a spacing of 406 mm. Steel piles are used for the foundation at both abutments and bents.

Based on the original construction drawings it was found that the concrete compressive strength was 34.5 MPa, the yield strength of the reinforcing steel was 345 MPa.

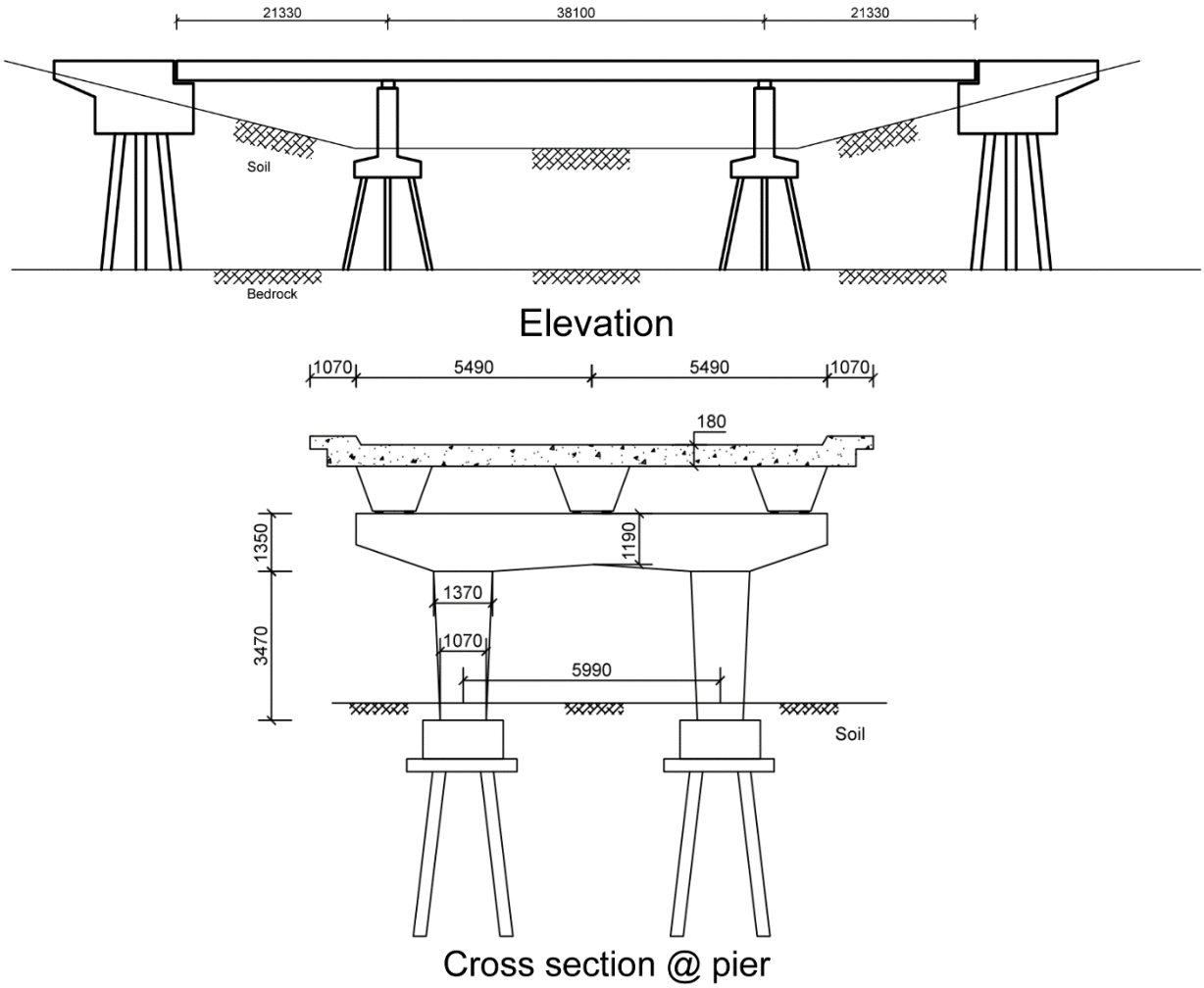

Figure 3.7 Geometric configuration of Bridge #7 adapted from Keivani (2003).

3.2.8 Bridge #8

Bridge #8 was built in 1973. It is a three-span continuous concrete bridge with the span lengths of 16.92 m, 28.04 m, 27.74 m (Fig. 3.8), respectively. This bridge is a typical slab-on-girder bridge, which is very similar to Bridge #2 except that the girders of Bridge #2 were made of steel while those of Bridge #8 were made of concrete. More specifically, the girders used on Bridge #8 are standard 1400 C.P.C.I (Canadian Prestressed Concrete Institute) girders. The thickness of the deck is 19 cm. The substructure at the bents consists of a cap beam and three circular columns. The minimum and maximum depths of the cap beam are 0.99 m (at the edge) and 1.24 m (at the supports), respectively. The diameter of the columns is 0.91 m, and the height is 4.79 m. Sixteen No. 11 bars are used to provide the longitudinal reinforcement, which gives a reinforcement ratio of 2.45%. The longitudinal bars are confined with a No. 5 spiral at a spacing of 89 mm. The ratio of the transverse reinforcement is 1.13%. Strip footings on the rock are used for both the abutments and bents.

The compressive strength of the concrete is 20.7 MPa. The yield strength for the reinforcement is 345 MPa. It is necessary to mention herein that the live load considered for the design was AASHTO HS-20-44 vehicle which is different from the all other bridges. The design of concrete components was based on ACI 515-57 (1957).

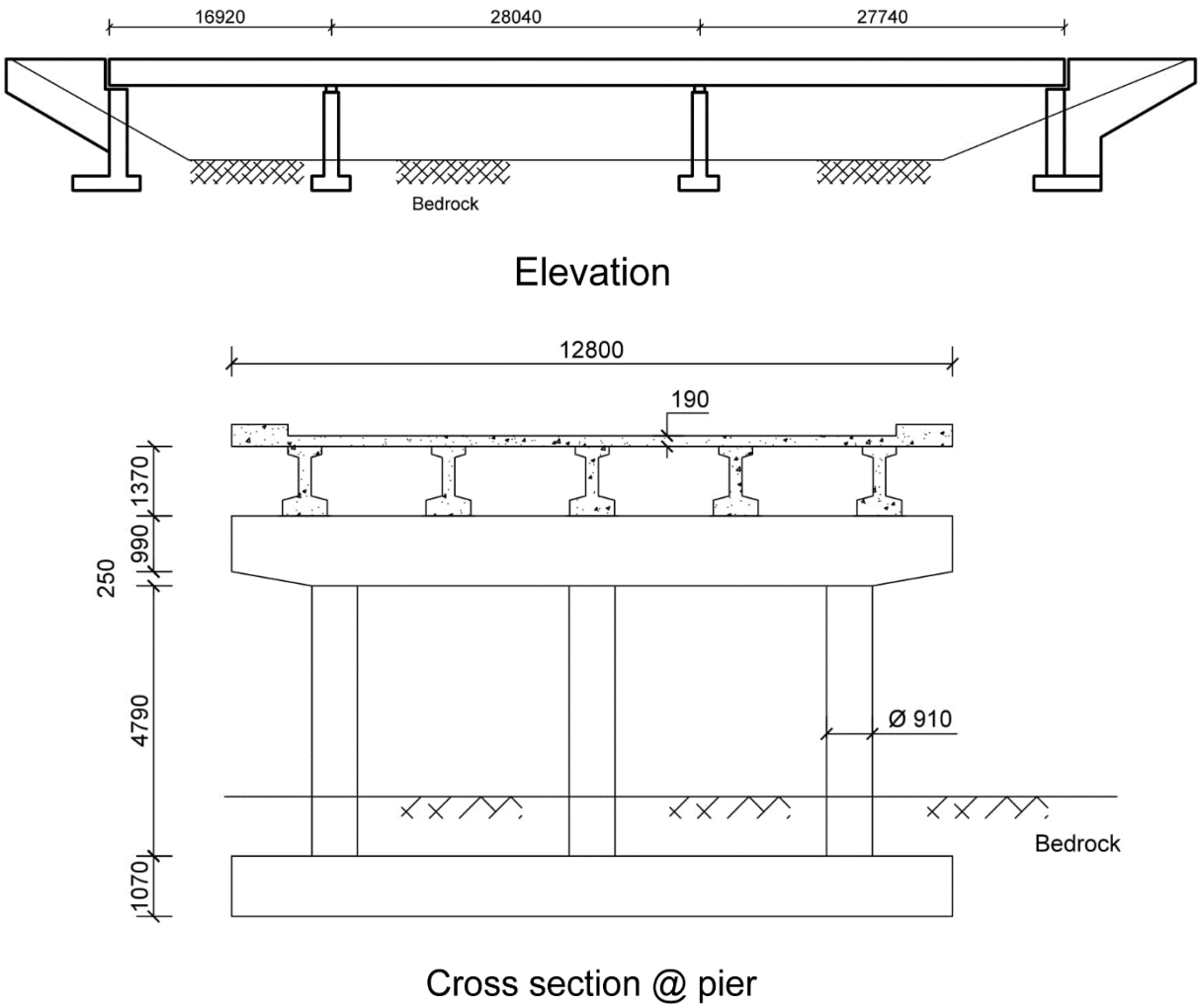

Figure 3.8 Geometric configuration of Bridge #8 adapted from Keivani (2003).

3.3 Summary

This chapter presents a detailed description of the eight bridges to be examined in this study, which includes geometric configuration, information on the reinforcing or prestressing steel, construction period, etc. Among all the bridges selected, two of them are steel bridges while the rest are reinforced concrete bridges. These bridges are representative of typical highway bridges in Canada.

Chapter 4

Modeling of Bridges

4.1 Introduction

The input files for the structural analysis models of the eight bridges considered in this study were based on those developed by Keivani (2003) with some corrections to the errors in the original files. In the study conducted by Keivani (2003), he used 2-D analysis software IDARC to investigate the seismic resistance of the bridges described in Chapter 3. Analyses for each bridge in the longitudinal and transverse direction were performed separately, i.e., a 2-D model was developed for both the longitudinal direction and the transverse direction for each bridge. It is worth mentioning that the program IDARC2D is widely used and accepted software for nonlinear analysis and has been used in many studies (e.g., Karbassi et al. 2012, Banerjee1 2014, Yousuf 2016, etc.).

It is known that structural analysis can be conducted using either a 2-D or a 3-D model. However, developing a 2-D model is less time and effort consuming compared to a 3-D model. On the other hand, a 3-D model could provide more accurate results than the 2-D model especially if a structure is sensitive to torsion. Therefore, using a 2-D model or a 3-D model for the analysis depends on the choice of an analyst. For example, Waller (2011) considered a 2-D IDARC model to conduct a seismic risk assessment of bridges in Ottawa. Thrall (2008) used a 2-D SAP model for their study. Some researchers (e.g., Pan et al. 2010, Nielson and DesRoches 2007) adapted a 3-D model in the analysis. With the recent advancing in the

technology, 3-D modeling is commonly used in academia for the purpose of research, and can be developed using most of the software, such as SAP2000 (CSI 2015), OpenSees (Mazzoni et al. 2009), Ruaumoko (Carr 2015), etc. On the contrary, engineering practitioners prefer to use a 2-D model for the sake of time (Personal communication) in which only longitudinal-vertical direction is considered. The preliminary results for the modal analysis on the eight bridges show that the vibration of the all the bridges was not dominated by torsion. Given this, IDARC2D analyses were conducted in the study.

Based on the structural system of the eight bridges presented in Chapter 3, bridges are classified into three groups for modeling. They are,

- **Group I:** include Bridges #1 and #5. The entire structure including the abutments and bents is modeled as a sway frame;

- **Group II:** include Bridges #3, #4, and #6. The abutments are simplified as a roller. A very short beam-element is introduced to model the bearing at the bent(s);

- **Group III:** include Bridges #2, #7, and #8. The bridge in the longitudinal direction is modeled as a single-degree-of-freedom (SDOF) system.

A detailed description of the modeling techniques for each of the above-mentioned groups of bridges is given in Sections 4.2 to 4.4 below.

4.2 Modeling of Group I Bridges

As described in Chapter 3, Bridge #1 and Bridge #5 have the same structural system: the superstructure consists of multiple T-beams (4 in total), there are 4 square columns in the bent in which each one supports an individual beam, and the foundation has two layers. The

major differences between Bridges #1 and #5 are, (i) Bridge #1 has three spans while Bridge #5 has four spans, (ii) crush struts are provided in Bridge #5 because the columns are relatively high (about 8 m). Therefore, the same techniques are applied to model both bridges. For ease of understanding, the details of modeling Bridge #5 are presented in the section below.

Figure 4.1 shows the model of Bridge #5 in the longitudinal direction. Each span of the superstructure is divided into four equal segments, which is the minimum number of elements required by ATC 32 (1996) for modeling. Every segment is modeled as a beam element, i.e., a flexural element without shear deformations coupled. A typical beam element with the corresponding 4 degrees of freedom is shown in Fig. 4.2 (Reinhorn et al. 2009), which are rotation and vertical displacement at each end. A lumped mass is added at each node based on the geometry of the superstructure from the original construction drawings. The vertical elements in the figure represent the substructure. As shown in Fig. 4.1, each vertical element consists of two parts, i.e., element I and element II. Element I is used to model the column (for the bents) or the retaining wall (for abutments), and the length is 8.47 m measured to the center of the superstructure. Element II is used to model the first layer of the foundation with a length of 2.74m. Both of them are modeled as a column element that considers the flexural and axial deformation with a total of six degrees of freedom as illustrated in Fig. 4.3. The connection between the superstructure and the substructure is rigid. The length of the rigid zone in the column of the element I at the top is taken as half depth of the T- beam. More specifically, it is 0.75 m for the piers, and 0.345 m for the abutments. The rigid length at the bottom of the element I is zero. Please note that the elastic flexural stiffness of the element II is assumed to be 10 times of the element I in order to take into account the extremely higher rigidity of the foundation. The foundations are fully fixed, i.e., all six degrees (three rotations and three translations) are restrained. Damping of 5% of critical was used for the dynamic analysis. It is

necessary to mention that axial deformations are neglected in beams, and no interaction between bending moment and axial load in columns are considered in the modeling.

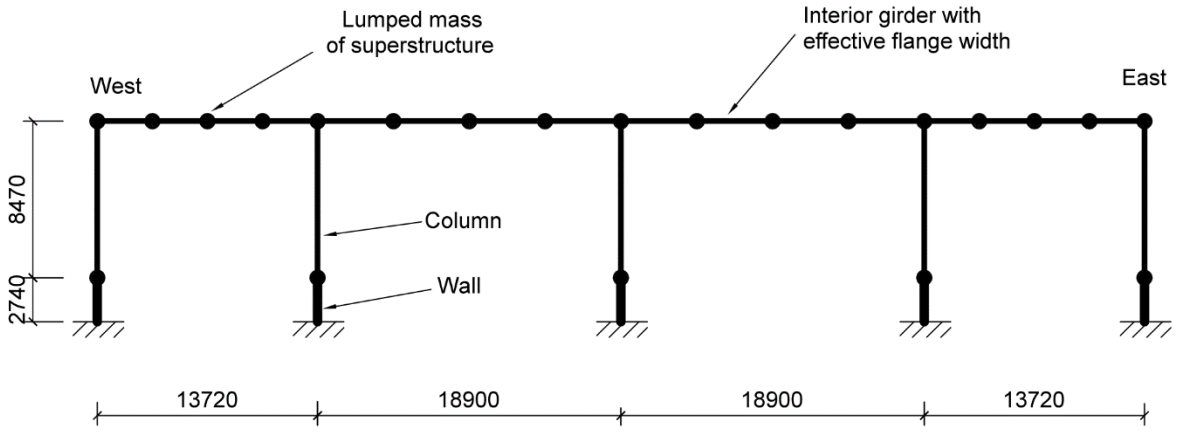

Figure 4.1 Finite element model of Bridge #5 in the longitudinal direction.

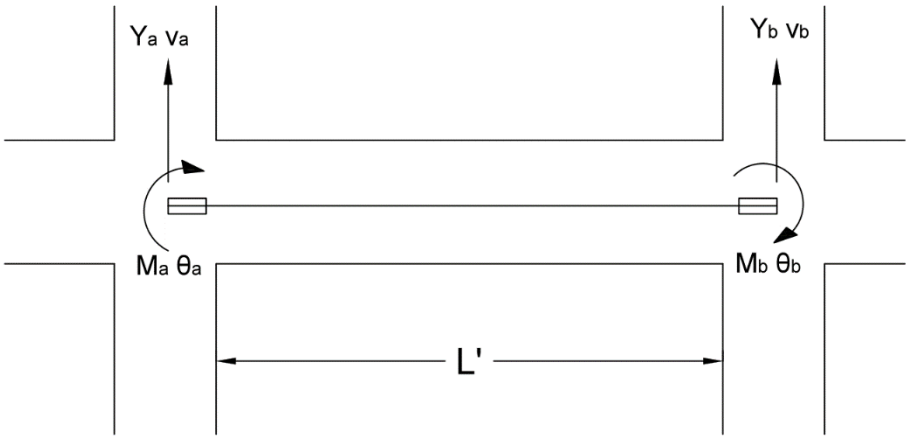

Figure 4.2 Typical beam element with degrees of freedom adapted from Reinhorn (2009).

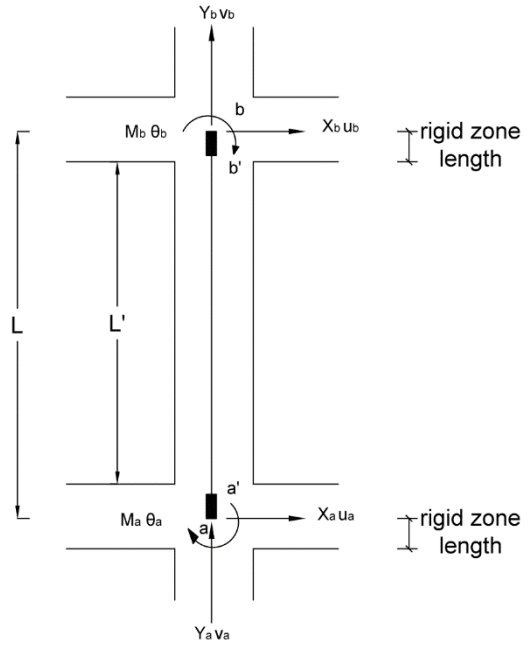

Figure 4.3 Typical column element with degrees of freedom adapted from Reinhorn (2009).

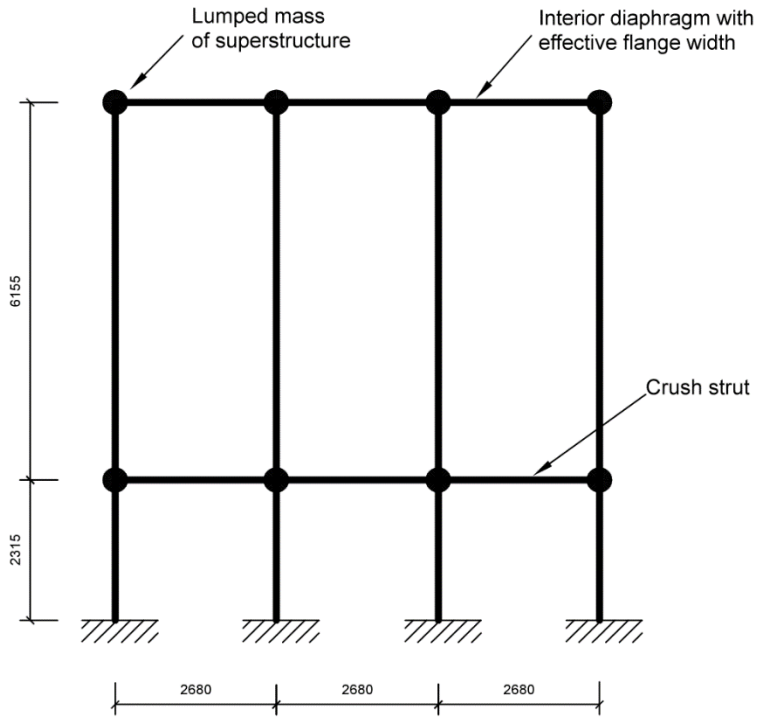

Figure 4.4 Finite element model of Bridge #5 in the transverse direction.

Figure 4.4 shows a finite element model of Bridge #5 in the transverse direction at one of the bents. It can be seen clearly that the bridge is modeled as a two-storey frame. The horizontal elements (i.e., beam elements) at the top and the bottom levels are used to model the diaphragms and the crush struts, respectively. The flexural stiffness of the crush struts is assumed to be five times of the girders. The vertical elements are used to model the columns that run over two storeys. More specifically, their height in the first storey is measured from the top of the foundation to the center of the crush strut, which gives 2.32 m as shown in Fig. 4.4; and that in the second storey is about 6.16 m measured between the center of the crush strut and the mid-height of the girder. The span length of the frame is the same as the center-to-center spacing of the columns (Figs. 3.5 and 4.4). All the connections are fully rigid. A lumped mass is assigned to each joint, which is determined according to the weight of the elements where they intersect.

4.3 Modeling of Group II Bridge

The bridges in Group II include Bridges #3, 4, and 6 as described in Chapter 3. The major difference of Group II bridges from Group I, is that expansion bearings are used at the abutments. Accordingly, the bridge system in the longitudinal direction is not modeled as a frame like the bridges in Group I. As an example, Figure 4.5 shows the model of Bridge #4 in the longitudinal direction. It can be seen in the figure that the bearings at the abutment on each end is modeled as a roller, i.e., both the translation and the rotation are allowed. The fixed bearings at the bent are modeled as a pin, i.e., the rotation is allowed and the translation is not permitted. In the finite element model, the bearings are modeled as artificial columns with a negligible height of 10 mm. The flexural stiffness of the bearings is taken as 10^4 times smaller than that of the columns. A very small shear stiffness (i.e., 100 kN/mm) is assigned to the

expansion bearings at the abutments while an extremely large shear stiffness (i.e., 1020 kN/mm) is assigned to the fixed bearings at the bent. The techniques for modeling girders and columns are the same as those for Group I bridges as described in the previous section.

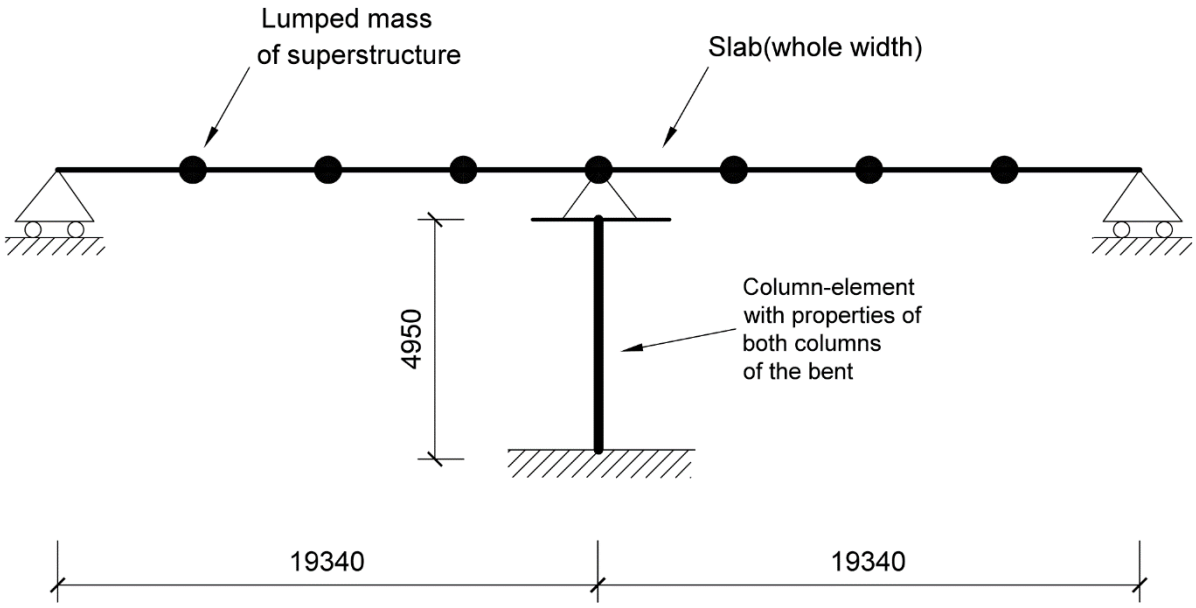

Figure 4.5 Finite element model of Bridge #4 in the longitudinal direction.

Figure 4.6 illustrates the model of the Bridge #4 for a section at the bent in the transverse direction. As presented in the figure, the bridge is modeled as a simply supported beam with a cantilever on both sides. The superstructure is divided into 4 beam elements. Fixed bearings are simulated as a pin on the top of each column. The flexural and shear stiffnesses of the bearings are the same as those of bearings in the model in the longitudinal direction. The techniques for modeling girders, columns, and bearings are the same as those explained above.

It is necessary to mention herein that Bridges #3 and #6 are modeled in the same way as Group I bridges (i.e., Bridges #1 and #5) except that the vertical columns used to model the abutments are replaced by rollers.

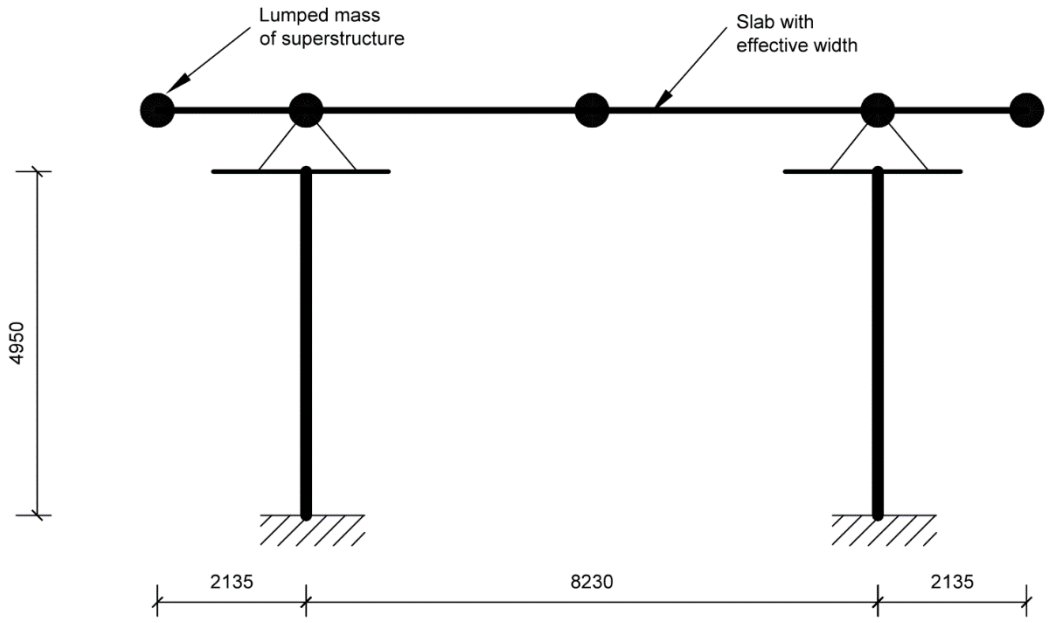

Figure 4.6 Finite element model of Bridge #4 in the transverse direction.

4.4 Modeling of Group III Bridges

The major difference of Bridges #2, #7 and #8 in Group III from those in Groups I and II is that the substructure of the bridges consists of a cap beam. Therefore, the bridge in the longitudinal direction is modeled as a single-degree-of-freedom system (SDOF) for each bent as presented in Fig. 4.7. The weight of the mass of SDOF corresponds to the half weight of superstructure, and the half weight of the substructure. The lateral stiffness of SDOF is taken as the total lateral stiffness of the three columns in the transverse direction. The vertical element of SDOF shown in Fig. 4.7 is modeled as a column element in IDARC. Its height of 6.03 m is measured up to the top of the cap beam (Fig. 3.8, Chapter 3). The bottom of the column is fully fixed, i.e., all the translations and rotations are restrained.

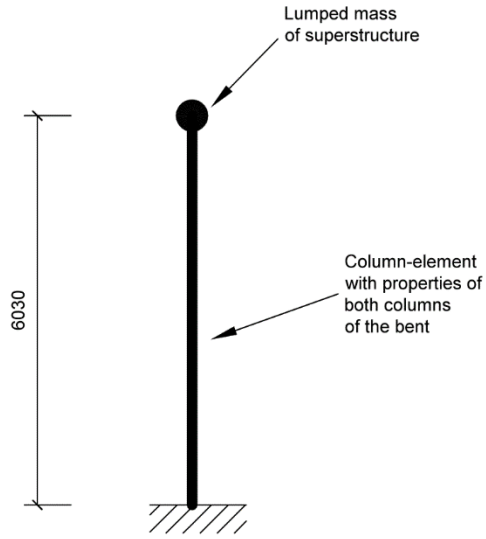

Figure 4.7 Finite element model of Bridge #8 in the longitudinal direction.

The models of Bridges #2, #7 and #8 in the transverse direction were developed in the same way as those of bridges in Groups I and II. For illustration, Figure 4.8 shows the model of Bridge #8. The horizontal elements represent the cap beams with a length of 4.57 m each, which is equal to the columns center-to-center spacing. The vertical members are used to simulate the columns, and the height is measured to the center of the cap beam. The beam-column connections are rigid. The bottom of the columns is fully fixed.

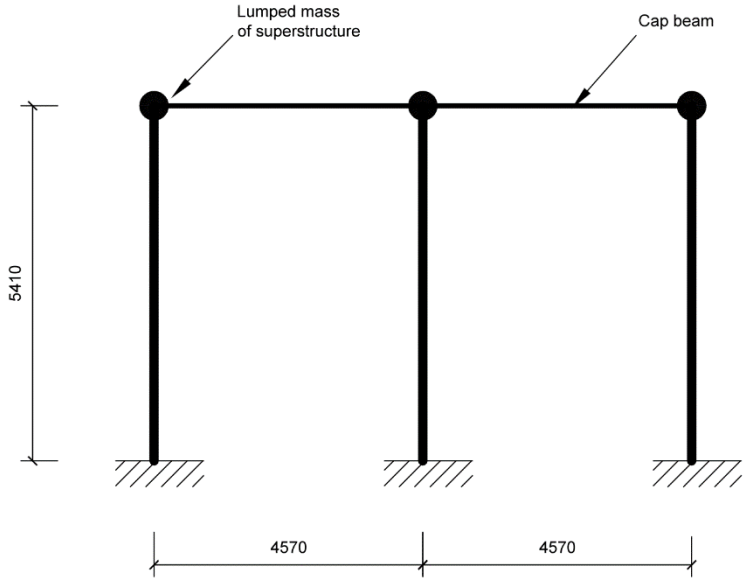

Figure 4.8 Finite element model of Bridge #8 in the transverse direction.

4.5 Modeling Hysteretic Behavior of Elements

4.5.1 Moment-curvature relationships

For the dynamic analysis, inelastic deformations are assumed to occur at the ends of the element where plastic hinges can be formed. More specifically, plastic hinges are concentrated at the ends of both the beam and column elements, which are referred to as "lumped plasticity model" in IDARC. In this study, a moment-curvature relation is used to represent the nonlinear behavior of the plastic hinges. As an example, Figures 4.9(a) and 4.9(b) illustrate response curves (i.e., moment *vs.* curvature) for a beam section and a column section of Bridge #1, respectively. It should be noted that these curves were idealized by three linear segments based on those curves computed according to the properties of the materials (concrete and steel) and cross section of the member (Keivani 2003).

Figure 4.10(a) shows the stress-strain curve for concrete proposed by Mander et al. (1988). Figure 4.10(b) illustrates the stress-strain model for the steel bars, which has three segments: yielding, post-yielding, and strain hardening. In this study, fracture of steel bars is assumed to occur when a stain of 0.1 is reached. The standard modulus of elasticity of the reinforcing steel 200 GPa is adopted. The yield strength of steel bars used in each bridge is described in Chapter 3.

(a)

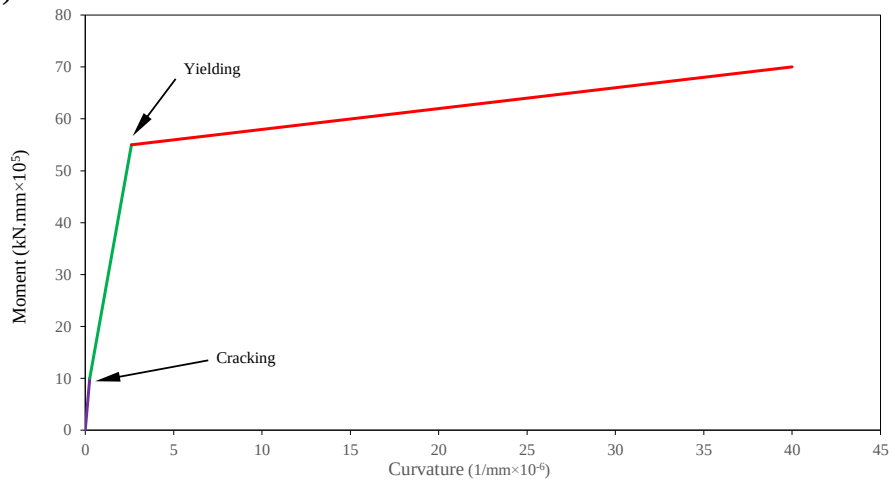

(b)

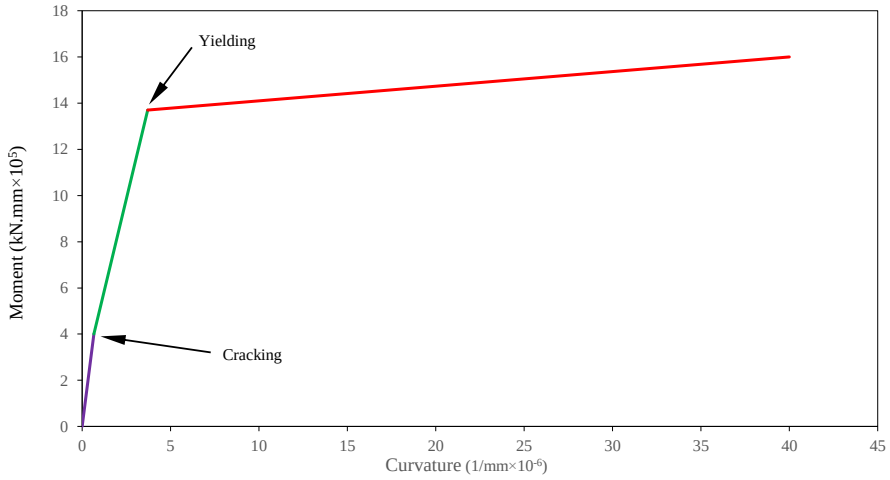

Figure 4.9 Moment-curvature relationship of Bridge #1:
(a) beam section; (b) column section.

(a)

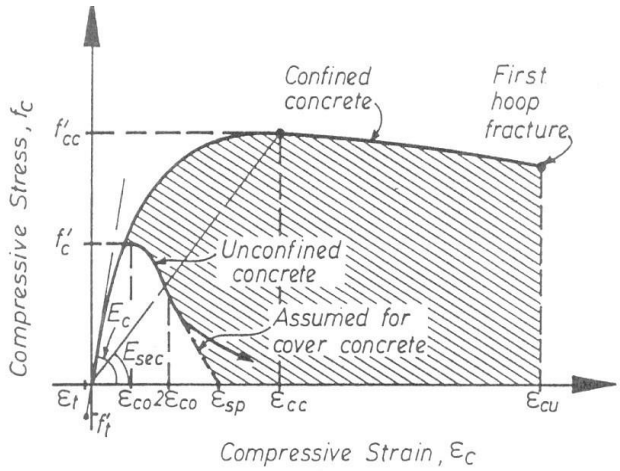

(b)

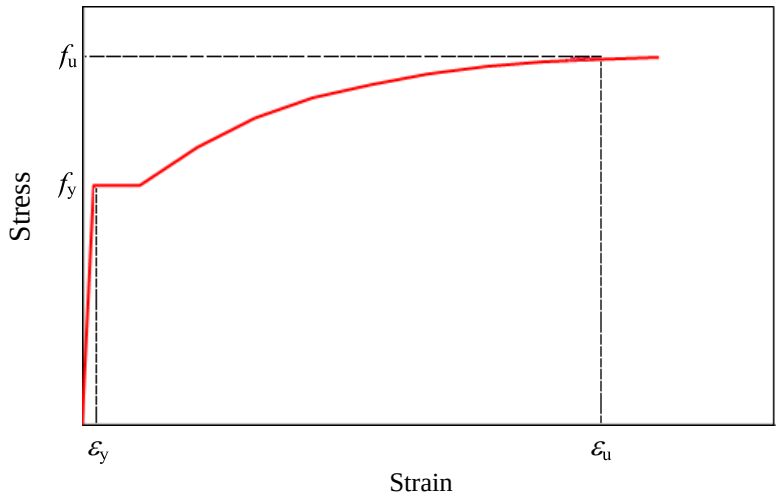

Figure 4.10 Stress-strain models:
(a) concrete in compression, adapted from Paulay and Prestley (1992);
(b) steel, adapted from Naumoski and Heidebrecht (1993).

4.5.2 IDARC Hysteretic modeling rules

The hysteretic modeling in IDARC takes into account the stiffness degradation, strength deterioration, and pinching behavior during cyclic loading. They are controlled by the following four parameters according to the user's guide,

- HC = Stiffness degrading coefficient, α in Fig. 4.11,
- HBD = Ductility-based strength decay parameter, β_1,
- HBE = Energy-based strength decay parameter, β_2,
- HS = Slip parameter, Υ in Fig. 4.12.

The typical values for hysteretic parameters defined in the IDARC user's guide are provided in Table 4.1. Please note that the nominal value of each parameter given in the table was based on the recommendation made by Reinhorn et al. (2009). Since seismic response of bridges depends very much on the hysteretic loop of the plastic hinges, sensitivity analyses were conducted in this study to choose the most suitable parameters to define hysteretic rules.

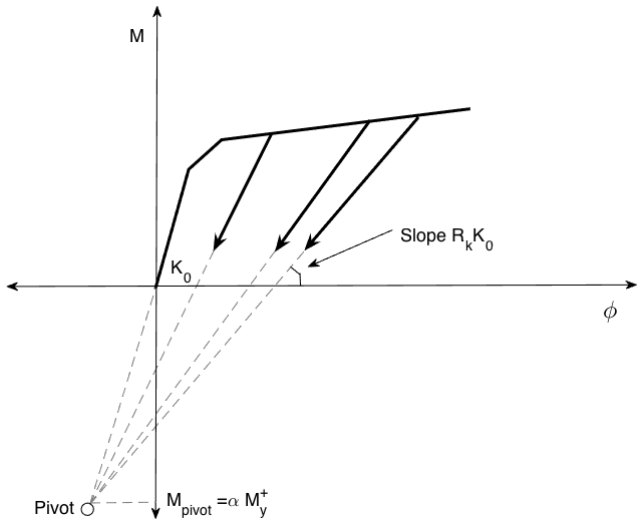

Figure 4.11 Modeling of stiffness degradation for positive excursion, adapted from Reinhorn et al. (2009).

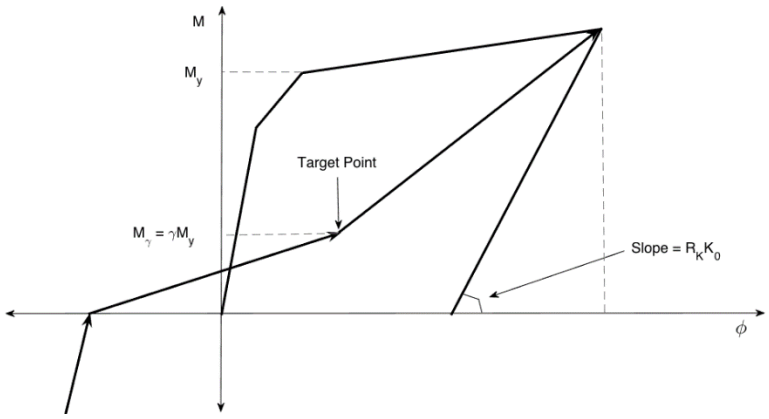

Figure 4.12 Modeling of slip, adapted from Reinhorn et al. (2009).

The model of Bridge #1 in the longitudinal direction was chosen to investigate the effects of different values of the parameters HC, HBD, HBE, and HS on the bridge response. Five earthquake records randomly selected from the set of records for the time-history analysis in this study, which is explained in Chapter 5, are used as excitations. They were scaled to three times the design earthquake level in order to assess the significant inelastic deformation of the element. The bridge response is represented by the column curvature. Figures 4.13(a) to 4.13(d) present the maximum column curvature associated with the different values for HC, HBD, HBE, and HS, respectively. Each point in the figure represents the maximum column curvature from one earthquake record. It can be seen clearly in Fig. 4.13 (a) that larger HC value leads to smaller curvature and vice versa. The ratio of the maximum to the minimum mean curvature associated with different values for HC of 4.0, 10.0, 15.0, and 40.0 is about 10%. The same finding is applied to the results from the sensitivity analysis on the parameter of HS shown in Figs. 4.13(d). The results shown in Fig. 4.13(c) indicate that the change of HBE has no effect on the curvature. With respect to the parameter HBD, the curvature decreases very slightly with the increasing of the value of HBD from 0.10 to 0.3. But when the value is set as 0.60, i.e., severe degrading is considered; there is a dramatic increase (about

12%) of the curvature. Given the observations described above, the nominal values controlled the IDARC hysteretic rules suggested by Reinhorn et al. (2009) are selected: 40.0 for HC, 0.10 for HBD and HBE, 0.50 for HS.

Table 4.1 Typical values for hysteretic parameters.

Hysteretic parameter	Value	Effect	Value type
HC	200.0	No degrading	**Default value**
	15.0	Mild degrading	
	10.0	Moderate degrading	
	4.0	Severe degrading	
	40.0	Nominal value	
HBD	0.01	No degrading	**Default value**
	0.15	Mild degrading	
	0.30	Moderate degrading	
	0.60	Severe degrading	
	0.10	Nominal value	
HBE	0.01	No degrading	**Default value**
	0.08	Mild degrading	
	0.15	Moderate degrading	
	0.60	Severe degrading	
	0.10	Nominal value	
HS	1.00	No pinching	**Default value**
	0.40	Mild pinching	
	0.25	Moderate pinching	
	0.05	Severe pinched loops	
	0.50	Nominal value	

(a)

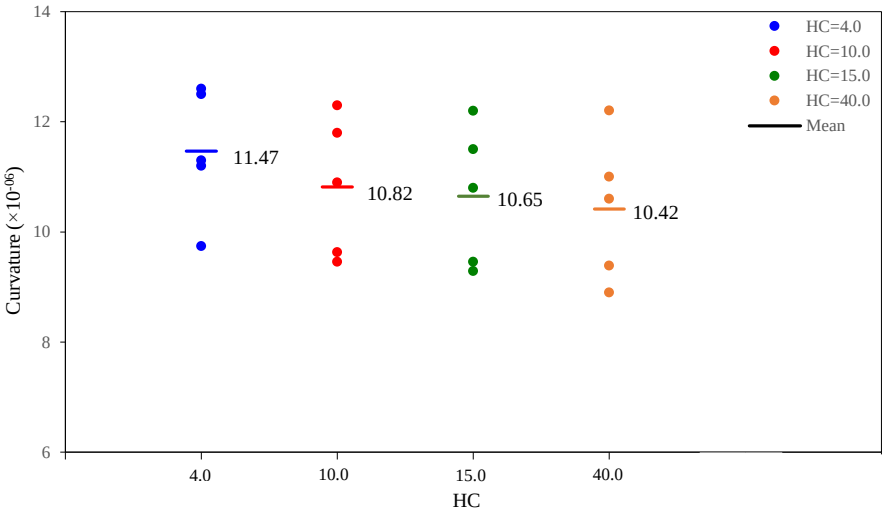
HC=4.0
HC=10.0
HC=15.0
HC=40.0
Mean
11.47
10.82
10.65
10.42
Curvature (×10-06)
HC
4.0
10.0
15.0
40.0

(b)

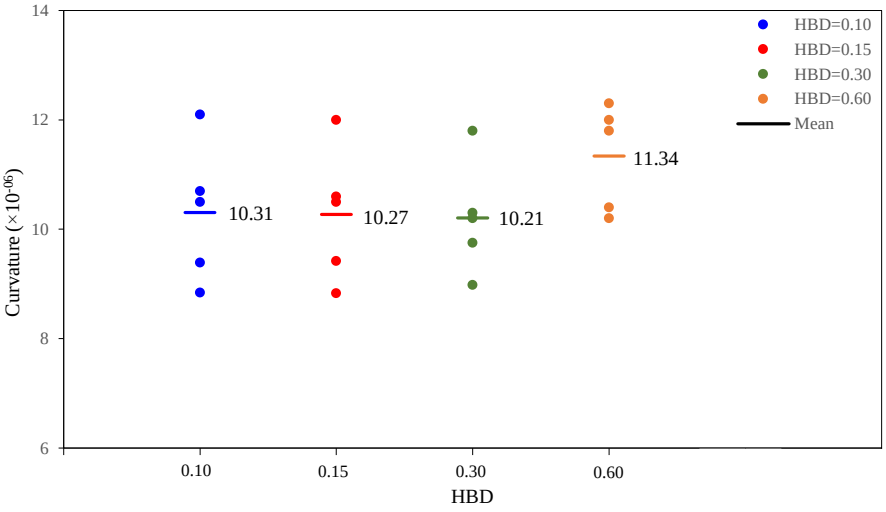
HBD=0.10
HBD=0.15
HBD=0.30
HBD=0.60
Mean
10.31
10.27
10.21
11.34
Curvature (×10-06)
HBD
0.10
0.15
0.30
0.60

(c)

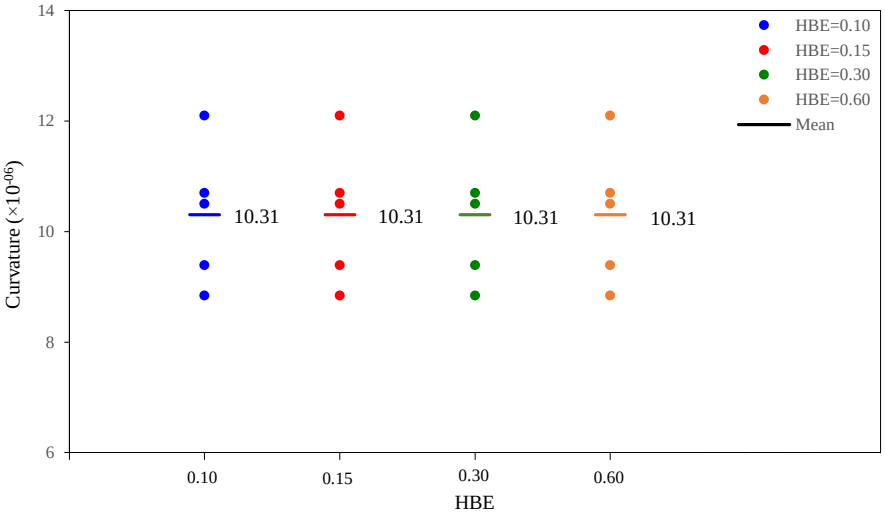
HBE=0.10
HBE=0.15
HBE=0.30
HBE=0.60
Mean
10.31
10.31
10.31
10.31
Curvature (×10-06)
HBE
0.10
0.15
0.30
0.60

(d)

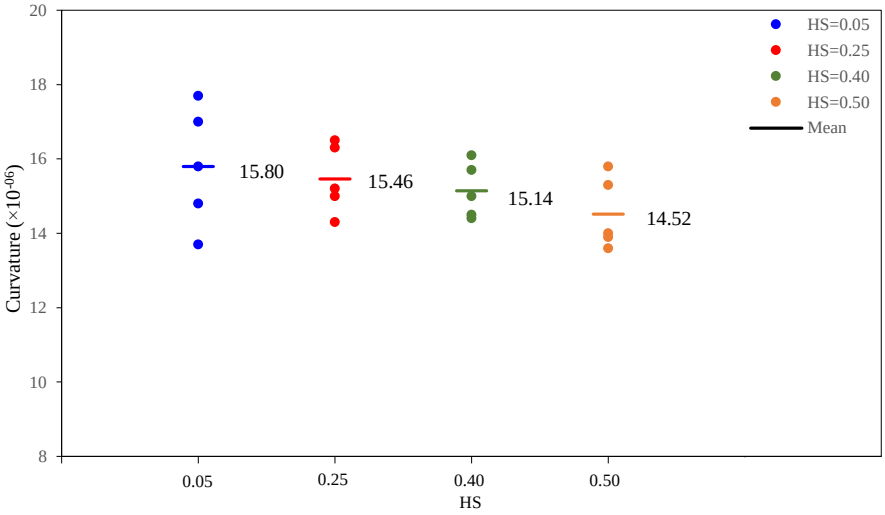

Figure 4.13 Results from the sensitivity analysis on the parameters for the hysteretic modeling rules; (a) HC; (b) HBD; (c) HBE; (d) HS.

4.6 Dynamics Characteristics of Bridge Models

Modal analysis was conducted on the model of each bridge in the longitudinal and transverse directions. Table 4.2 provides the periods of the first three models along with the direction of each mode from the modal analysis. It can be seen in the table that the shortest period of the model models is about 0.27s (Bridge #1) while the longest period is about 1.36 s (Bridge #4). Generally speaking, the dominant period of the bridges examined is less than 1.0s. Regarding the direction of the vibration, it is governed by the longitudinal direction. Therefore, the 2-D analysis as explained in Section 4.1 is appropriate for the study since torsion does not govern the vibration.

Table 4.2 Dynamic characteristics of bridge models.

Bridge ID	Mode Number	Period (s)	Vibration direction
#1	1	0.269	Longitudinal
	2	0.203	Transverse
	3	0.018	Longitudinal
#2	1	0.450	Longitudinal
	2	0.193	Transverse
	3	0.033	Transverse
#3	1	0.752	Longitudinal
	2	0.751	Transverse
	3	0.048	Longitudinal
#4	1	1.361	Longitudinal
	2	0.959	Transverse
	3	0.016	Longitudinal
#5	1	0.692	Longitudinal
	2	0.412	Transverse
	3	0.037	Longitudinal
#6	1	1.080	Longitudinal
	2	0.551	Transverse
	3	0.029	Transverse
#7	1	0.596	Longitudinal
	2	0.123	Transverse
	3	0.031	Transverse
#8	1	0.597	Longitudinal
	2	0.223	Transverse
	3	0.044	Transverse

4.7 Summary

This chapter explains the techniques for modeling the eight bridges to be examined in the study. These bridges are divided into three groups according to its structural system. Sensitivity analyses are conducted on the input for modeling the hysteretic behavior of the plastic hinges regarding stiffness degradation, strength deterioration, and pinching behavior. The nonlinear behavior of the plastic hinges is represented by the moment-curvature relation.

Chapter 5

Selection of Earthquake Records

5.1 Background of Acceleration Selection in Canada

Canada is divided into three parts according to its seismicity, i.e., western Canada where British Columbia is located is the most seismically prone area; eastern Canada where Ontario and Québec are placed is characterized by moderate seismic hazard; and "Stable Canada", which is the zone between western and eastern Canada with very low seismicity. The seismic hazard of western Canada is governed by several types of earthquakes, such as crustal earthquakes, deep subcrustal earthquakes, and Cascadia earthquakes. The hazard of the east is generally dominated by crustal earthquakes. It is also known that the seismic ground motions in eastern Canada are characterized by relatively high frequency content compared to those in western Canada (Adams and Halchuk 2003; Naumoski et al. 1988).

Since the real records from strong earthquakes are not available for almost all parts of Canada, they are often selected from other countries having similar characteristics of ground motions. For example, for the time-history analysis of structures in Vancouver, records from crustal earthquakes are often considered, and they are normally selected from earthquakes in California through PEER database. This is because the seismic characteristics of crustal earthquakes in Vancouver are believed to be very similar to those in California (Atkinson 2009).

The earthquake records available from eastern Canada are very limited. The most

significant earthquakes happened were M5.7 1988 Saguenay, Québec earthquake; and M5.0 1982 Miramichi, New Brunswick earthquake. Researchers and practitioners have difficulties in choosing accelerograms for the seismic analysis of structures in eastern Canada.

5.2 Seismic Excitations for Time-history Analysis

Huang (2014) conducted a comprehensive study on the selection of acceleration time series for the seismic analysis of bridges in eastern Canada. Four types of accelerograms were considered in the study. Set 1 consists of real records obtained from earthquakes around the world that represent the characteristics of ground motions in eastern Canada. There were compiled by Naumoski et al. (1988), and have been used in several studies, such as Yousuf and Bagchi (2010); Hatami and Bathurst (2001); and Marianchik et al. (2000). Accelerograms of Sets 2, 3 and 4 are all synthetic. More specifically, Sets 2 and 3 time histories were generated using the real records of Set 1 as seeds. Each was modified iteratively until its spectrum matches the prescribed design spectrum for the bridge location. The simulated accelerograms of Set 4 were generated using a stochastic finite-fault method (Atkinson 2009). They were compatible with uniform hazard spectra for eastern Canada defined in the 2005 edition of the National Building Code of Canada (NBCC). Among these four sets of accelerograms, Huang (2014) recommended using the simulated time series generated by Atkinson for the time-history analysis of bridge in eastern Canada. It is necessary to mention herein that Lin et al. (2013) made the same recommendation from their study on buildings.

Following the suggestions given in Huang (2014), Lin et al. (2013), and the Commentary of the 2014 CHBDC, two sets (namely Set I and Set II) of simulated time series generated by Atkinson was selected for use in this study in which each set has 30 accelerograms that are the minimum number of time histories as required by NIST (2011).

Table 5.1 Characteristics of the selected records of Set I (soil class C).

Record No.	Record name	Magnitude	Distance to fault (km)	Azimuth (degree)	A (g)	V (m/s)	A/V
1	E7C2_05	7.0	50.3	255.4	0.148	0.110	1.35
2	E7C2_06	7.0	50.3	255.4	0.122	0.092	1.33
3	E7C2_07	7.0	45.2	85.6	0.204	0.104	1.97
4	E7C2_08	7.0	45.2	85.6	0.184	0.096	1.93
5	E7C2_10	7.0	50.3	174.8	0.125	0.118	1.06
6	E7C2_11	7.0	50.3	174.8	0.127	0.083	1.54
7	E7C2_12	7.0	50.3	174.8	0.122	0.077	1.59
8	E7C2_14	7.0	50.3	257.7	0.163	0.137	1.19
9	E7C2_16	7.0	62.6	297	0.090	0.071	1.26
10	E7C2_17	7.0	62.6	297	0.104	0.069	1.51
11	E7C2_21	7.0	51.9	318.8	0.101	0.076	1.32
12	E7C2_22	7.0	69.9	166.6	0.090	0.096	0.94
13	E7C2_23	7.0	69.9	166.6	0.098	0.076	1.30
14	E7C2_24	7.0	69.9	166.6	0.097	0.084	1.15
15	E7C2_26	7.0	70.2	257.9	0.107	0.091	1.19
16	E7C2_27	7.0	70.2	257.9	0.092	0.098	0.94
17	E7C2_28	7.0	47.8	328.4	0.123	0.113	1.09
18	E7C2_29	7.0	47.8	328.4	0.134	0.076	1.76
19	E7C2_30	7.0	47.8	328.4	0.113	0.069	1.64
20	E7C2_31	7.0	95.9	128.8	0.090	0.075	1.19
21	E7C2_33	7.0	95.9	128.8	0.112	0.068	1.65
22	E7C2_35	7.0	100.2	226.7	0.097	0.062	1.55
23	E7C2_36	7.0	100.2	226.7	0.085	0.067	1.27
24	E7C2_37	7.0	95.5	124	0.109	0.074	1.47
25	E7C2_38	7.0	95.5	124	0.100	0.064	1.58
26	E7C2_39	7.0	95.5	124	0.111	0.085	1.32
27	E7C2_41	7.0	94.3	90.6	0.097	0.072	1.34
28	E7C2_42	7.0	94.3	90.6	0.107	0.071	1.51
29	E7C2_44	7.0	98.6	157.7	0.142	0.093	1.52
30	E7C2_45	7.0	98.6	157.7	0.105	0.070	1.51

Table 5.2 Characteristics of the selected records of Set II (soil class D).

Record No.	Record name	Magnitude	Distance to fault (km)	Azimuth (degree)	A (g)	V (m/s)	A/V
1	E7E2_01	7.0	41.6	304.4	0.384	0.329	1.17
2	E7E2_02	7.0	41.6	304.4	0.345	0.270	1.28
3	E7E2_03	7.0	41.6	304.4	0.390	0.308	1.27
4	E7E2_04	7.0	50.3	255.4	0.263	0.180	1.46
5	E7E2_05	7.0	50.3	255.4	0.273	0.267	1.02
6	E7E2_06	7.0	50.3	255.4	0.237	0.227	1.05
7	E7E2_07	7.0	45.2	85.6	0.378	0.242	1.56
8	E7E2_08	7.0	45.2	85.6	0.302	0.208	1.45
9	E7E2_09	7.0	45.2	85.6	0.308	0.300	1.03
10	E7E2_10	7.0	50.3	174.8	0.222	0.278	0.80
11	E7E2_11	7.0	50.3	174.8	0.227	0.177	1.28
12	E7E2_12	7.0	50.3	174.8	0.195	0.183	1.06
13	E7E2_13	7.0	50.3	257.7	0.270	0.171	1.57
14	E7E2_14	7.0	50.3	257.7	0.268	0.329	0.82
15	E7E2_15	7.0	50.3	257.7	0.235	0.274	0.86
16	E7E2_19	7.0	51.9	318.8	0.232	0.176	1.32
17	E7E2_20	7.0	51.9	318.8	0.194	0.193	1.00
18	E7E2_21	7.0	51.9	318.8	0.167	0.172	0.97
19	E7E2_22	7.0	69.9	166.6	0.163	0.231	0.70
20	E7E2_23	7.0	69.9	166.6	0.170	0.171	0.99
21	E7E2_24	7.0	69.9	166.6	0.168	0.186	0.90
22	E7E2_28	7.0	47.8	328.4	0.226	0.277	0.82
23	E7E2_29	7.0	47.8	328.4	0.246	0.186	1.32
24	E7E2_30	7.0	47.8	328.4	0.202	0.155	1.30
25	E7E2_38	7.0	95.5	124	0.190	0.139	1.36
26	E7E2_39	7.0	95.5	124	0.200	0.196	1.02
27	E7E2_40	7.0	94.3	90.6	0.176	0.185	0.95
28	E7E2_42	7.0	94.3	90.6	0.210	0.162	1.29
29	E7E2_43	7.0	98.6	157.7	0.210	0.133	1.58
30	E7E2_44	7.0	98.6	157.7	0.257	0.210	1.22

(a)

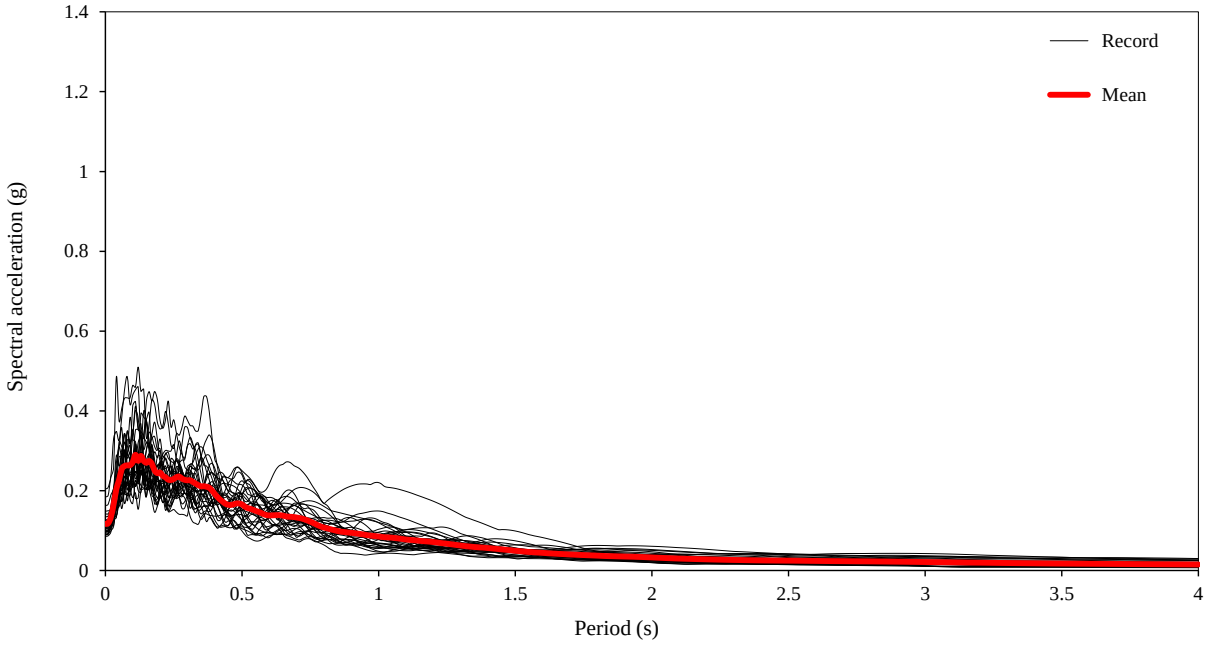

(b)

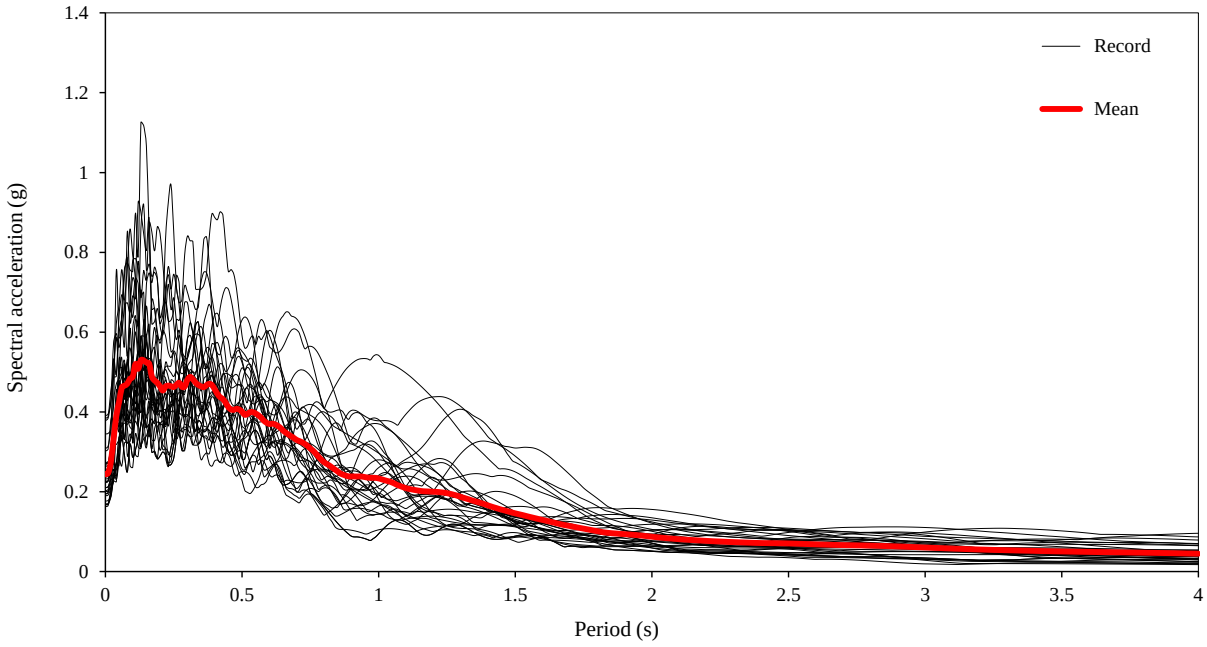

Figure 5.1 Acceleration response spectra of the simulated records, 5% damping: (a) soil class C; (b) soil class D.

The characteristics of the time histories are presented in Tables 5.1 and 5.2. It can be seen in the tables that the selected accelerograms correspond to an earthquake magnitude of 7.0; distances from 50 km to 100 km. The accelerograms of Sets I and II are associated with the soil classes C (very dense soil and soft rock, shear velocity is between 360 m/s and 760 m/s) and D (stiff soil, shear velocity is between 180 m/s and 360 m/s), respectively. The Set II time histories will be used for the analyses of Bridges #2, #3 and #7 since the foundations sit on the soft soil. The average ratios of the peak acceleration (A, in g) to peak velocity (V, in m/s) of the two sets are 1.40 and 1.15. That is consistent with the characteristics of the ground motions in eastern Canada that a typical value of the A/V ratio is between 1.0 and 2.0 as reported in Naumoski et al. (1988). The acceleration response spectra of the selected accelerograms for this study are presented in Fig. 5.1 along with the mean spectrum of each set. As expected, the spectra of Set II are much higher than those of Set I since the soft soil tends to amplify the structural response.

5.3 Summary

Two sets of simulated accelerograms generated by Atkinson are selected for the time-history analysis in the study, i.e., one set for soil class C while the other set is for soil class D. Each set consists of 30 accelerograms, which is the minimum number of accelerograms required by NIST.

Chapter 6

Analysis Results

6.1 Introduction

As described in Introduction, Chapter 1, the main objective of this study is to assess the force reduction factor of typical highway bridges for seismic design. For ease of discussion, the force reduction factor is designated as R-factor, hereafter.

The two models (i.e., one for the longitudinal direction, the other for the transverse direction) of each of the eight bridges were subjected to thirty ground motions represented by either Set I or Set II depending on the soil class where the foundations are located. More specifically, Bridges #2, #3, and #7 were analyzed using the accelerograms of Set II while all other bridges were examined using the accelerograms of Set I. The accelerograms were scaled according to the intensity measure of the spectral acceleration at the fundamental period T_1 of the bridge, i.e., $Sa(T_1)$. The 5%-damped design spectrum for Montreal for the probability of exceedance of 10% in 50 years was considered as the design earthquake level. It is worth mentioning that this probability level is the lowest defined in the latest edition of CHBDC (i.e., 2014 CHBDC), and it was the only level specified in the 2006 edition. Three excitation levels were considered, i.e., $1.0Sa(T_1)$, $2.0Sa(T_1)$ and $3.0Sa(T_1)$. The latter two intensity levels were selected based on the recommendation made by Heidebrecht and Naumoski (2002) that seismic ground motions about two to three times the design level might occur at the location of the structure.

Among a number of response parameters, the bending moment and curvature ductility at the end sections (top and bottom) of the column were selected to evaluate the value of R. Generally speaking, bending moment is a global response parameter and it has a direct relation with the external seismic force applied to the structure. The curvature ductility, on the other hand, is a local deformation parameter and represents the extent of inelastic deformations at a specified section of a structural member. The curvature ductility for a given section of a member represents the ratio of the maximum curvature experienced during the response to the yield curvature of the section. For each excitation motion, maximum values of the bending moment the curvature ductility were extracted from IDARC. Then they were statistically analyzed to compute the mean value, which is arithmetic mean.

6.2 Investigation of the Force Reduction Factor

For the purpose of investigation of the force reduction factor R, both elastic and inelastic analyses were conducted on the models for the longitudinal and transverse directions of each bridge. As described in Chapter 4, the nonlinear behavior of the columns in this study was represented by a tri-linear moment-curvature (M-ϕ) envelope (Fig. 4.9) to include the responses at the following three stages, cracking, yielding, and post-yielding. For the elastic analysis, the slope of the linear relation of the M-ϕ is taken the same as that of the tri-linear M-ϕ relation up to the cracking. As an example, Figure 6.1 shows the results of M-ϕ from elastic and inelastic analyses for a model of Bridge #1 in the longitudinal direction in which the excitations were scaled to $1.0Sa(T_1) = 1.0Sa(0.27s)$. Each point in the figure represents the maximum response from a single time-history analysis. As expected, the responses of the top and bottom sections are not the same. For this case, both the moment and curvature ductility of the top section (Fig. 6.1 (a)) are much larger than those of the bottom section (Fig. 6.1(b)).

(a)

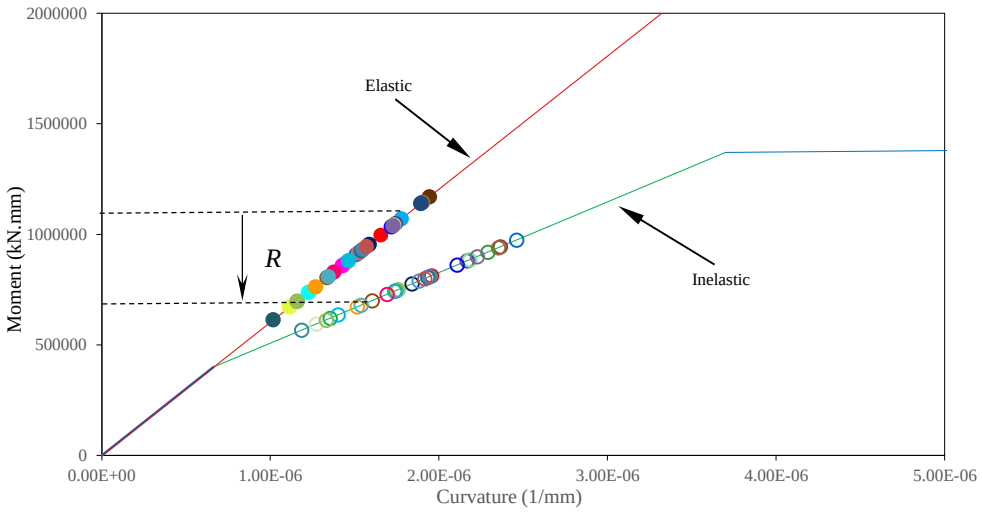

(b)

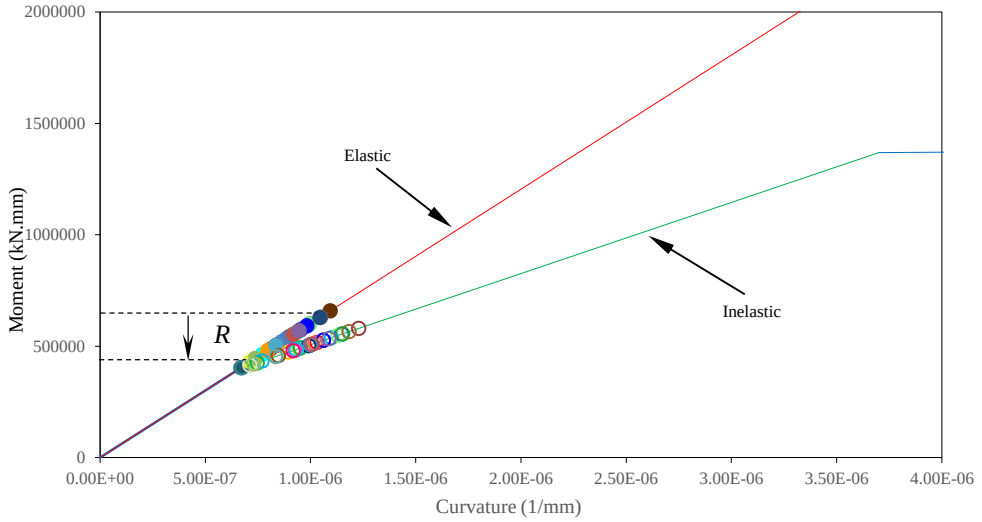

Figure 6.1 Analysis results of Bridge #1 (longitudinal model), 1.0Sa(T_1): (a) Top section; (b) Bottom section.

Once the elastic and inelastic responses are extracted from IDARC, the R-factor and the ductility from each accelerogram can be determined using Eqs. 6.1 and 6.2

$$R = \frac{M_{elastic}}{M_{inelastic}} \tag{6.1}$$

$$\mu = \frac{\phi_{inelastic}}{\phi_{yield}} \tag{6.2}$$

Where,

$M_{elastic}$ = maximum response moment from elastic analysis,

$M_{inelastic}$ = maximum response moment from inelastic analysis,

$\phi_{inelastic}$ = maximum response curvature from inelastic analysis,

ϕ_{yield} = yield curvature defined on the tri-linear M-Ø envelope.

6.2.1 Results from Group I bridges

6.2.1.1 Force reduction factor vs ductility

As mentioned in Chapter 4, Group I bridges consist of Bridge #1 and Bridge #5 due to the similarity of their structural system. The results for the value of R *vs* the ductility for Bridge #1 and Bridge #5 are presented in Figs. 6.2 and 6.3, respectively where the symbols in blue, black, and red are associated with the intensity levels of 1.0 Sa(T_1), 2.0 Sa(T_1) and 3.0Sa(T_1). Figures 6.2 (a) and 6.3(a) represent the results obtained from the model in the longitudinal direction while figures 6.2 (b) and 6.3(b) illustrate those from the model in the transverse direction. Please note that each point (i.e., R-factor and ductility pair) in the figure corresponds to the maximum response from a single time-history that can be found on either the top or bottom section of the column. In total, there are thirty points in each figure for each excitation level. It can be seen in the figures that the R-factor increases with the increase of the ductility. The relationship between the two parameters fits a power function very well with a coefficient of determination (i.e., R^2) of the regression line about at least 0.98 (Fig. 6.3a). Another observation of the results in Figs. 6.2 and 6.3 is, the data are much more scattered at the excitation level of 3.0Sa(T_1) than 1.0Sa(T_1). This is because the bridge response is elastic

associated with the ground motions scaled to 1.0Sa(T_1) while it becomes inelastic when the ground motions are scaled to 3.0Sa(T_1). Table 6.1 provides the mean value for R-factor and ductility for the Bridge #1 and Bridge #5. It can be seen in the table that the column ductility (top and bottom sections) from the two models, i.e., longitudinal and transverse directions, is less than 1.0 at the intensity level of 1.0 Sa(T1). When the intensity level reaches 2.0Sa(T_1) and 3.0Sa(T_1), the top section of the column in the two bridges yields except the one in Bridge #5, at the excitation level of 2.0Sa(T_1). Regarding the bottom section, yielding only occurs at the excitation levels of 2.0Sa(T_1) and 3.0Sa(T_1), for Bridge #5, transverse model; for the rest of the cases, the response is still at the elastic stage. With respect to the R-factor, it is governed by the response in the ***transverse*** direction (see the highlights in Table 6.1). For example, for Bridge #1, the R-factors from the analyses at 1.0Sa(T_1), 2.0Sa(T_1) and 3.0Sa(T_1) are 1.93, 2.43, and 2.67, respectively; which is about 3.0. For Bridge #5, they are 1.61, 1.79, and 1.85 that yields roughly about 2.0. The smaller R-factor observed in Bridge #5 is mainly due to the crush struts provided in the bridge transverse direction.

Table 6.1 Mean R-factor and ductility of Group I bridges.

Bridge ID	Direction	Response	Top Section			Bottom Section		
			1.0Sa(T_1)	2.0Sa(T_1)	3.0Sa(T_1)	1.0Sa(T_1)	2.0Sa(T_1)	3.0Sa(T_1)
#1 (without crush struts)	Long.	R	1.35	1.54	1.86	1.13	1.24	1.27
		ϕ	0.50	1.08	2.36	0.26	0.36	0.40
	Tran.	R	1.86	2.23	2.26	1.93	2.43	2.67
		ϕ	0.39	1.10	1.79	0.26	0.36	0.40
#5 (with crush struts)	Long.	R	1.27	1.70	1.90	1.07	1.37	1.44
		ϕ	0.27	0.58	0.86	0.17	0.31	0.39
	Tran.	R	1.62	1.81	2.15	1.60	1.77	1.81
		ϕ	0.54	1.24	2.66	0.52	1.16	1.85

(a)

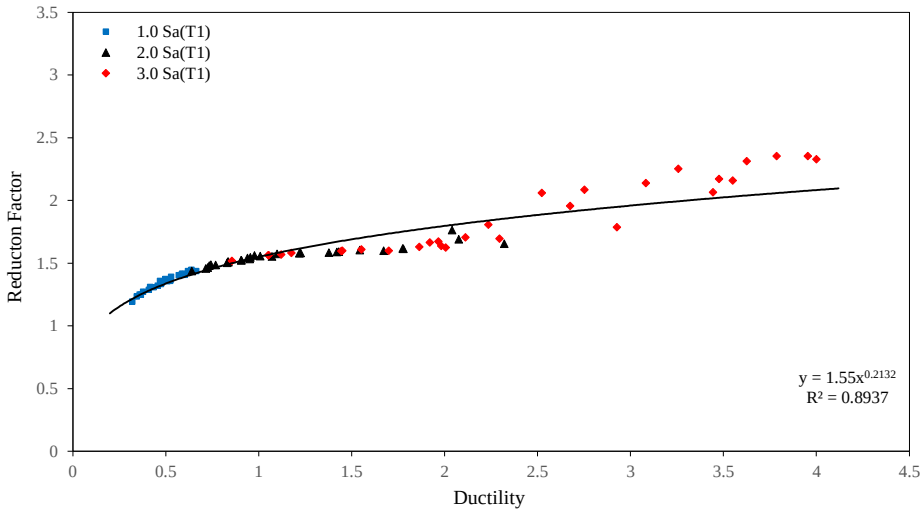

(b)

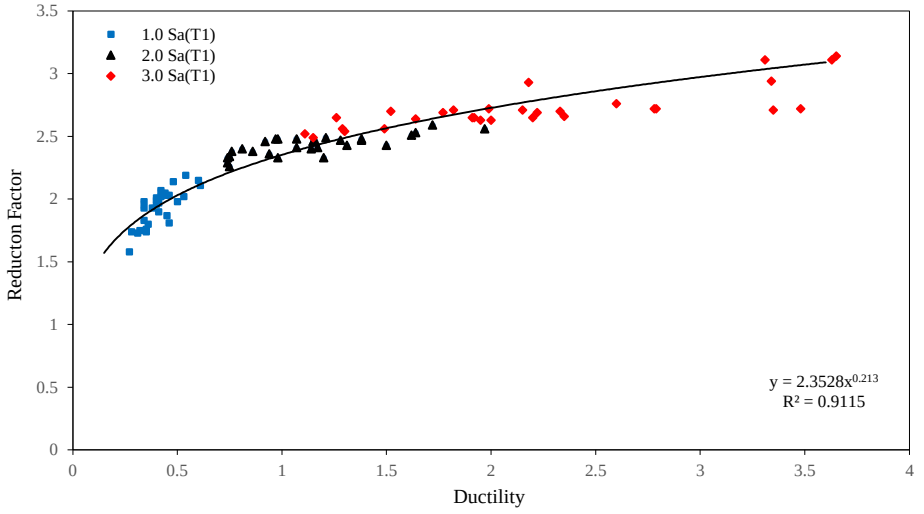

Figure 6.2 Results of R-factor vs ductility for Bridge #1:
(a) longitudinal direction, $Sa(T_1) = 0.5g$;
(b) transverse direction, $Sa(T_1) = 0.5g$.

(a)

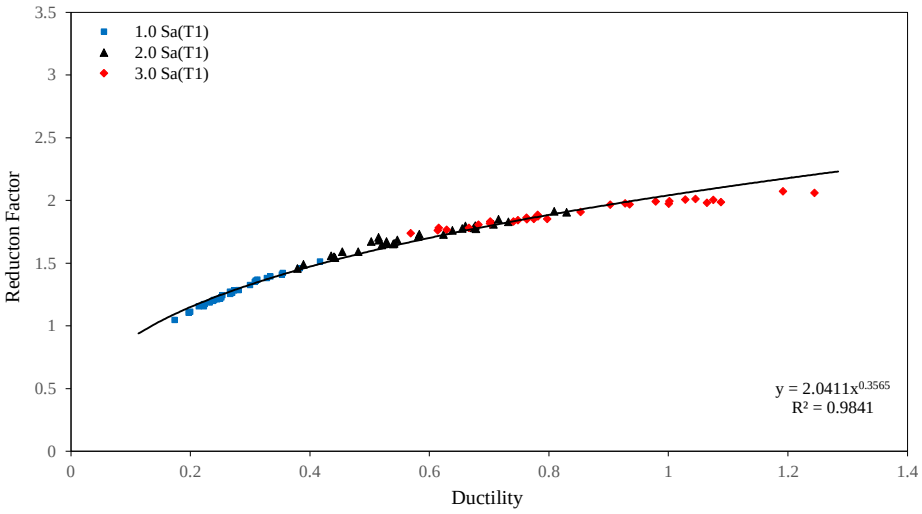

(b)

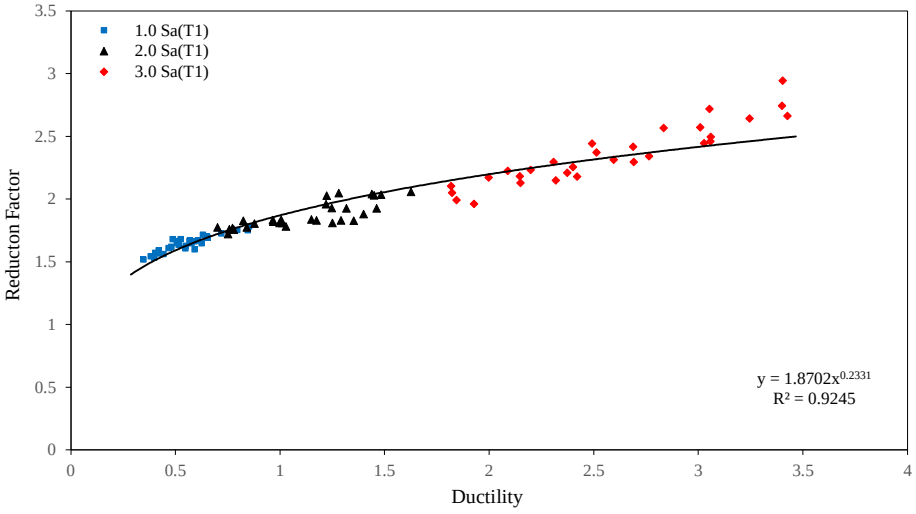

Figure 6.3 Results of R-factor vs ductility for Bridge #5:
(a) longitudinal direction, $Sa(T_1) = 0.307g$;
(b) transverse direction, $Sa(T_1) = 0.435g$.

6.2.1.2 Force reduction factor vs period

In order to investigate the relationship between the R-factor and the dominant period of the bridge, the height of the column of Bridge #1 and Bridge #5 was changed manually in order to cover a range of periods for the statistics analysis. It is necessary to mention that the original reinforcement design of columns was examined due to the change of the column height to assure the design did not fail. Time-history analysis was conducted on six new models of each bridge, i.e., three models for each direction. Then, the maximum R-factor was determined at each intensity level. The results are illustrated in Figs. 6.4 (for Bridge #1) and 6.5 (for Bridge #5). It should be noted that the results in Fig. 6.4 are governed by the bottom section while those in Fig. 6.5 are dominated by the top section. For ease understanding, the mean R-factor is also provided in each figure.

Table 6.2 Period and column height of original model and modified models, Group I bridges.

Bridge ID.	Model direction		Model input data			
			Original model	Modified model		
#1	Longitudinal	Col. height (mm)	4390	6000	8100	10000
		Period (s)	0.27	0.34	0.50	0.66
	Transverse	Col. height (mm)	4390	6000	8100	10000
		Period (s)	0.20	0.33	0.56	0.79
#5	Longitudinal	Col. height (mm)	8470	4000	6000	10000
		Period (s)	0.69	0.32	0.49	0.93
	Transverse	Col. height (mm)	6155	4000	8000	10000
		Period (s)	0.41	0.33	0.56	0.70

The results in Fig. 6.4 show that a parabolic function fits the data between R-factor and period very well except the results for the intensity level of $1.0Sa(T_1)$. More specifically, for the intensity levels of $2.0Sa(T_1)$ and $3.0Sa(T_1)$, the value of R^2 is almost 1.0 that indicates that the data is extremely close to the fitted regression line. It is also observed that the R-factor does not change significantly with the period. For example, at the excitation level of $2.0Sa(T_1)$, the ratio

of the R-factor at the longest period to that at the shortest period is only about 8%. At the excitation level of 3.0Sa(T_1), the ratio becomes even smaller to reach 5%. From the structural design of view, such small change of R-factor can be ignored, i.e., the R-factor can be considered constant regardless of the bridge period. The observations of the results for Bridge #5 are slightly different from those for Bridge #1. It can be seen in Fig. 6.5 that at the intensity level of 1.0Sa(T_1), the R-factor is almost the same for the four periods considered. At the intensity level of 2.0Sa(T_1), the variation of the R-factor with the period is negligible that is about 3% between the maximum (1.85) and the minimum (1.79). However, the variation becomes obvious at the intensity level of 3.0Sa(T_1). The ratio of the maximum to the minimum R-factor is about 37%. Furthermore, the R-factor is almost linearly increased with the increasing of the period. Based on the results given in Figs. 6.4 and 6.5, it can be concluded that the R-factors for Bridge #1 and Bridge #5 are about 3.0 and 2.0, respectively.

(a)

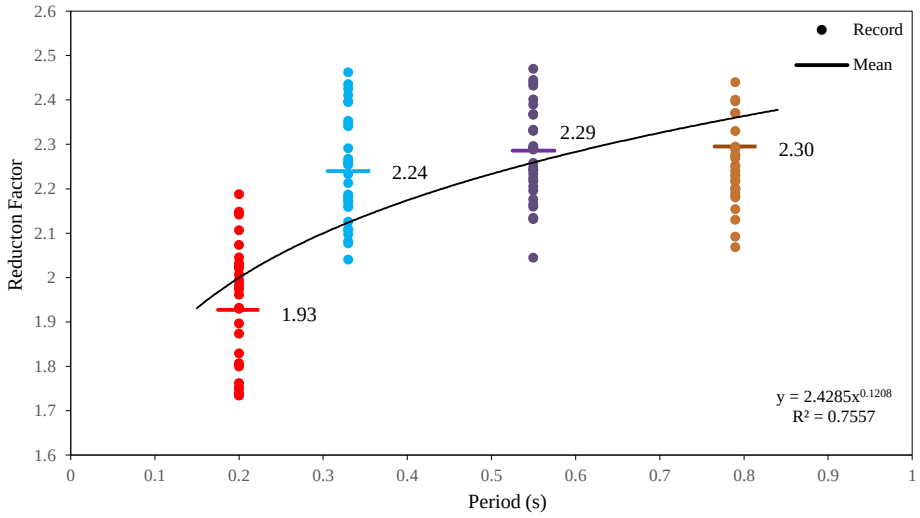

(b)

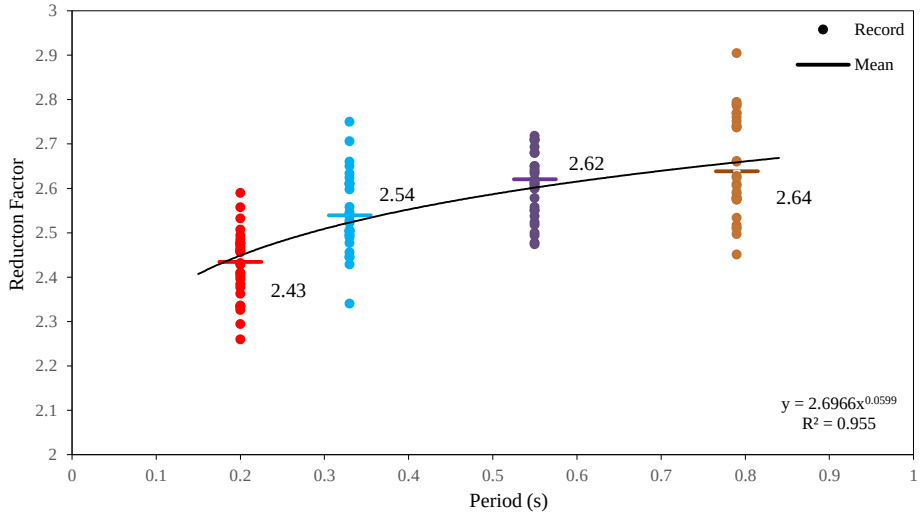

(c)

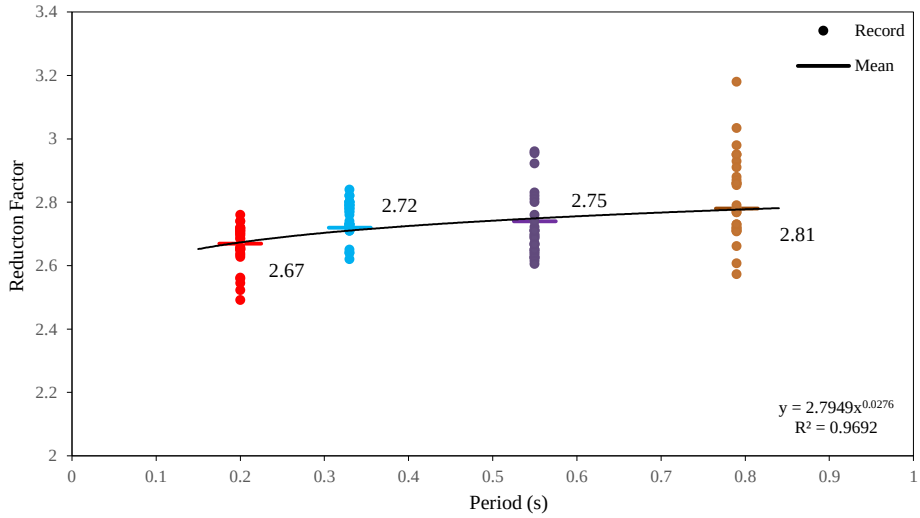

Figure 6.4 R-factor *vs* period for Bridge #1 at three excitation levels: (a) 1.0Sa(T_1); (b) 2.0Sa(T_1); (c) 3.0Sa(T_1).

(a)

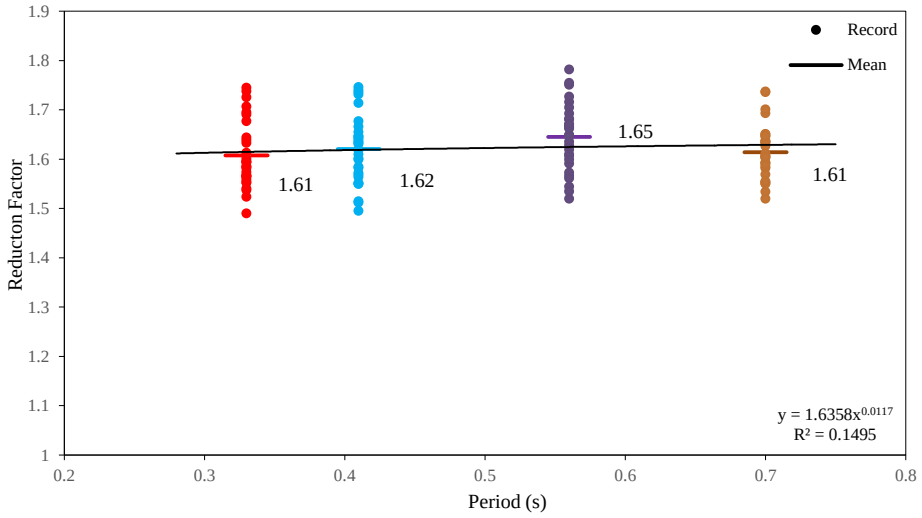

(b)

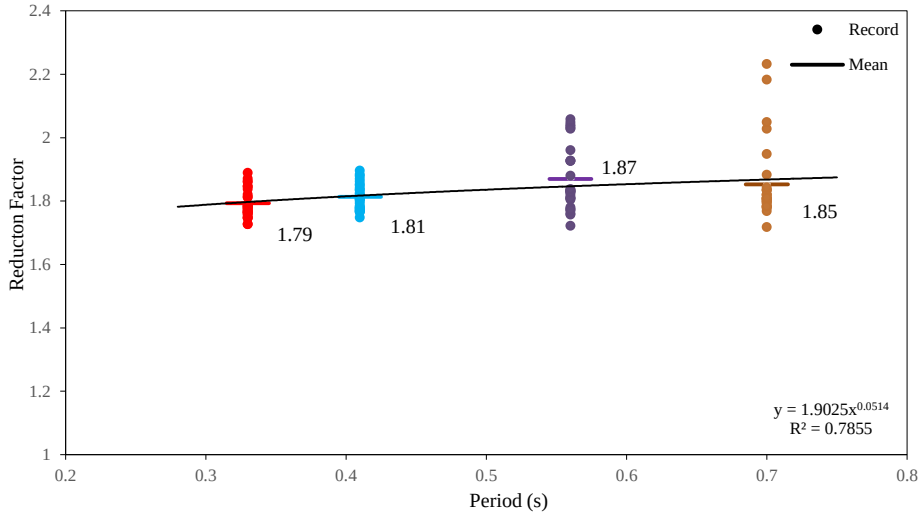

(c)

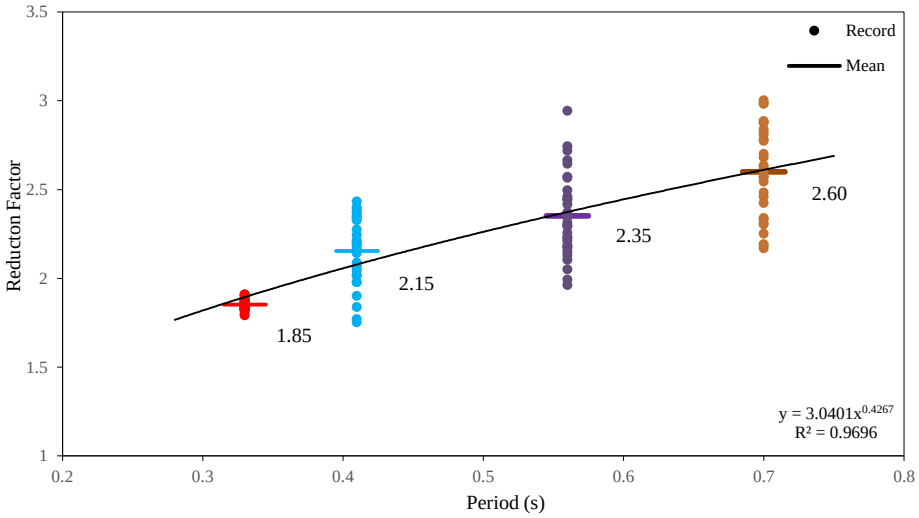

Figure 6.5 R-factor *vs* period for Bridge #5 at three excitation levels: (a) 1.0Sa(T_1); (b) 2.0Sa(T_1); (c) 3.0Sa(T_1).

6.2.2 Results from Group II bridges

6.2.2.1 Force reduction factor vs ductility

The bridges in Group II consist of Bridges #3, #4, and #6. It should be noted that the structural system of Bridge #3 is very similar to that of Bridge #1; Bridge #6 is very similar to that of Bridge #5 in Group I. The major difference is that the abutments of Bridges #3 and #6 were modeled as a roller in the longitudinal direction while both Bridges #1 and #5 were modeled as a rigid frame in the longitudinal direction. In the transverse direction, the structural model of Bridge #3 (Group II) and Bridge #1 (Group I); Bridge #6 (Group II) and Bridge #1 (Group I) is the same except that the model of Bridges #3 and #6 in Group II has 2 spans while that of Bridges #1 and #5 in Group II has 3 spans. The structural system of Bridge #4 is different from that of Bridges #3 and #6. In both Bridges #3 and #6, the columns are monolithically cast with the girders. However, in Bridge #4, a fixed bearing is used on the top of each column, which allows the rotation only.

The results for Bridges #3 and #6 are presented in Figs. 6.6 and 6.7, respectively. By comparing the results obtained from the model in the longitudinal direction with those in the transverse direction, it can be noticed that the maximum R-factor for Bridge #3 is governed by the transverse direction while for Bridge #6 it is governed by the longitudinal direction. In Figs. 6.6 (b) and 6.7(a), it can be seen that both power function and linear function fit the data reasonably well from the regression analysis. The only difference is that the value of R^2 of the power function is slightly larger than that of the linear function. Furthermore, it can be seen that the results in Fig. 6.6 (b) are very different from those shown in Fig. 6.2 (b) even though Bridge #3 and Bridge #1 have the same structural system in the transverse direction. The same observation was obtained for Bridge #6 and Bridge #5. Such difference clearly indicates that the R-factor depends on the number of columns in the transverse direction.

The mean R-factor and the ductility for the top and bottom section of the column of each bridge in Group II are presented in Table 6.3. It can be seen in the table that, for Bridge #3, the minimum R-factor obtained from the analyses is 2.78 corresponding to the top section at the intensity of the 1.0Sa(T_1) while the maximum is 5.25 corresponding to the bottom section at the intensity of the 3.0Sa(T_1). For Bridge #6, the minimum is 1.69 and the maximum is 4.63. The maximum R-factor of both bridges is governed by the responses on the bottom section of the column (see highlights in Table 6.3). The results in Table 6.3 also show that the R-factors of Bridge #6 are smaller than those of Bridge #3. More specifically, the R-factors of Bridge #6 are about 56%, 58%, 15% smaller than those of Bridge #3 at the three intensity levels. The smaller R-factors observed in Bridge #6 are due to the use of the crush struts in the bridge transverse direction. This observation is consistent with that from Group I bridges. It is also noticed that the R-factors of Bridges #3 and #6 in Group II are larger than that of Bridges #1 and #5 in Group I. Such finding was not expected. Since Bridges #3 and #6 have three columns while Bridges #1 and #5 have four columns in the transverse direction, a larger R-factor is expected in Bridges #1 and #5. The larger R-factor in Bridge #6 compared with Bridge #5 might be due to the system of the superstructure. More specifically, internal diaphragms were provided in the superstructure of Bridge #5 while they were not present in Bridge #6 since the superstructure of Bridge #6 consists of solid slab only. The larger stiffness of these diaphragms tends to prevent the substructure from yielding. It is also interesting to point out that according to the 2014 CHBDC, the R-factor for the bridge bents with multiple columns in the transverse direction is 5.0. It was observed that in the examined Bridge #3 at the excitation levels of 2.0Sa(T_1) and 3.0Sa(T_1), which are 5.07 and 5.25, respectively as shown in Table 6.3. With respect to Bridge #4, no significant force reduction was found in which the R-factor is only about 1.2. Such results are not surprising as a larger portion of the bending in the bridge substructure is carried by the

bearings. Therefore, the moment developed in the column is relatively small. Given this, no further investigation was conducted on Bridge #4.

Table 6.3 Mean R-factor and ductility of Group II bridges.

Bridge ID	Direction	Response	Top Section			Bottom Section		
			1.0Sa(T_1)	2.0Sa(T_1)	3.0Sa(T_1)	1.0Sa(T_1)	2.0Sa(T_1)	3.0Sa(T_1)
#3 (without crush struts)	Long.	R	2.78	2.83	3.76	3.47	4.39	4.98
		ϕ	1.87	3.21	4.44	1.89	3.32	4.43
	Tran.	R	3.06	3.79	3.89	3.23	5.07	5.25
		ϕ	1.60	4.00	4.53	1.85	3.26	3.72
#6 (with crush struts)	Long.	R	1.93	2.83	4.27	2.06	3.19	4.63
		ϕ	1.12	1.64	3.10	1.27	1.83	3.01
	Tran.	R	2.14	2.49	3.43	1.69	1.85	1.88
		ϕ	0.74	1.46	2.74	0.35	0.50	0.54
#4	Long.	R	------	------	------	1.01	1.08	1.19
		ϕ	------	------	------	0.09	0.17	0.23
	Tran.	R	------	------	------	1.00	1.04	1.10
		ϕ	------	------	------	0.07	0.14	0.19

(a)

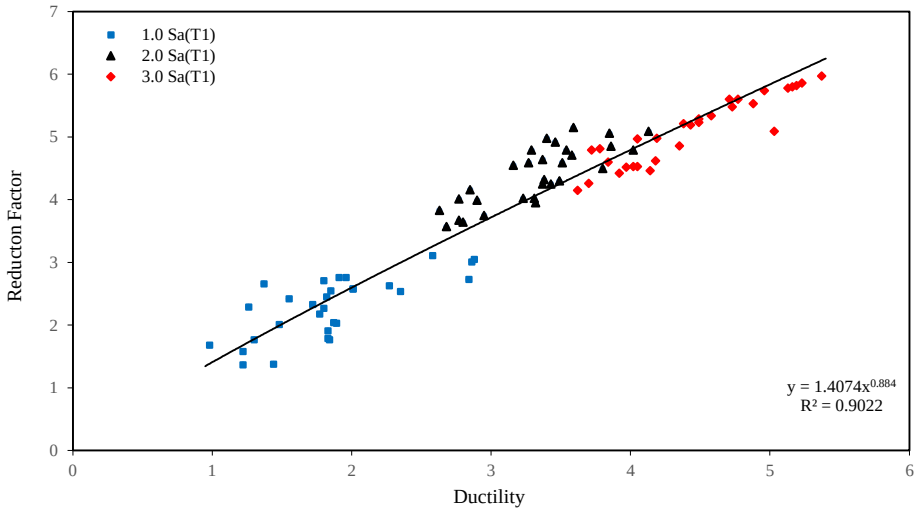

(b)

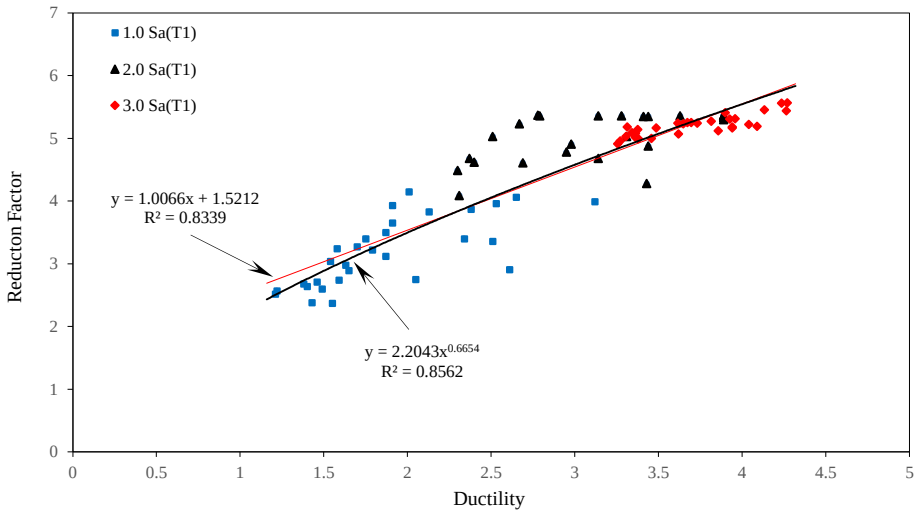

Figure 6.6 Results of R-factor vs ductility for Bridge #3:
(a) longitudinal direction, $Sa(T_1) = 0.5g$;
(b) transverse direction, $Sa(T_1) = 0.5g$.

(a)

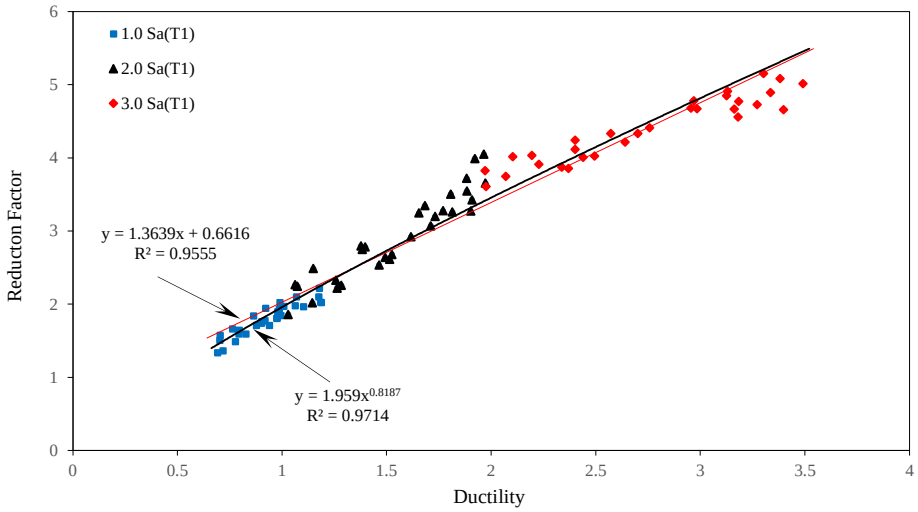

(b)

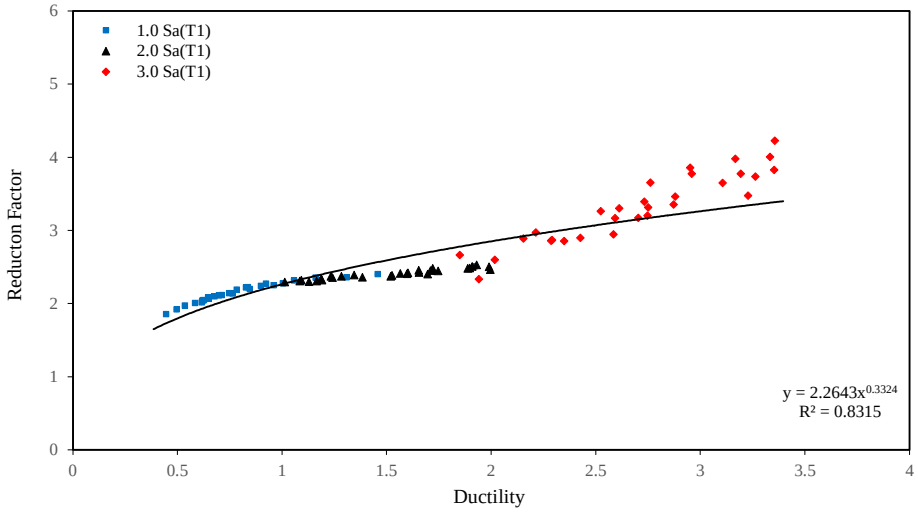

Figure 6.7 Results of R-factor vs ductility for Bridge #6:
(a) longitudinal direction, Sa(T_1) = 0.228g;
(b) transverse direction, Sa(T_1) = 0.358g.

6.2.2.2 Force reduction factor vs period

The relation between R-factor and the period was also investigated on the bridges in Group II. As discussed in the previous section, the largest R-factor observed for Bridge #4 was about 1.2, which occurred at the highest intensity level of $3.0Sa(T_1)$. Such extremely small factor can be compensated by the material factors and the factors for load combinations in the design process. Therefore, Bridge #4 was not analyzed to develop the relationship between R-factor and the period of the structure. Table 6.4 lists the change of the height of the column in the original model of Bridges #3 and #6 in each direction for the purpose of investigation. Figures 6.8 and 6.9 illustrate the results for Bridges #3 and #6, respectively. It can be seen in the figures that the R-factor is almost constant throughout periods. More specifically, for Bridge #3, the ratios of the largest to the smallest R-factors at the excitation levels $1.0Sa(T_1)$, $2.0Sa(T_1)$ and $3.0Sa(T_1)$ are 22%, 6%, and 4% while for Bridge #6, they are 14%, 9%, and 5%. It is not surprising that a relatively larger ratio was observed at the intensity level of $1.0Sa(T_1)$ as discussed in the previous section about Group I bridges. At the excitation levels $2.0Sa(T_1)$ and $3.0Sa(T_1)$, the R-factor can be treated the same, and this observation is consistent with that in Group I bridges. Based on the results presented in Fig. 6.8 and 6.9, one might suggest R-factor of 5.0 for Bridge #3; 3.0 and 5.0 for Bridge #6 at the intensity levels $2.0\ Sa(T_1)$ and $3.0\ Sa(T_1)$, respectively.

Table 6.4 Period and column height of original model and modified models, Group II bridges.

Bridge ID	Model direction		Model input data			
			Original model	Modified models		
#3	Longitudinal	Col. height (mm)	6460	4000	5000	8000
		Period (s)	0.75	0.4	0.55	1.09
	Transverse	Col. height (mm)	6460	4000	5000	8000
		Period (s)	0.75	0.42	0.58	1.17
#6	Longitudinal	Col. height (mm)	9220	3000	5000	7000
		Period (s)	1.08	0.24	0.47	0.75
	Transverse	Col. height (mm)	5495	3500	7500	9500
		Period (s)	0.55	0.34	0.84	1.17

(a)

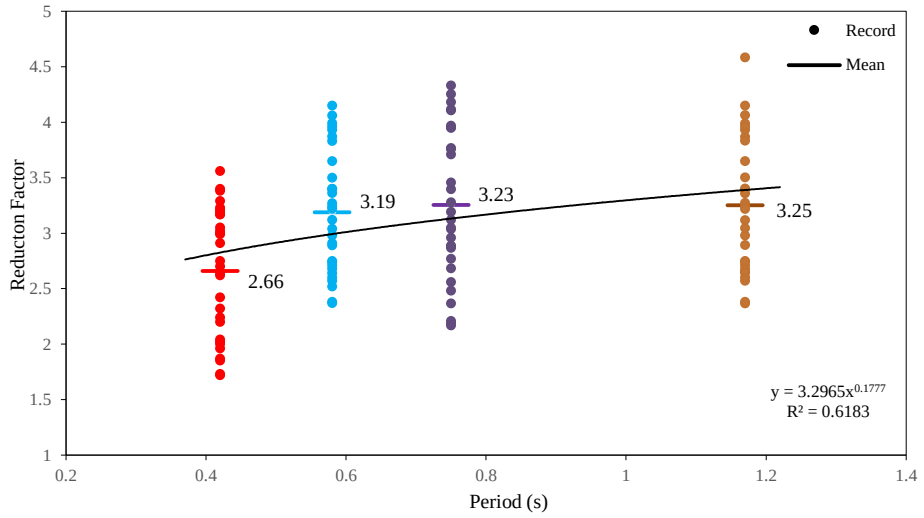

(b)

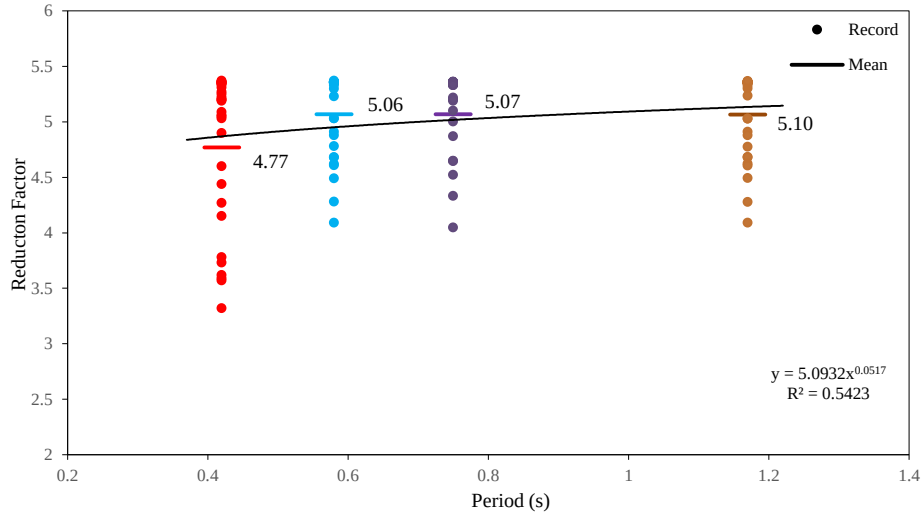

(c)

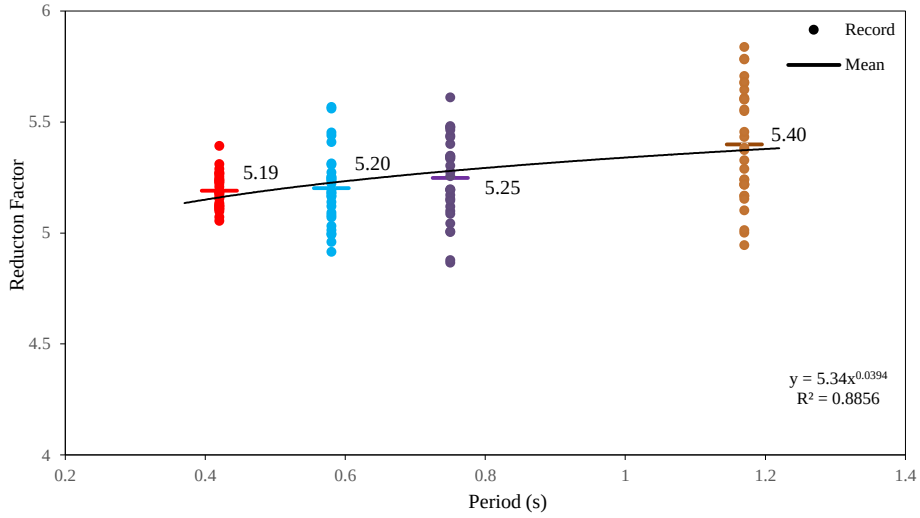

Figure 6.8 R-factor *vs* period for Bridge #3 at three excitation levels: (a) 1.0Sa(T_1); (b) 2.0Sa(T_1); (c) 3.0Sa(T_1).

(a)

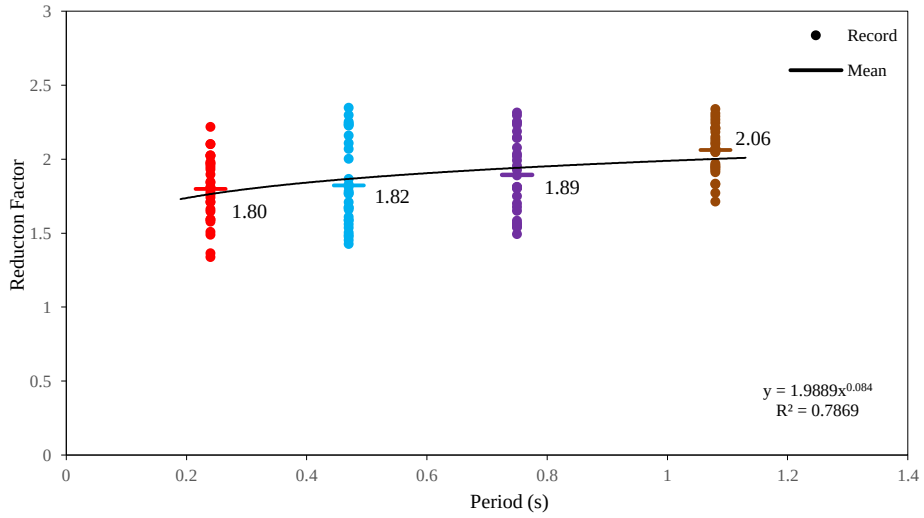

(b)

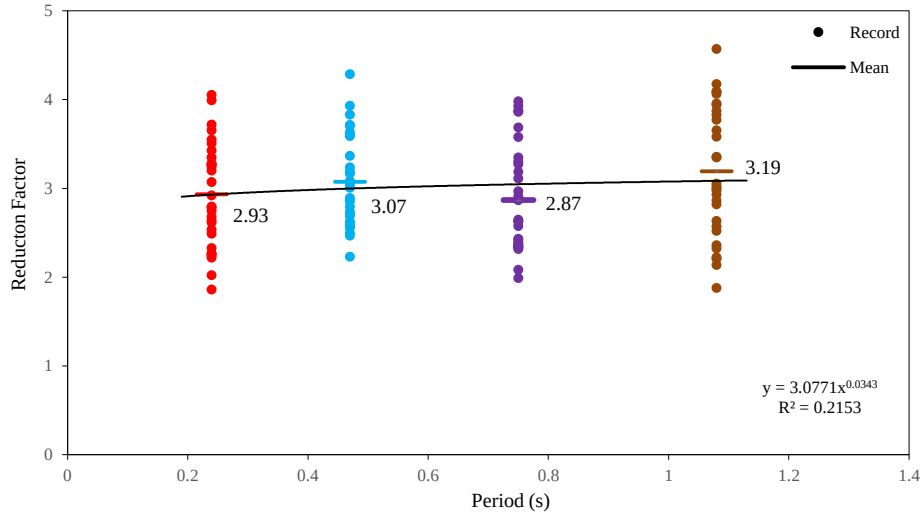

(c)

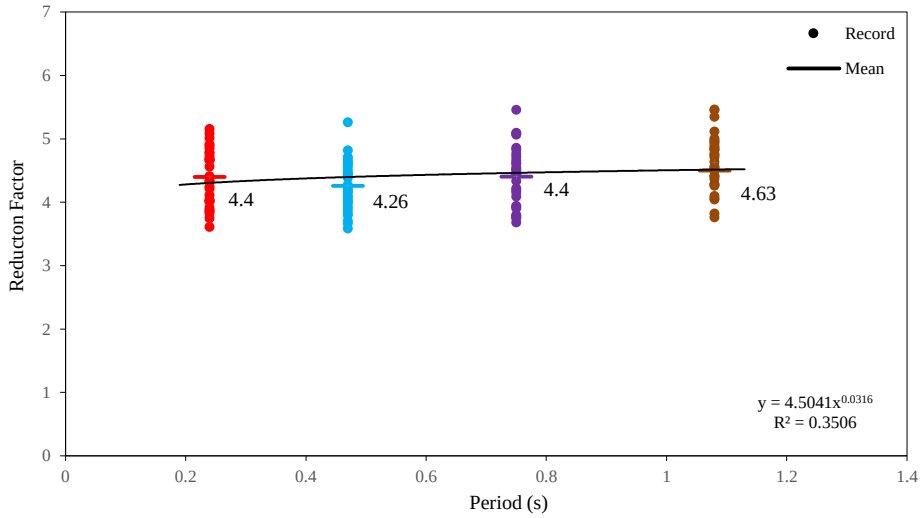

Figure 6.9 R-factor *vs* period for Bridge #6 at three excitation levels: (a) 1.0Sa(T_1); (b) 2.0Sa(T_1); (c) 3.0Sa(T_1).

6.2.3 Results from Group III bridges

6.2.3.1 Force reduction factor vs ductility

The bridges in Group III are Bridges #2, #7, and #8 as described in Chapter 4. All the three bridges were modeled as a single-degree-of-freedom in the longitudinal direction. The transverse direction of Bridges #2 and #8 was modeled in the same way like Bridges #1 and #5 in Group I, and Bridge #3 in Group II. The only difference is, the beam elements in the models of Bridges #2 and #8 (Fig. 4.8, Chapter 4) are representative of the cap beam in the superstructure while those in the models of Bridges #1 and #5 in Group I, and Bridge #3 in Group II are representative of the diaphragms in the transverse direction. The model of Bridge #7 in the transverse direction is different than Bridges #2 and #8 in which the beam element is cantilevered on both sides of the frame, and the section of beam and column elements is variable along its span length or the height as described in Chapter 3.

The results for the maximum mean of R-factor *vs* ductility for the three bridges are presented in Figs. 6.10 to 6.12. It can be observed in the figures that a scatter of the data in the longitudinal and transverse directions is very different. More specifically, in the longitudinal direction, the R-factor is almost constant at each scaling level of $1.0Sa(T_1)$, $2.0Sa(T_1)$, and $3.0Sa(T_1)$ (Fig. 6.11 (a)) while in the transverse direction, the data distribution is very similar to the results presented in the previous section. Table 6.5 provides detailed results on the maximum mean R-factor and ductility for the three bridges. The results in the table indicate that the maximum R-factor of the three bridges is governed by the longitudinal direction. It should be noted that for Bridge #7, the top section in the transverse direction provides the largest R-factor. However, they were eliminated because of the extremely small ductility, which indicates the section is far from yielding. Another observation of the results in Table 6.5 is the ductility of the section in the transverse direction is much smaller than in the longitudinal direction. For

example, for Bridge #2, the range of the ductility of the section in the transverse direction is between 0.33 and 1.40 while in the longitudinal direction it is between 0.96 and 4.19. This is not a surprising result since the bridge moves as a rigid frame in the transverse direction; therefore, each column provides resistance to the seismic loads. The R-factors of Bridges #2 and #8 are very close to those of Bridge #3 in Group II due to the similarity of the structural system.

Table 6.5 Mean R-factor and ductility of Group III bridges.

Bridge ID	Direction	Response	Top Section			Bottom Section		
			1.0Sa(T_1)	2.0Sa(T_1)	3.0Sa(T_1)	1.0Sa(T_1)	2.0Sa(T_1)	3.0Sa(T_1)
#2	Long.	R	------	------	------	2.18	3.12	4.60
		ϕ	------	------	------	0.96	2.48	4.19
	Tran.	R	1.65	1.95	2.08	1.68	1.98	2.16
		ϕ	0.33	0.77	1.37	0.34	0.79	1.40
#7	Long.	R	------	------	------	1.53	2.71	3.62
		ϕ	------	------	------	1.09	1.86	3.36
	Tran.	R	2.56	2.99	3.17	1.00	1.06	1.08
		ϕ	0.11	0.22	0.35	0.25	0.48	0.70
#8	Long.	R	------	------	------	1.68	2.54	3.75
		ϕ	------	------	------	0.85	2.01	3.69
	Tran.	R	1.46	1.62	1.64	1.48	1.66	1.90
		ϕ	0.48	0.97	1.75	0.48	1.07	1.77

(a)

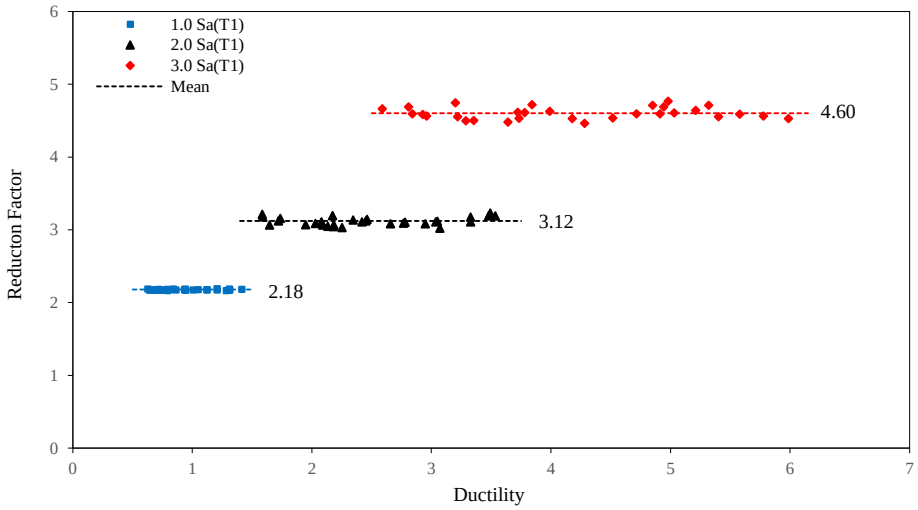

(b)

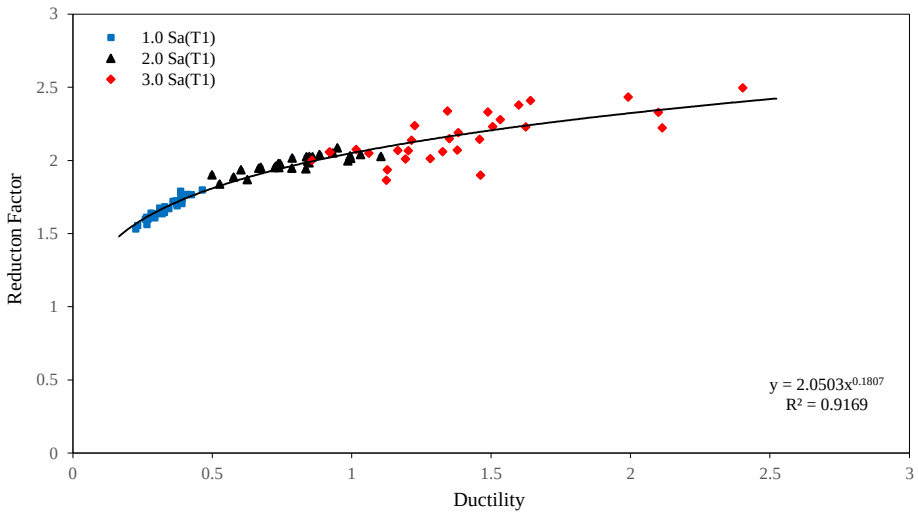

Figure 6.10 Results of R-factor vs ductility for Bridge #2:
(a) longitudinal direction, $Sa(T_1) = 0.5g$;
(b) transverse direction, $Sa(T_1) = 0.5g$.

(a)

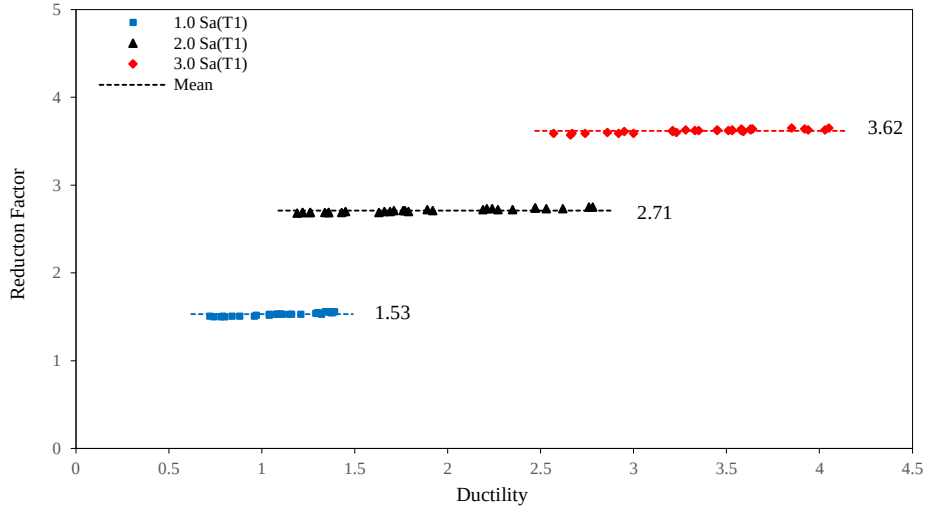

(b)

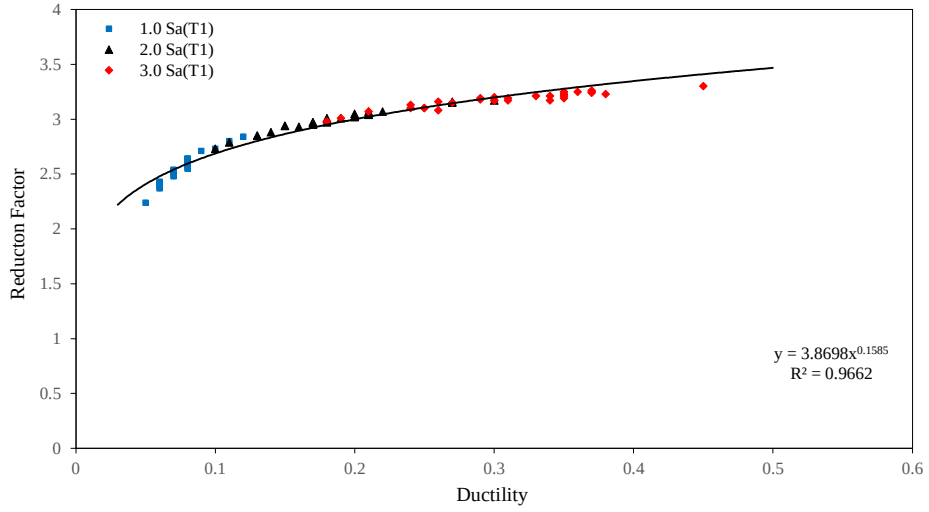

Figure 6.11 Results of R-factor vs ductility for Bridge #7:
(a) longitudinal direction, Sa(T_1) = 0.5g;
(b) transverse direction, Sa(T_1) = 0.5g.

(a)

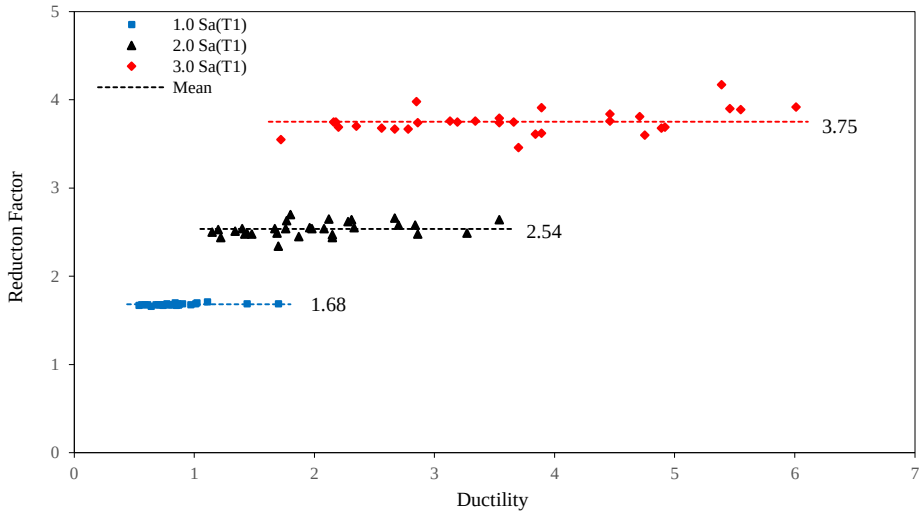

(b)

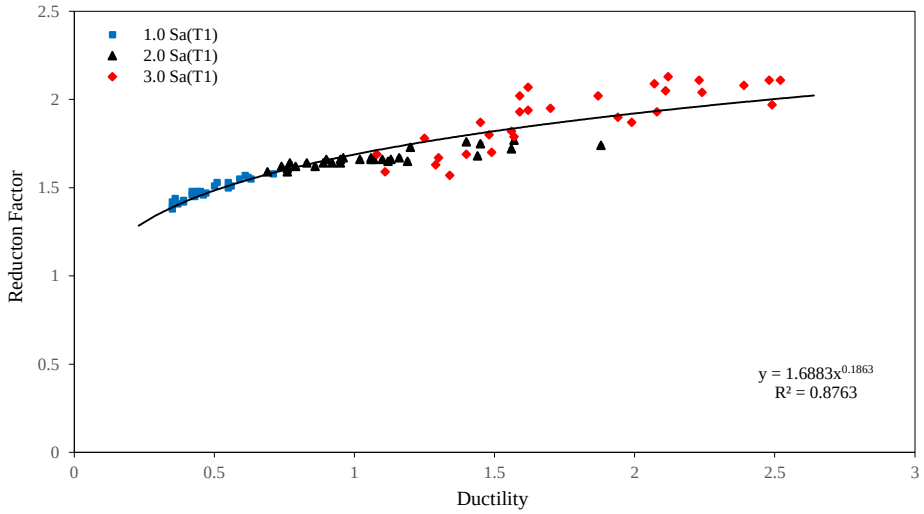

Figure 6.12 Results of R-factor vs ductility for Bridge #8:
(a) longitudinal direction, Sa(T_1) = 0.337g;
(b) transverse direction, Sa(T_1) = 0.5g.

6.2.3.2 Force reduction factor vs period

The results for the R-factor *vs* period are presented in Figs. 6.13 to 6.15 for Bridges #2, #7, and #8, respectively. The heights of the columns modified to achieve different periods of the each model are provided in Table 6.6. Please note that the R-factors shown in the figures are governed by the model in the longitudinal direction, which is represented by a SDOF. It can

be seen in Fig. 6.13 that for Bridge #2, the models at the first two periods, i.e., 0.45 s and 0.69 s develop almost constant reduction factors from each time-history at each excitation level while those at the other two periods, i.e., 0.86 s and 1.06 s generate non-uniform factors. Among the four periods considered, at the scaling level of 1.0Sa(T_1), the smallest mean R-factor is about 2.2, the largest is about 2.6; at the scaling level of 3.0Sa(T_1), the smallest R-factor is about 4.6, the largest is about 7.3. For Bridge #7 (Fig. 6.14), all the models produce almost the same R-factor in which the variation is extremely small. It is a very special observation, which was not observed in other bridges examined in this study. Furthermore, the R-factor is linearly increased with the period. The largest R-factor from the model with the longest period at the highest scaling level of 3.0Sa(T_1) is around 5.0. The regression analysis results of Bridge #8 are similar to those of Group I and Group II bridges, i.e., the relation between R-factor and period can be fitted with a linear function or a power function. The highest R-factor observed in Fig. 6.15 is about 4.0.

Table 6.6 Period and column height of original model and modified models, Group III bridges.

Bridge ID	Model direction		Model data			
			Original model	Modified models		
#2	Longitudinal	Col. height (mm)	5170	6000	7000	8000
		Period (s)	0.45	0.69	0.86	1.06
	Transverse	Col. height (mm)	4530	6000	7000	8000
		Period (s)	0.14	0.36	0.45	0.76
#7	Longitudinal	Col. height (mm)	4820	3000	7000	9000
		Period (s)	0.59	0.20	1.04	1.59
	Transverse	Col. height (mm)	4145	6000	8000	10000
		Period (s)	0.12	0.24	0.37	0.53
#8	Longitudinal	Col. height (mm)	6030	4000	8000	10000
		Period (s)	0.6	0.3	1.0	1.5
	Transverse	Col. height (mm)	5410	4000	7000	9000
		Period (s)	0.22	0.16	0.44	0.66

(a)

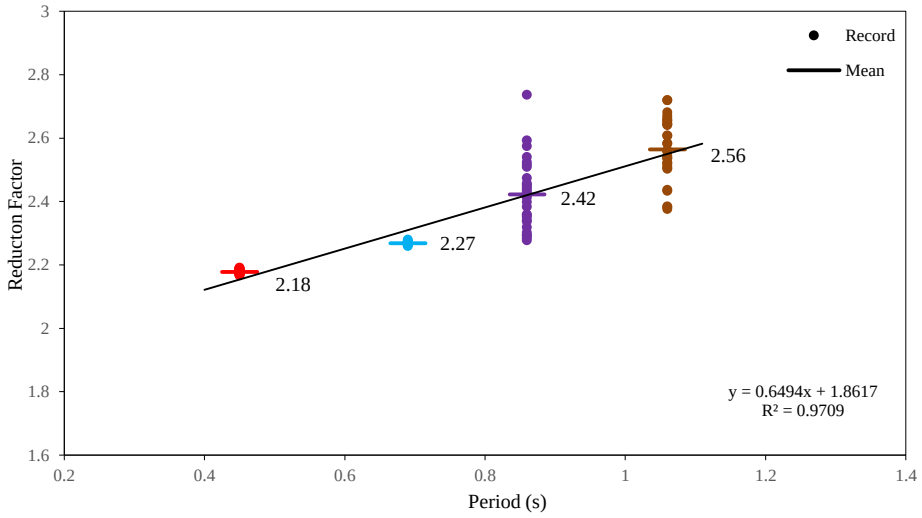

(b)

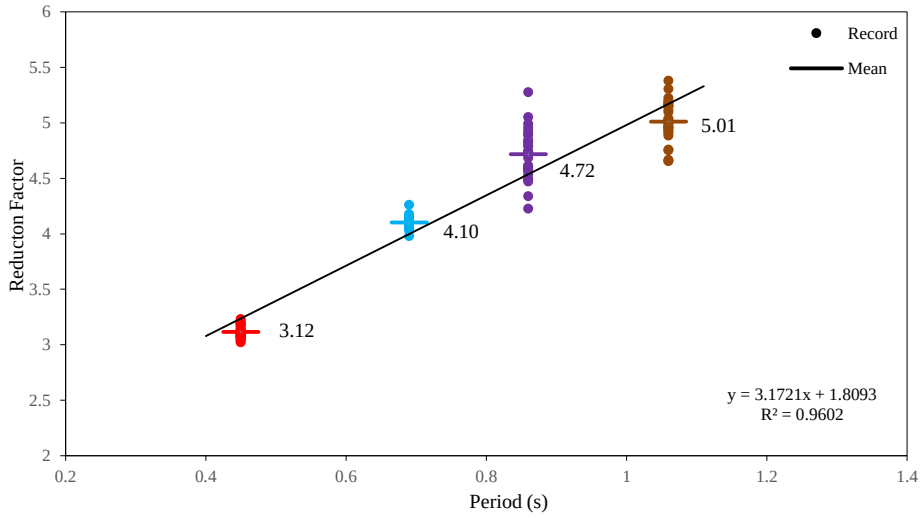

(c)

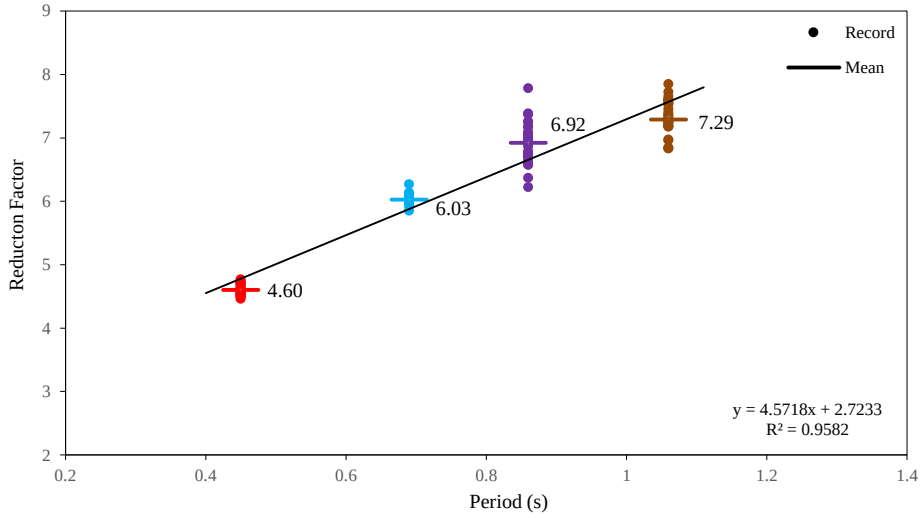

Figure 6.13 R-factor *vs* period for Bridge #2 at three excitation levels: (a) 1.0Sa(T_1); (b) 2.0Sa(T_1); (c) 3.0Sa(T_1).

(a)

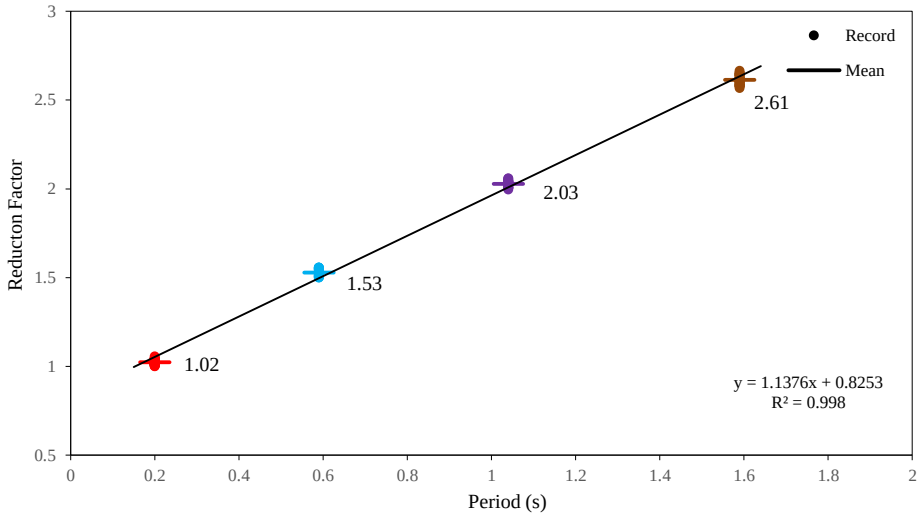

(b)

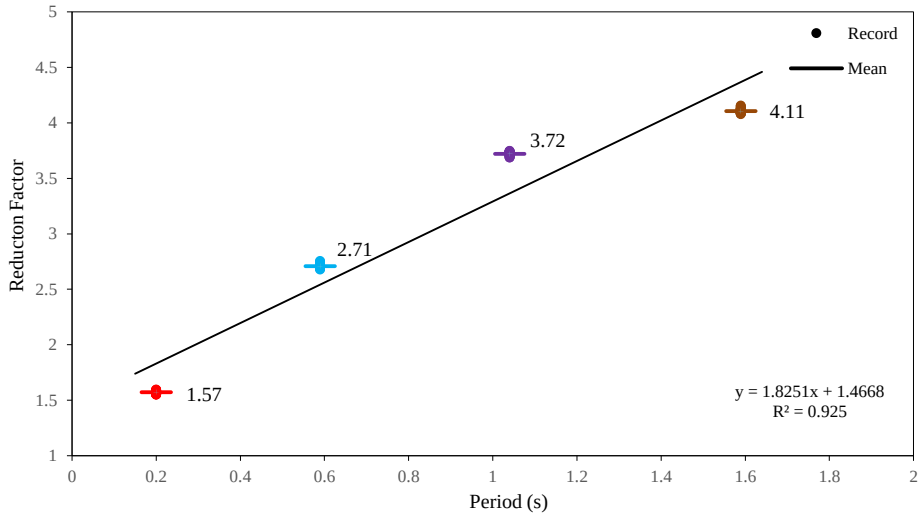

(c)

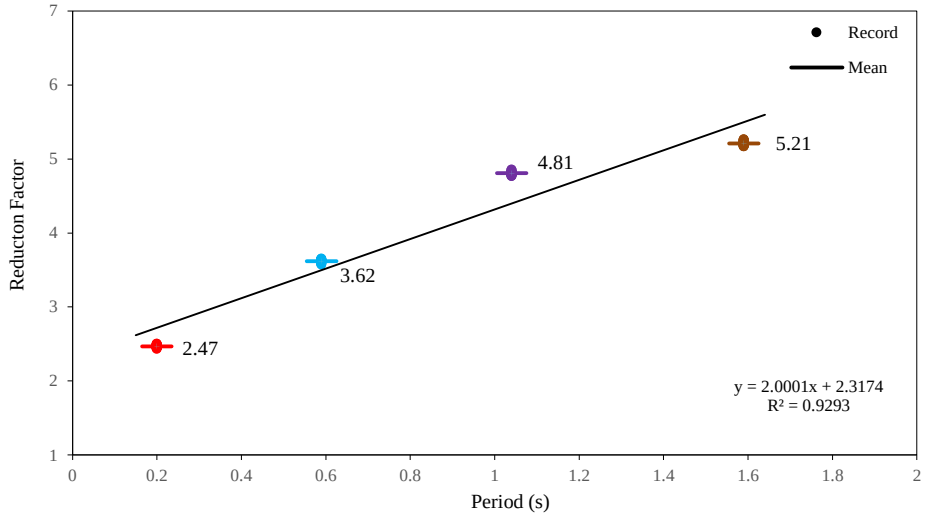

Figure 6.14 R-factor *vs* period for Bridge #7 at three excitation levels: (a) 1.0Sa(T_1); (b) 2.0Sa(T_1); (c) 3.0Sa(T_1).

(a)

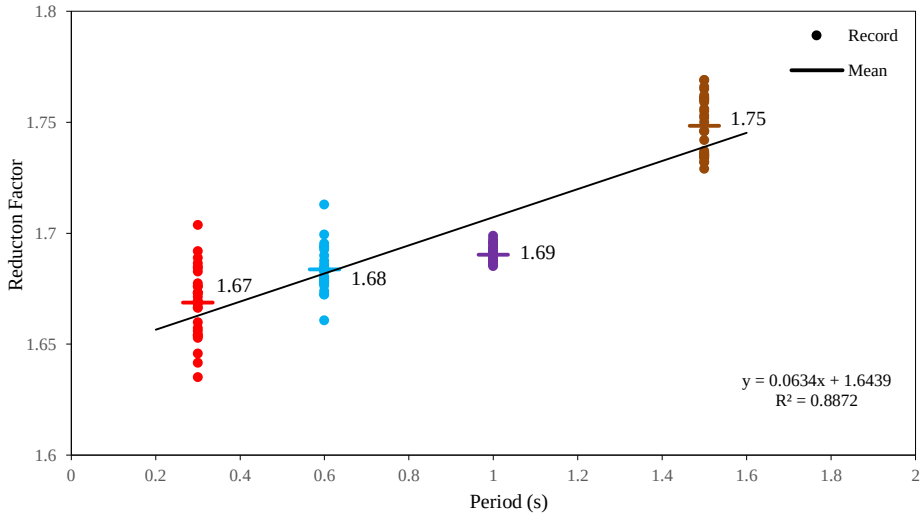

(b)

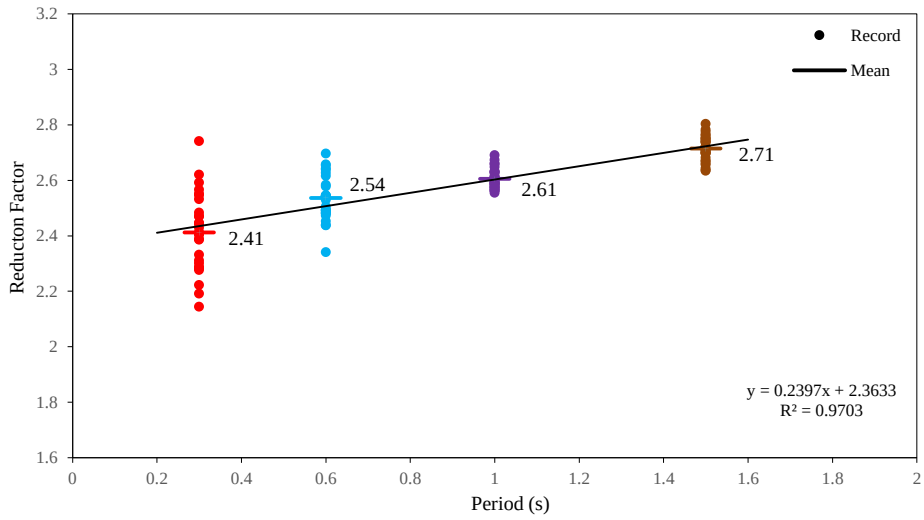

(c)

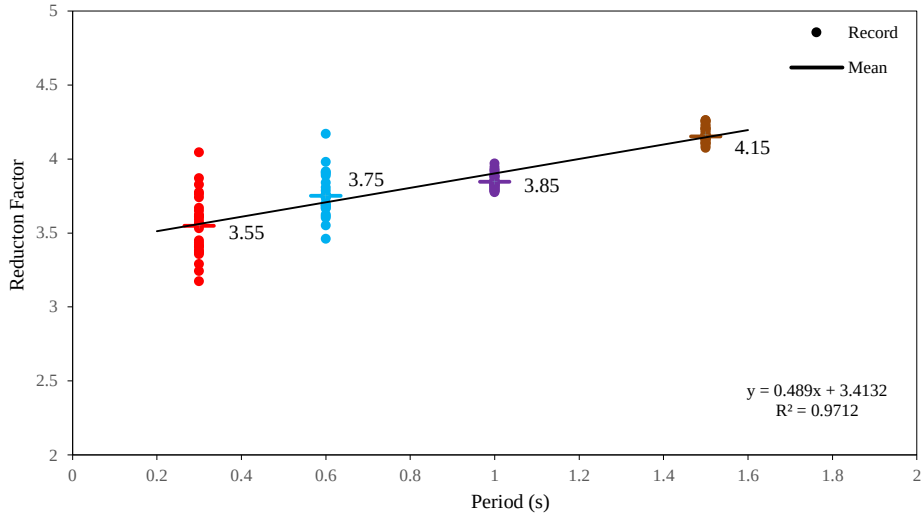

Figure 6.15 R-factor *vs* period for Bridge #8 at three excitation levels: (a) 1.0Sa(T_1); (b) 2.0Sa(T_1); (c) 3.0Sa(T_1).

6.2.4 Summary of the results

Table 6.7 summarizes the maximum R-factors based on analyses on the models of the eights bridges in the transverse direction associated with the three intensity levels 1.0Sa(T_1), 2.0Sa(T_1), and 3.0Sa(T_1). The results in the table show that the R-factor decreases with the increasing of the number of spans. More specifically, the R-factor obtained from a frame with two spans is about two times of that with three spans. It is also noticed that using the crush struts would reduce the R-factor. A bridge substructure system with cap beam shows much smaller R-factor compared with the system in which the columns are monolithically cast with the superstructure. Furthermore, the maximum R-factor for the substructure with cap beam is about 2.0. However, if the cap beam is cantilevered, the R-factor is increased to about 3.0. Furthermore, if fixed bearings are used on the top of the column with the cap beam system, the maximum R-factor from the examined bridge (Bridge #4) is about 1.1, which is negligible.

Table 6.8 provides the maximum mean R-factors for the eight bridges examined in this study based on the analyses on the models in the longitudinal and transverse directions of each bridge. It can be seen in the table that the mean R-factors of Bridges #1, #5, and #3 are governed by the transverse direction while those of the rest bridges are dominated by the longitudinal direction. Furthermore, the maximum R-factor of Bridges #3, #6, and #2 are about 5.0 that is very close to the value recommended by CHBDC. The maximum R-factor of Bridges #7 and #8 are about 4.0, which is slightly less than the value recommended by CHBDC. The R-factors of Bridge #1 and #5 are appropriately 3.0 and 2.0, respectively. As mentioned above, the R-factor for Bridge #4 is extremely small that can be neglected.

Table 6.7 Maximum R-factors observed in the models of bridges in transverse direction.

Group ID.	Bridge ID.	Schematic model	Max. mean R-factor		
			$1.0Sa(T_1)$	$2.0Sa(T_1)$	$3.0Sa(T_1)$
I	#1	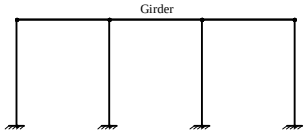	1.93	2.43	2.67
	#5	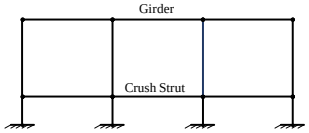	1.62	1.81	2.15
II	#3	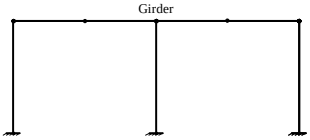	3.23	5.07	5.25
	#6	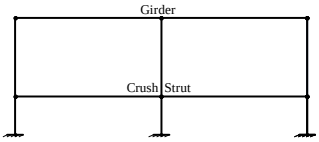	2.14	2.49	3.43
III	#2	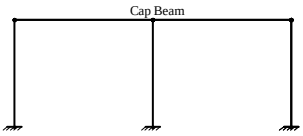	1.68	1.98	2.16
	#8	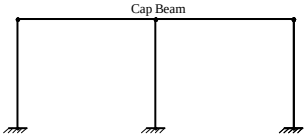	1.48	1.66	1.90
	#7	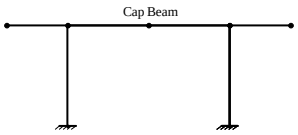	2.56	2.99	3.17
II	#4	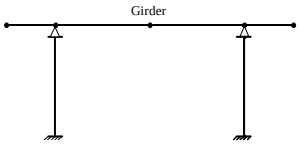	1.00	1.04	1.10

Table 6.8 Maximum R-factors of the original bridges.

Group ID.	Bridge ID.	Schematic model		Max. mean R-factor			Recommended	
		Long	Tran.	1.0Sa(T_1)	2.0Sa(T_1)	3.0Sa(T_1)	CHBDC	AASHTO
I	#1	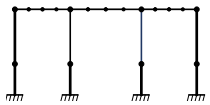	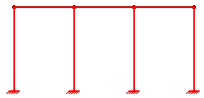	1.93	2.43	2.67	5.0	5.0
	#5	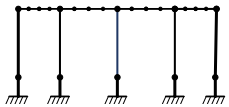	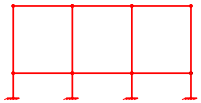	1.62	1.81	2.15		
II	#3	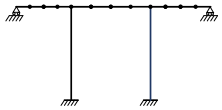	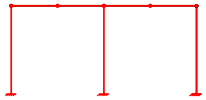	3.23	5.07	5.25		
	#6	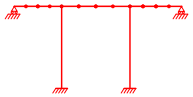	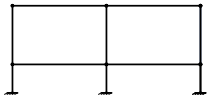	2.06	3.19	4.63		
	#4	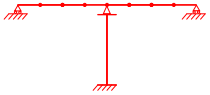		1.01	1.08	1.19		
III	#2		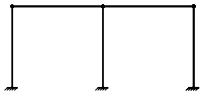	2.18	3.12	4.60		
	#7		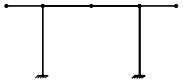	1.53	2.71	3.62		
	#8		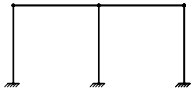	1.68	2.54	3.75		

As described in the previous sections, the height of the columns of each bridge was changed (Tables 2, 4, and 6) in order to investigate how the R-factor would change with the period of the bridge. Table 6.9 presents the minimum and the maximum R-factors based on the original model of each bridge in which the height of the columns was obtained from the construction drawings, and the modified models in which the height is artificial for the purpose of the study. The results clearly show that the R-factor changes the period slightly. For most of the cases, the difference between the maximum and the minimum R-factor is less than 15%. Extremely large difference (about 162%) was observed on Bridge #7 of Group III bridges. This might be due to relatively its small cross-section and small lateral stiffness of the column compared to other bridges. It also can be seen in the table that for some bridges (Bridges #1, #3, and #6), the difference at the lower intensity level 1.0Sa(T_1) is smaller than that at the higher level 3.0Sa(T_1) while for others it is are opposite observation. Both results are expected due to the different ductility and different properties of the plastic hinges.

Table 6.9 Ranges of the R-factor of the original and the modified models.

Group ID.	Bridge ID.	1.0Sa(T_1)			2.0Sa(T_1)			3.0Sa(T_1)		
		Min. R	Max. R	Difference* (%)	Min. R	Max. R	Difference (%)	Min. R	Max. R	Difference (%)
I	#1	1.93	2.27	18%	2.43	2.64	9%	2.67	2.81	5%
	#5	1.61	1.65	2%	1.79	1.85	3%	1.85	2.54	**37%**
II	#3	2.66	3.25	22%	4.77	5.07	6%	5.19	5.4	4%
	#6	1.8	2.06	14%	2.93	3.19	9%	4.4	4.63	5%
	#4	1.01	1.21	20%	1.08	1.38	28%	1.19	1.49	25%
III	#2	2.18	2.56	17%	3.12	5.01	**61%**	4.6	7.33	**59%**
	#7	1.02	2.61	**156%**	1.57	4.11	**162%**	2.47	5.21	**111%**
	#8	1.67	1.75	5%	2.41	2.71	12%	3.55	4.17	17%

* Difference is calculated with respect to the minimum R-factor.

The R-factors for the bridges examined in this study are summarized in Table 6.10. For the purpose of comparison, the R-factor specified in CHBDC is provided in the table. According to CHBDC, the R-factor is the same for all the bridges, which is 5.0 regardless of the configuration of the superstructure. However, the results in Table 6.10 clearly show that the R-factors from the detailed time-history analyses are much smaller that the CHBDC value. The only exception is the R-factor for the column bents without crush struts and cap beam obtained from the responses due to the excitations subjected to $3.0Sa(T_1)$ is compatible with the code value. In addition, the R-factor is almost 1.0 when the fixed bearings are used.

Table 6.10 Summary of the values for R-factor from the current study.

Type of substructure		Current study	CHBDC
Multiple column bent	with crush struts	2.15~3.43	5.0
	without crush struts	2.67~5.25	
	with cap beam	2.16~3.17	
	without cap beam	4.63~5.25	
	with fixed bearing	1.10~1.19	

6.3 Comparison with Code Requirement and other Studies

The response modification factor (R) specified in the CHBDC depends on the type and the material of the column bent as listed in Table 2.1, Chapter 2. It should be noted that the R factors defined in CHBDC are the same as those in AASHTO. According to CHBDC requirement, the value of the R factor for all the eight bridges considered in this study is 5.0. However, detailed time-history analysis results show that this factor was achieved only in three cases i.e., Bridges #3 and #6 (Group II), and Bridge #2 (Group III) at the excitation level of $3.0Sa(T_1)$, which is the highest intensity level for the nonlinear analysis. The "satisfactory" rate success rate is about 13% (=3/24) in which 24 is the total number of analysis cases using the

original model. For the rest of the cases, the R-factor is extremely much smaller than the code value.

Borzi (2000) conducted a comprehensive study on the response modification factor and proposed the following three equations (i.e., Eqs. 6.1 to 6.3) to determine *R* factor. It is necessary to mention that the original notations used in the equations proposed by Borzi (2000) were revised slightly to be consistent with those used in current study. The notation *T* in Eqs. 6.1 to 6.3 represents the dominant period of the bridge while the variables T_1, R_1, and R_2 can be determined using Eqs. 6.4 and 6.5 in which μ represents the ductility. For the purpose of comparison, the R-factors of the original model of each eight bridges along with the three additional models described in the previous sections were calculated using Eqs. 6.1 to 6.3. The results are presented in Table 6.11. It can be seen that the R-factors obtained from the analysis in current study are compatible with those predicted using Eqs. 6.1 to 6.3 proposed by Borzi (2000) except there are few cases that the difference is larger than 20%. Further more, it is noticed that the difference of the R-factor between current study and Borzi (2000) is larger if it is dominated by the response in the transverse direction.

$$T<T_1 \qquad R = 1 + (R_1 - 1)\frac{T}{T_1} \tag{6.1}$$

$$T_1<T<T_2 \qquad R = 1 + R_1 + (R_2 - R_1)\frac{T - T_1}{T_2 - T_1} \tag{6.2}$$

$$T>T_2 \qquad R = R_2 \tag{6.3}$$

Where,

$$T_1 = b_{T1} \qquad T_2 = a_{T2}\mu + b_{T2} \tag{6.4}$$

$$R_1 = a_{R1}\mu + b_{R1} \qquad R_2 = a_{R2}\mu + b_{R2} \tag{6.5}$$

$b_{T1} = 0.25$, $a_{T2} = 0.163$, $b_{T2} = 0.60$, $a_{R1} = 0.69$, $b_{R1} = 0.90$, $a_{R2} = 1.01$, $b_{R2} = 0.24$.

Table 6.11 Comparison of the R-factor between current study and Borzi (2000).

Group ID	Bridge ID.	Governing Direction	Model	R-factor		
				Current Study	Borzi (2000)	Difference*
I	#1	Transverse	Original Model	2.67	2.02	24%
			Modified Model #1	2.75	2.27	17%
			Modified Model #2	2.72	2.27	17%
			Modified Model #3	2.81	2.26	20%
	#5	Transverse	Original Model	2.15	2.65	-23%
			Modified Model #1	1.85	2.27	-23%
			Modified Model #2	2.35	2.68	-14%
			Modified Model #3	2.24	2.26	-1%
II	#3	Transverse	Original Model	5.25	4.04	23%
			Modified Model #1	5.19	3.91	25%
			Modified Model #2	5.2	3.86	26%
			Modified Model #3	5.4	4.23	22%
	#6	Longitudinal	Original Model	4.63	4.17	10%
			Modified Model #1	4.4	3.81	13%
			Modified Model #2	4.26	3.79	11%
			Modified Model #3	4.4	3.97	10%
	#4	Longitudinal	Original Model	1.19	1.25	-5%
			Modified Model #1	1.39	1.25	10%
			Modified Model #2	1.4	1.25	11%
			Modified Model #3	1.49	1.25	16%
III	#2	Longitudinal	Original Model	4.6	5.06	-10%
			Modified Model #1	6.03	5.13	15%
			Modified Model #2	6.92	5.28	24%
			Modified Model #3	7.33	5.43	26%
	#7	Longitudinal	Original Model	3.62	3.38	7%
			Modified Model #1	2.47	2.58	-4%
			Modified Model #2	4.81	4.15	14%
			Modified Model #3	5.21	4.28	18%
	#8	Longitudinal	Original Model	3.75	3.64	3%
			Modified Model #1	3.55	3.69	-4%
			Modified Model #2	3.85	3.68	4%
			Modified Model #3	4.17	3.78	9%

* The difference is calculated with respect to the value from current study.
* The positive percentage indicates the R-factor from current study is larger than that predicted by Borzi (2000).

Chapter 7

Conclusions and Recommendations

7.1 Introduction

As one of the major natural hazards, earthquakes have caused severe damage to bridges. Some of the magnificent earthquakes are, the 1994 Northridge and the 1989 Loma Prieta earthquakes in California, the 1995 Kobe earthquake in Japan, 1999 Chichi earthquake in Taiwan, and 2010 Chile earthquake. The lessons from the past earthquakes have led to sustainable research on the assessment of the performance of bridges due to seismic loads, which in turn helps to improve the seismic provisions in the bridge design codes.

The current seismic design of bridges is based on a well-known principle, capacity design, in which the superstructure remains elastic during earthquake events while the nonlinear deformation, i.e., plastic hinges, should occur in the substructure and must be ductile in term of flexure. Given this, the Canadian bridge design code CHBDC allows to reduce the demands for the design of substructure elements (mainly columns) by a response modification factor R. These demands include moment, shear, and axial force. The value of R-factor specified in CHBDC is between 2.0 and 5.0 depending on the material of the column and the type of the column bents. For example, the R-factor is 3.0 for single column bents, and it is 5.0 for multiple-column bents.

Since the R-factor will affect the design forces for the substructure elements significantly, the objective of the study is to examine its value from detailed nonlinear analyses,

and its relationship with the ductility and the bridge dominant period. For the purpose of the study, eight existing highway bridges in Montreal were selected to be examined. These include slab type bridges, slab-girder type bridges, and box-girder type bridges, which represent typical highway bridges in Quebec. The substructure consists of multiple columns from two to four columns in a column bent. Linear and nonlinear time-history analyses were conducted on each bridge model using finite element analysis software IDARC. In total, thirty simulated accelerograms representative of the characteristics of ground motions in eastern Canada were used as input for the seismic excitations. The accelerograms were scaled to three intensity levels according to the first mode period of the bridge, namely, $1.0Sa(T_1)$, $2.0Sa(T_1)$, and $3.0Sa(T_1)$. In order to investigate the relation between the R-factor and the bridge dominate vibration period, the original column height, which was obtained from the construction drawings, was modified for additional three heights, and the analyses were repeated.

7.2 Conclusions

The main conclusions of the study are summarized as follows:

- Both equal displacement and equal energy rules are not observed in this study. The results from this study indicate that a power function or linear function can be used to express the relation between R-factor and the ductility.

- The R-factor does not change significantly with the bridge dominant period. In general, a bridge with a longer dominant period is expected to have a relatively larger R-factor.

- The R-factor increase with the increase of the seismic excitation levels. The R-factor at the excitation level of $3.0Sa(T_1)$ is about two times at the excitation level of $2.0Sa(T_1)$. Given this, we recommend using the excitation level of $2.0Sa(T_1)$ to estimate the R-

factor.

- The configuration of the substructure should be considered to specify R-factor. The results from the current study show that the R-factors for columns bents w/o crush struts are about 3.5 and 5.0; w/o cap beams are about 3.0 and 5.0.

- The R-factor depends on the number of columns on the bent. For example, the R-factor for the 2 (or 3)-column bents from the current study is about 5.3, which is very close to the number specified in CHBDC. However, for the 4-column bents, the R-factor is about half of CHBDC value.

7.3 Recommendations

- The column bents of all the bridges examined are made of concrete. Similar studies can be performed on steel bridges in order to understand the reduction of responses of steel columns because the nonlinearity of concrete and steel is very different.

- Effects of seismic excitations in the two orthogonal directions (longitudinal direction and transverse direction) applied simultaneously could be investigated.

- Bridges with a skew angle could also be examined.

References

AASHTO. (1961). Standard specifications for highway bridges. 8th Edition, Washington, DC.

AASHTO (2014). AASHTO LRFD Bridge design specifications, customary U.S. units, 7th Edition. American Association of State Highway and Transportation Officials, Washington, DC.

Abdel-Mohti, A. (2010). Effect of skew on the seismic response of RC box-girder bridges. Proceedings of the 9th US National and 10th Canadian Conference on Earthquake Engineering, Toronto, ON, Canada.

ACI 515-57 (1958). A guide to the use of waterproofing, dampproofing, protective and decorative barrier systems for concrete. ACI Committee 515, Manual of Concrete Practice.

Adams, J., and Halchuk, S. (2003). Fourth generation seismic hazard maps of Canada: Values for over 650 Canadian localities intended for the 2005 National Building Code of Canada. Open File Report 4459, Geological Survey of Canada, Ottawa, ON, Canada.

Alemdar, F. Z. (2010). Plastic hinging behavior of reinforced concrete bridge columns. PhD. Thesis, University of Kansas, Lawrence, Kansas, U.S.

Amiri-Hormozaki K. (2003). Effects of scaling of earthquake excitations on dynamic response of reinforced concrete frame buildings. M.A.Sc Thesis, Department of Civil Engineering, University of Ottawa, Ottawa, Ont., 2003.

ASCE/SEI7-10. (2010). Minimum design loads for buildings and other structures. ASCE standard, American Society of Civil Engineers.

ATC-32. (1996). Improved seismic design criteria for California bridges: provisional recommendations. Applied Technology Council, Redwood City, CA.

Atkinson, G.M. (2009). Earthquake time histories compatible with the 2005 National building code of Canada uniform hazard spectrum. Canadian Journal of Civil Engineering, 36(6): 991-1000.

Aviram, A., Mackie, K.R., and Stojadinovic, B. (2008). Guidelines for nonlinear analysis of bridge structures in California. PEER Report, Pacific Earthquake Engineering Research Center, Berkeley, CA.

Baker, J.W., and Cornell, C.A. (2005). A vectored-valued ground motion intensity measure consisting of spectral acceleration and epsilon. Earthquake Engineering and Structural Dynamics, 34(10): 1193-1271.

Balendra, T., Huang, X. (2003). Overstrength and ductility factors for steel frames designed according to BS 5950. Journal of Structural Engineering, 129(8): 1019–1035.

Banerjee1, S., Patro, S.K., and Rao, P. (2014). Inelastic seismic analysis of reinforced concrete frame building with soft storey. International Journal of Civil Engineering Research, 5(4): 373-378.

Billah, A. M., and Alam, M. S. (2016). Plastic hinge length of shape memory alloy (SMA) reinforced concrete bridge pier. Engineering Structures, 117 (15): 321-331.

Borzi, B., and Elnashai, A.S. (2000). Refined force reduction factors for seismic design. Engineering Structures, 22:1244–1260.

Caltrans (2013). Seismic design criteria, version 1.7. California Department of Transportation, Sacramento, CA.

Carr, A.J. (2015). RUAUMOKO – Inelastic dynamic analysis program. Department of Civil Engineering, University of Canterbury, Christchurch, New Zealand.

CHBDC. (1966). Canadian highway bridge design code. Standards CAN/CSA-S-6, Canadian Standards Association, Mississauga, Ontario.

CHBDC (2014). Canadian Highway Bridge Design Code, CAN/CSA S6-14. Canadian Standards Association, Rexdale, ON, Canada.

Computers and Structures, Inc. (2015). SAP2000 - Computer program for three dimensional static and dynamic finite element analysis and design of structures, Berkley, CA.

Dowell, R. K., and Hines, E. M. (2002). Plastic hinge length of reinforced concrete bridge columns. Proceedings of the Third National Seismic Conference and Workshop on Bridges and Highways, Portland, Ore.

Erdem, A. (2010). Seismic design of bridges: analytical investigation of AASHTO LRFD response modification factors and seismic performance levels of circular bridge columns. Saarbrücken: LAP LAMBERT Academic Publishing.

European Committee for Standardization (CEN). (2005). Design of structures for earthquake resistance – Part 2: Bridges. Eurocode 8, EN 1998-2, Brussels.

FHWA. (2012). Manual for design, construction, and maintenance of orthotropic steel bridges, FHWA-IF-12-027. US Department of Transportation Federal Highway Administration, Washington, DC.

Hartzell, S.H. (1978). Earthquake aftershocks as Green's functions. Geophysical Research Letters, 5(1): 1-4.

Hatami, K., and Bathurst, R.J. (2001). Investigation of seismic response of reinforced soil retaining walls. Proceedings of the 4th International Conference on Recent Advances in Geotechnical Earthquake Engineering and Soil Dynamics, San Diego, California.

Haselton, C.B., Whittaker, A.S., Hortacsu, A., Baker, J., Gray, J., and Grant, D.N. (2012). Selecting and scaling earthquake ground motions for performing response-history analysis. Proceedings of the 15th World Conference on Earthquake Engineering. Lisbon, Portugal.

Heidebrecht, A.G., and Naumoski, N. (2002). The influence of design ductility on the seismic performance of medium height reinforced concrete buildings. ACI Special Publications SP-197, American Concrete Institute, Farmington Hills, MI, 239-264.

Hines, E. M., Seible, F., and Priestley, M.J.N. (2000). Cyclic Tests of Structural Walls with Highly - Confined Boundary Elements, Structural Engineering Report SSRP 2001/27, University of California, San Diego, 260 pp.

Hobbs, W.H. (1908). A Study of the damage to bridges during earthquakes. The Journal of Geology, 16(7): 636-653.

Huang, K. (2014). Minimum number of accelerograms for time-history analysis of typical highway bridges. M.A.Sc. Thesis, Department of Building, Civil, and Environmental Engineering, Concordia University, Montreal, QC, Canada.

ICC, (2000), The International Building Code, IBC-2000, International Code Council, Falls Church, VA.

Itani, A., Gaspersic, P., and Saiidi, M. (1997). Response modification factors for seismic design of circular reinforced concrete bridge columns. Structural Journal, 94(1): 23–30.

Kang, C.K., and Choi, B.J. (2011). New approach to evaluate the response modification factors for steel moment resisting frames. International Journal of Steel Structures, 11(3): 275-286.

Kappos, A. J., Paraskeva, T. S., and Moschonas, I. F. (2013). Response modification factors for concrete bridges in Europe. Journal of Bridge Engineering, 18(12): 1328–1335.

Karbassi, A., Lestuzzi, P., and Mohebi, B. (2012). Development and application of damage spectra for RC buildings in Europe. Proceedings of the 15th World Conference on Earthquake Engineering, Lisboan, Portugal.

Keivani, S.B. (2003). Seismic evaluation of existing reinforced concrete bridges in Ottawa region. M.A.Sc Thesis, Department of Civil Engineering, University of Ottawa, Ottawa, Ont.

Kim, J. K., and Choi, H.H. (2005). Response modification factors of chevron-braced frames. Engineering Structures, 27: 285-300.

Lin, L., Naumoski, N., Saatcioglu, M., Booth, E., and Gao, Y.L. (2013). Selection of seismic excitations for nonlinear analysis of reinforced concrete frame buildings. Canadian Journal of Civil Engineering, 40(5): 411-426.

Mander, J.B., Priestley, M.J., and Park, R. (1988). Theoretical stress-strain model for confined concrete. Journal of Structural Engineering, 114(8): 1804-1826.

Marianchik, E., Levy, R., Rutenberg, A., and Segal, F. (2000). Optimal seismic design of friction damped braced frames based on existing earthquake records. Proceedings of the 12th World Conference on Earthquake Engineering, Auckland, New Zealand.

Mazzoni, S., McKenna, F., Scott, H.F. Fenves, G.L. (2009). Open System for Earthquake Engineering Simulation (OpenSees), Pacific Earthquake Engineering Research Center, Berkeley, California.

Miranda, E., and Bertero, V. (1994). Evaluation of strength reduction factors for earthquake resistant design. Earthquake Spectra, 10(2): 357-379.

Mitchell, D. Huffman, S., Tremblay, R., Saatcioglu, M., Palermo, D., Tinawi, R., and Lau, D. (2013). Damage to bridges due to the 27 February 2010 Chile earthquake. Canadian Journal of Civil Engineering, 40(8): 675-692.

Mitchell, D., Tremebaly, R., Karacabeyli, E., Paultre, P., Saatcioglu, M., and Anderson, D.L. (2003). Seismic force modification factors for the proposed 2005 edition of the National Building Code of Canada. Canadian Journal of Civil Engineering, 30(2): 308–327.

Mortezaei, A. (2014). Plastic hinge length of RC columns under the combined effect of near-fault vertical and horizontal ground motions. Journal of Civil Engineering, 58(3): 243-253.

Naumoski, N.N., Heidebrecht, A.C., and Rutenberg, A.V. (1993). Representative ensembles of strong motion earthquake records. EERG report 93-1, Department of Civil Engineering, McMaster University, Hamilton, ON, Canada.

Naumoski, N.N., Heidebrecht, A.C., and Tso, W.K. (1988). Selection of representative strong motion earthquake records having different A/V ratios. EERG Report 88-01, Department of Civil Engineering, McMaster University, Hamilton, Ontario.

Naumoski, N.N., and Heidebrecht, A.C. (1998). Seismic level of protection of medium height reinforced concrete frame structures, member properties for seismic analysis. EERG report 98-01, Department of Civil Engineering, McMaster University, Hamilton, ON, Canada.

Naumoski, N., and Tso, W.K. (1990). Period-dependent seismic force reduction factors for short-period structures, Canadian Journal of Civil Engineering, 18(4): 568-574.

Nassar, A. A., and Krawinkler, H. (1991). Seismic demands for SDOF and MDOF systems. Report No. 95, The John A. Blume Earthquake Engineering Center, Stanford University, CA.

Newmark, N.M., and Hall, W.J. (1973). Procedures and criteria for earthquake resistant design. National Bureau of Standards, Washington, DC, pp. 209-236.

Nielson, B.G., and DesRoches, R. (2007). Seismic fragility methodology for highway bridges using a component level approach. Earthquake Engineering and Structural Analysis, 36: 823-839.

NIST. (2011). Selecting and scaling earthquake ground motions for performing response history analysis. NIST/GCR 11-917-15, prepared by NEHRP Consultants Joint Venture for the National Institute of Standards and Technology, Gaithersburg, Maryland.

NRCC (2010). National Building Code of Canada. Institute for Research in Construction, National Research Council of Canada, Ottawa, ON.

Pan, Y., Agrawal, A.K., Ghosn, M., and Alampalli, S. (2010). Seismic fragility of multispan simply supported steel highway bridges in New York State. I: Bridge Modelling, Parametric Analysis, and Retrofit Design. Journal of Bridge Engineering, 15(5): 448-461.

Paulay, T. and Priestley, M.J.N. (1992). Seismic design of reinforced concrete and masonry buildings. John Wiley & Sons, Inc., Hoboken, NJ.

Priestley, M. J. N., Calvi, G. M., and Kowalsky, M. J. (2007). Displacement based seismic design of structures. IUSS PRESS, Italy.

Priestley, M.J.N., Seible, F. and Calvi, G.M. (1996). Seismic design and retrofit of bridges. John Wiley & Sons, Inc., Hoboken, NJ.

Reinhorn, A.M., Roh, H., Sivaselvan, M., Kunnath, S.K., Valles, R.E., Madan, A., Li, C., Lobo, R., and Park, Y.J. (2009). IDARC2D version 7.0: a program for the inelastic damage analysis of structures. Report MCEER-09-0006, University at Buffalo, The State University of New York.

Reyes, J.C., and Kalkan, E. (2011). Required number of records for ASCE/SEI 7 ground motion scaling procedure. US Geological Survey, Open File Report 108, 334 p.

Sebai, E.D.A. (2009). Comparisons of international seismic code provisions for bridges. M.A.Sc. Thesis, Department of Civil Engineering an Applied Mechanics, McGill University, Montreal, QC.

Tavares, D.H., Padgett, J.E., and Paultre, P. (2012). Fragility curves of typical as-built highway bridges in eastern Canada. Engineering Structures, 40: 107-118.

Thrall, A.P., and Billington D.P. (2008). Bayonne Bridge: the work of Othmar Ammann, master builder. Journal of Bridge Engineering, 13(6): 635–43.

Uang, C. M., Tsai, K. C., and Bruneau, M., (2000). Seismic design of steel bridges. Bridge Engineering Handbook, CRC Press.

Waller, C.L. (2011). A methodology for probabilistic performance-based seismic risk assessment of bridge inventories. M.A.Sc. thesis, Department of Civil and Environmental Engineering, Carleton University, Ottawa, ON.

Watanabe, G., and Kawashima, K. (2002). An evaluation of the force reduction factor in the force based seismic design, NIST special publication SP, pp 201–218.

Wilson, J.C. (2003). Repair of new long-span bridges damaged by the 1995 Kobe Earthquake. Journal of Performance of Constructed Facilities, 4(4): 196-205.

Yousuf, M.D., and Bagchi, A. (2010). Seismic performance of a 20-story steel-frame building in Canada. The Structural Design of Tall and Special Buildings, 19(8): 901-921.

Yousuf, N. (2016). Seismic analysis of RC frame with and without shear walls. International Journal of Civil and Structural Engineering, 6(3): 168-176.

Zafar, A. (2009). Response modification factor of reinforced concrete moment resisting frames in developing countries. M.A.Sc. Thesis, Graduate College, University of Illinois Urbana-Champaign, Urbana, Illinois, U.S.

Zhe, L. (2017). Personal communication.